doi : 10.17596/0003794

戦略的イノベーション創造プログラム
Cross-ministerial Strategic Innovation Promotion Program

Cruise Report

SIP-HOT I "Pathfinder"

(SIP-Hydrothermal deposit in Okinawa Trough)

CK14-04 (Exp. 907)

JAMSTEC

National Institute of Advanced Industrial Science and Technology
AIST

国立研究開発法人
国立環境研究所
National Institute for Environmental Studies

July 8 - 26, 2014

This cruise report is a preliminary documentation as of the end of the cruise.

This report may not be corrected even if changes on contents (i.e. taxonomic classifications) may be found after its publication. This report may also be changed without notice. Data on this cruise report may be raw or unprocessed. If you are going to use or refer to the data written on this report, please ask the Chief Scientist/Associate Chief Scientist for latest information.

Users of data or results on this cruise report are requested to inform their results to the Planning and Coordination Unit, Project Team for Development of New-generation Research Protocol for Submarine Resources of JAMSTEC (sip-pc@jamstec.go.jp).

This report is to be cited as,
Takai, K., Kumagai, H., Kubo, Y. and CK1404 on-board member (2015) Cruise Report SIP-HOT I "Pathfinder" (SIP-Hydrothermal deposit in Okinawa Trough) CK14-04 (Exp. 907), JAMSTEC, pp. 116, Yokosuka, Japan,
(http://www.godac.jamstec.go.jp/catalog/data/doc_catalog/media/CK14-04-907_all.pdf).

CK14-04(Exp.907)　Cruise Report Contents (draft plan 140714 final rv. 151001)

Expedition CK14-04 (Exp 907) Cruise Report

Chapter 1: Introduction

1.1 Background and Scientific Objectives

K.Takai

Since the first discovery of submarine hydrothermal activity at Iheya Knoll and Izena Hole (Halbach et al., 1989; Sakai et al., 1990a) in the mid Okinawa Trough, approximately 20 active hydrothermal fields, some are published and some are known but unpublished, have been discovered to date. Among them, several representative hydrothermal systems such as the Minani-Ensei Knoll, the Iheya North, the Izena Hole, the Hatoma Knoll and the Yonaguni Knoll IV systems have been relatively well investigated (Aoyama et al., 2014; Gamo et al., 1991; Ishibashi et al., 2014; Kawagucci et al., 2011; 2013a; 2013b; Konno et al., 2006; Nakagawa et al., 2005; Nunoura and Takai, 2009; Nunoura et al, 2008; Takai et al., 2011; 2012; Yanagawa et al., 2013; 2014). When the abundance of presently known seafloor hydrothermal fields and the spatial extension of seafloor hydrothermal activity in each of the fields such as high- and low-temperature fluid discharges, widespread microbial mats and macrofaunal colonies is compared among the deep-sea hydrothermal systems in the entire Okinawa Trough (totally more than 1000 km length), it seems likely that there are found relatively many and large seafloor hydrothermal systems specifically in the mid Okinawa Trough, e.g., Izena Hole JADE and Hakurei fields and Iheya North field (Ishibashi et al., 2014; Kawagucci et al., 2011; Nakagawa et al., 2005). It has been predicted that not only the emerging seafloor hydrothermal activities but also potential subseafloor hydrothermal fluid flow paths and reservoirs of the Izena Hole and Iheya North systems are relatively large and long-lived (Ishibashi et al., 2014; Kawagucci et al., 2011; 2013a; Kinoshita et al., 1995; Noguchi et al., 2007; Tsuji et al., 2012). The high abundance and large scale of the mid Okinawa Trough hydrothermal systems could be driven by the geological settings such as heavy rifting in backarc basin, many and sporadic magmatic intrusions, thick terrigenous sediments and repeated extension and deposition of volcanoclastics (Ikegami et al., 2014; Tsuji et al., 2012).

In September 2010, the scientific expedition (IODP Exp 331) was conducted in the Iheya North field by a deep-sea drilling vessel ‘Chikyu’ (Takai et al., 2010; 2011). Although the primary scientific objective of this expedition was to characterize

functionally active and metabolically diverse subseafloor microbial communities just beneath the hydrothermal discharging regions of the Iheya North field, the preliminary results obtained from the drilling operations and cored samples indicated the possible existence of enormous subseafloor hydrothermal fluid reservoirs that were much more expansive that expected from the extension of seafloor hydrothermal activities (Takai et al., 2011; 2012). Probably at around the cap rock layers that sealed the hydrothermal fluid reservoirs, the subseafloor massive black-ores (Kuroko) were found (Takai et al., 2011; 2012). These findings suggested that the subseafloor hydrothermal fluid regimes of the Iheya North field, even of other mid Okinawa Trough hydrothermal systems, had great potentials to host subseafloor hydrothermal mineral deposits such as noble metals and rarely found metals for future marine mineral resources of Japan. In addition, during the IODP Exp 331, artificial hydrothermal vents (complete casing and capping) were deployed at several deep holes and new vents were also created (Takai et al., 2011; 2012). Immediately after the development of artificial and post-drilling vents, the hydrothermal fluid patterns and chemistry, the growth and chemical composition of chimney structures and the distribution and propagation of chemosynthetic animal communities have been monitored for almost 4 years at an interval of every 6 months (Kawagucci et al., 2013b). The post-drilling investigation of artificial and new hydrothermal vents pointed that the artificial hydrothermal vents brought previously untouchable deep source brine-enriched hydrothermal fluids on the seafloor and established very fast growing hydrothermal mineral deposits containing abundant metal sulfides (Kawagucci et al., 2013b). In addition, the artificial hydrothermal vents provided excellent seafloor platforms for long-term in situ experiments and monitoring of hydrothermal activities and macrofaunal ecosystems in response to drilling operations and other anthropogenic environmental disturbances. Thus, further to explore the subseafloor microbial ecosystem associated with hydrothermal fluid discharges, to estimate the developmental potential to hydrothermal mineral deposits and to understand the biological resilience to the future industrial development of seafloor mineral and energy resources, we have undertaken another scientific drilling expedition for the Iheya North field and/or similar hydrothermal systems in the mid Okinawa Trough.

As a different discipline of JAMSTEC research, we have been developing a new, easy, fast and effective exploration scheme of seafloor hydrothermal systems in the

Okinawa Trough. As already described, approximately 20 active hydrothermal fields have been discovered in the Okinawa Trough. However, all the previously found hydrothermal systems were discovered by chances or by pinpoint surveys based on the topographic nature of seafloor such as volcano caldera structures or for other purposes. It has been recently reported that near-bottom acoustic reflection and geophysical surveys by remotely operative vehicles (ROV) and autonomous underwater vehicles (AUV) can visualize seafloor hydrothermal discharges and detect subseafloor hydrothermal alteration zones (Kumagai et al., 2010; Nakamura et al., 2012). The AUV acoustic and geophysical surveys can be integrated to the fast and widespread exploration of seafloor hydrothermal activities. In addition, the AUV can load many in situ physical (temperature and turbidity) and chemical (pH, Eh, Mn, H_2S, H_2, CH_4) sensors for detection of hydrothermal plumes and for prediction of subseafloor hydrothermal circulation patterns and extent (Kawagucci et al., 2011; 2013a). Thus, the systematic and interdisciplinary AUV surveys will be a powerful scheme for the fast and effective exploration of seafloor hydrothermal activities and their additional scientific and resource potentials, that means the biogeochemical processes and subseafloor microbial community development and functions, the extent and age of hydrothermal fluid circulations and the extent and quality of subseafloor hydrothermal mineral deposits. However, the systematic and interdisciplinary AUV surveys are still money- and time-consuming operations and are not an easy exploration scheme. Currently, we have found that the acoustic surveys from the surface ship, e.g., commercially available, relatively high frequency multiple narrow beam topography, can also detect the seafloor hydrothermal discharges. Since the acoustic surveys from the surface ship are much easier and faster than those by AUV, it can be used as the preliminary fast and widespread exploration of seafloor hydrothermal activities. Thus, we have proposed a new, easy, fast and effective exploration scheme of seafloor hydrothermal systems that consist of the 1st-round fast and widespread acoustic survey by surface ship for hydrothermal activities and the 2nd-round fine and detail acoustic, geophysical and geochemical survey by AUV for nature and extent of subseafloor hydrothermal fluid circulations and mineral deposits.

Using this new exploration scheme of seafloor hydrothermal systems, we have successfully found two new hydrothermal systems in the Iheya North Knoll in October 2013 – January 2014. The new hydrothermal fields named as Iheya North

Natsu and Aki fields are located at 1.5 km south-southeast and 3.0 km south from the Iheya North Original field, respectively. Based on the comparison of hydrothermal fluid chemistry and macrofaunal community compositions obtained from preliminary ROV observations and samplings between the Iheya North Original, Natsu and Aki fields, these hydrothermal systems are likely related with each other. Then, it has been hypothesized that these seafloor hydrothermal systems within 4 km diameter area of the Iheya North Knoll may be derived from the same hydrothermal reaction and fluid source. This implies that an enormous subseafloor hydrothermal fluid reservoir (about 10 km diameter level of coverage) may be present beneath the three hydrothermal fields of the Iheya North Knoll.

The primary scientific objective of the SIP Chikyu Drilling cruises is to test a hypothesis that the Iheya North Original, Natsu and Aki fields form an enourmous, complex hydrothermal system rooted from a common gigantic subseafloor hydrothermal fluid reservoir potentially covering the whole Iheya North Knoll. Surely, justification of this hypothesis is directly coupled with finding of a gigantic subseafloor hydrothermal mineral (Kuroko) deposit from an aspect of marine mineral resource development. In the 1st-round of SIP Chikyu Drilling cruises, Pathfinder (CK14-04 Exp. 907), LWD tools (logging while drilling) are attempted quickly to detect a common gigantic subseafloor hydrothermal fluid reservoir beneath the three hydrothermal fields. Particularly, temperature monitoring, resistibility and gamma ray intensity while drilling are tested to find the rapid temperature increase by breakout of cap rock structure of the subseafloor hydrothermal fluid paths, the complex structures of porous layered subseafloor hydrothermal fluid paths and the localization of thickness of subseafloor hydrothermal mineral (Kuroko) deposits. In the 2nd-round of SIP Chikyu Drilling cruises, Explorer (CK14-05 Exp. 908), the predicted 3D map of gigantic subseafloor hydrothermal fluid reservoir and mineral deposit structures will be justified by a number of coring and core sample characterizations.

References

Aoyama, S., Nishizawa, M., Takai, K., and Ueno, Y., 2014. Microbial sulfate reduction within the Iheya North subseafloor hydrothermal system constrained by quadruple sulfur isotopes. Earth Planet. Sci. Lett., 398, 113-126.

Gamo, T., Sakai, H., Kim, E.S., Shitashima, K., and Ishibashi, J., 1991. High alkalinity due to sulfate reduction in the Clam Hydrothermal Field, Okinawa Trough. Earth Planet. Sci. Lett., 107:328-338.

Halbach, P., Nakamura, K., Wahsner, M., Lange, J., Sakai, H., Kaselitz, L., Hannsen, R. D., Yamano, M., Post, J., Prause, B., Seiffert, R., Michaelis, W., Teichmann, F., Kinoshita, M., Martchen, A., Ishibashi, J., Czerwinski, S., and Blum, N., 1989. Probable modern analogue of Kuroko-type massive sulphide deposits in the Okinawa Trough back-arc basin. Nature, 338:496-499.

Ikegami, F., Tsuji, T., Kumagai, H., Ishibashi, J., and Takai, K., 2014. Active rifting structures in Iheya Graben and adjacent area of the mid-Okinawa Trough observed through seismic reflection surveys. In Ishibashi, J., Okino, K., Sunamura, M. (Eds), Subseafloor biosphere linked to hydrothermal systems, Tokyo, Springer, in press.

Ishibashi, J., Noguchi, T., Toki, T., Miyabe, S., Yamagami, S., Onishi, Y., Yamanaka, T., Yokoyama, Y., Omori, E., Takaihashi, Y., Hatada, K., Nakaguchi, Y., Yoshizaki, M., Konno, U., Shibuya, T., Takai, K., Inagaki, F., and Kawagucci, S., 2014. Diversity of fluid geochemistry affected by processes during fluid upwelling in active hydrothermal fields in the Izena Hole, the middle Okinawa Trough back-arc basin. Geochemical J., 48, doi:10.2343/geochemj.2.0311.

Kawagucci, S., Chiba, H., Ishibashi, J., Yamanaka, T., Toki, T., Muramatsu, Y., Ueno, Y., Makabe, A., Inoue, K., Yoshida, N., Nakagawa, S., Nunoura, N., Takai, K., Takahata, N., Sano, Y., Narita, T., Teranishi, G., Obata, H., and Gamo, T., 2011. Hydrothermal fluid geochemistry at the Iheya North field in the mid-Okinawa Trough: Implication for origin of methane in subseafloor fluid circulation systems. Geochem. J., 45, 109-124.

Kawagucci, S., Ueno, Y., Takai, K., Toki, T., Ito, M., Inoue, K., Makabe, A., Yoshida, N., Muramatsu, Y., Takahata, N., Sano, Y., Narita, T., Teranishi, G., Obata, H., Nakagawa, S., Nunoura, T., and Gamo, T., 2013a. Geochemical origin of hydrothermal fluid methane in sediment-associated fields and its relevance with the geographical distribution of whole hydrothermal circulation. Chem. Geol., 339, 213-225.

Kawagucci, S., Miyazaki, J., Nakajima, R., Nozaki, T., Takaya, Y., Kato, Y., Shibuya, T., Konno, U., Nakaguchi, Y., Hatada, K., Hirayama, H., Fujikura, K., Furushima, Y.,

Yamamoto, H., Watsuji, T., Ishibashi, J., and Takai, K., 2013b. Post‐drilling changes in fluid discharge pattern, mineral deposition, and fluid chemistry in the Iheya North hydrothermal field, Okinawa Trough. Geochem. Geophys. Geosyst., 14, 4774-4790.

Kinoshita, M., 1995. Localized heat flow anomalies in the midlle Okinaw Trough associated with hydrothermal circulation. *In* Sakai, H., Nozaki, Y. (Eds), Biogeochemical processes and ocean flux in the western Pacific, Tokyo, TerraPub, 537-559.

Konno, U., Tsunogai, U., Nakagawa, F., Nakaseama, N., Ishibashi, J., Nunoura, T., and Nakamura, K., 2006. Liquid CO_2 venting on the seafloor: Yonaguni Knoll IV hydrothermal system, Okinawa Trough. Geophys. Res. Lett., 33:L16607, doi:10.1029/2006GL026115.

Kumagai, H., Tsukioka, S., Yamamoto, H., Tsuji, T., Shitashima, K., Asada, M., Yamamoto, F., and Kinoshita, M., 2010. Hydrothermal plumes imaged by high-resolution side-scan sonar on a cruising AUV, Urashima. Geochem. Geophys. Geosyst., 11, Q12013.

Nakagawa, S., Takai, K., Inagaki, F., Chiba, H., Ishibashi, J., Kataoka, S., Hirayama, H., Nunoura, T., Horikoshi, K., and Sako, Y., 2005. Variability in microbial community and venting chemistry in a sediment-hosted backarc hydrothermal system: impacts of subseafloor phase-separation. FEMS Microbiol. Ecol., 54(1):141–155. doi:10.1016/j.femsec.2005.03.007.

Nakamura, K., Toki, T., Mochizuki, N., Asada, M., Ishibashi, J., Nogi, Y., Yoshikawa, S., Miyazaki, J., and Okino, K., 2012. Discovery of a new hydrothermal vent based on an underwater, high-resolution geophysical survey. Deep-Sea Res. Part I, 74, 1-10.

Nunoura, T., and Takai, K. 2009. Comparison of microbial communities associated with phase-separation-induced hydrothermal£uids at the Yonaguni Knoll IV hydrothermal field, the Southern Okinawa Trough. FEMS Microbiol. Ecol., 67:351-370.

Nunoura, T., Oida, H., Nakaseama, M., Kosaka, A, Ohkubo, S, Kikuchi, T., Kazama, H., Tanabe, S. H., Nakamura, K., Kinoshita, M., Hirayama, H, Inagaki, F., Tsunogai, U., Ishibashi, J., and Takai, K., 2010. Archaeal diversity and distribution along thermal and geochemical gradients in hydrothermal sediments at the Yonaguni Knoll IV, the Southern Okinawa Trough. Appl. Environ. Microbiol., 76:1198-1211.

Sakai, H., Gamo, T., Kim, E.S., Shitashima, K., Yanagisawa, F., Tsutsumi, M., Ishibashi, J., Sano, Y., Wakita, H., Tanaka, T., Matsumoto, T., Naganuma, T., and Mitsuzawa, K., 1990. Unique chemistry of the hydrothermal solution in the Mid-Okinawa Trough Backarc Basin. Geophys. Res. Lett., 17:2133-2136.

Takai, K., Mottl, M. J., Nielsen, S. H., and the Expedition 331 Scientists, 2011. Proceedings of IODP, 331: Tokyo (Integrated Ocean Drilling Program Management International, Inc.). doi:10.2204/iodp.proc.331.2011.

Takai, K., Mottl, M. J., Nielson, S. H. H., and the IODP Expedition 331 Scientists, 2012. IODP Expedition 331 finds enormous hydrothermally altered lithostratigraphy comparable to typical Kuroko deposits and chemically stratified hydrothermal fluid reservoir, and points to possible existence of functionally active microbial communities beneath the Iheya North hydrothermal system, the Okinawa Trough. Scientific Drilling, 13, 19-27.

Tsuji, T., Takai, K., Oiwane, H., Nakamura, Y., Masaki, Y., Kumagai, H., Kinoshita, K., Yamamoto, F., Okano, T., and Kuramoto, S., 2012. Hydrothermal fluid flow system around the Iheya North Knoll in the mid-Okinawa Trough based on seismic reflection data. J. Volcanol. Geotherm. Res., 213-214, 41-50.

Yanagawa, K., Nunoura, T., McAllister, S., Hirai, M., Breuker, A., Brandt, L., House, C., Moyer, C. L., Birrien, J.-L., Aoike, K., Sunamura, M., Urabe, T., Mottl, M., and Takai, K., 2013. The first microbiological contamination assessment by deep-sea drilling and coring by the D/V Chikyu at the Iheya North hydrothermal field in the Mid-Okinawa Trough (IODP Expedition 331). Frontier Microbiol., 4, doi: 10.3389/fmicb.2013.00327.

Yanagawa, K., Breuker, A., Schippers, A., Nishizawa, M., Ijiri, A., Hirai, M., Takaki, Y., Sunamura, M., Urabe, T., Nunoura, T., and Takai, K. 2014. Microbial community stratification controlled by the subseafloor fluid flow and geothermal gradient at the Iheya North hydrothermal field in the Mid-Okinawa Trough (IODP Expedition 331). Appl. Environ. Microbiol., in press.

You, C.F., Butterfield, D.A., Spivack, A.J., Gieskes, J.M., Gamo, T., and Campbell, A. J., 1994. Boron and halide systematics in submarine hydrothermal systems - effects of phase-separation and sedimentary contributions. Earth Planet. Sci. Lett., 123:227-238.

1.2. Geological settings and backgrounds

H.Kumagai

As one of the prominent findings at IODP Exp. 331 “Deep-hot biosphere,” a km-wide fluid reservoir may extend beneath Iheya-North Knoll (Takai et al., 2011). This implication was mainly derived from unexpected discharge of hydrothermal fluid If such a reservoir extends beneath to the newly located two hydrothermal sites, their spatial scale exceeds a few kilometer in length, which corresponds to the scale of Kuroko-type VMS deposit on land. If it is the case, the spatial discrepancy between land and submarine sulfide deposits may be resolved.

The Okinawa Trough is a seafloor depression extending southwestward from Kyushu Island, southwest Japan, of which fore-arc is a Islands of Ryukyus (Figure 2-1). There are two models of its evolutional history. One model argues that its rifting started at the southern part and propagated northeastward (e.g. Glasby and Notsu, 2003). Another model argues that its rifting started its middle part and propagated both north and southward. These models are to be investigated by further geological and geochronological studies. In either model, the Okinawa Trough is regarded to be in an initial rifting stage prior to the normal/stable seafloor spreading as a main stage of back arc basin formation (e.g. Glasby and Notsu, 2003). In a framework of arc-backarc volcanism, the present day’s volcanic front is at the eastern edge of Okinawa Trough although exact position is still under arguments especially in the southern extension from Tokara Islands. Recently, new model has been proposed: the volcanic front in Okinawa Trough passes upon Izena-Hole (Yokose et al., 2014). This new model seems to be consistent with the recent discovery rush of active hydrothermal field lining on the NE-SW trending centered by Izena-Hole (see. Press-releases by JCG and AIST).

The Iheya-North Knoll is a volcanic complex located near the Eurasian continental slope on the flat basin forming middle part of Okinawa Trough (Figure 2-2). It has two peak points; those altitudes are almost similar, shallower than 800mWD at 126°55.7’E, 27°46.3N, 126°56.1’E, 27°48.0’N, respectively. These peaks are on respective N-S or W-E trending ridge formed as small domy volcanic features (ca. ~100 in diameters), sometimes associating with small craters on the top. Such morphological feature suggests that its magmatic activity is mainly siliceous. In fact, siliceous pumices were widely observed and retrieved in the shallow lithological units on the top of knoll (Oiwane et al., 2008). Some of the pumiceous layers showed graded bedding for upward in the piston-cored samples in the pre-drilling survey by JAMSTEC (Kinoshita et al., 2008). A relatively fresh banded pumice was sampled at the site of KY08-01

HFPC-23, which suggests that the recent volcanic activity of the Knoll (KY08-01 Leg.3 Cruise Report). The sedimentary fills were also widely found in local topographic lows even on the top of the knoll.

References

Glasby G.P, and Notsu K (2003) Submarine hydrothermal mineralization in the Okinawa Trough, SW of Japan: an overview. Ore Geol Rev, 23, 299–339.

Kinoshita, M., Y. Masaki, H. Kumagai, H. Oiwane, H. Hamamoto, and K.-S. s. party (2008), Hydrothermal system beneath Iheya-north hydrothermal site, mid-Okinawa Trough - Preliminbary results from KY8-01 cruise-, in *Japan Geosciences Union Meeting 2008*, Chiba, http://www2.jpgu.org/meeting/2008/program/pdf/J164/J164-005_e.pdf.

Momma, H., R. Iwase, K. Mitsuzawa, Y. Kaiho, Y. Fujiwara, Y. Amitani, and M. Aoki (1996), Deep tow survey in nanseisyoto Region (K95-07-NSS), *Jamstec J. Deepsea Research*, *12*, 195-210.

Oiwane, H., H. Kumagai, Y. Masaki, H. Tokuyama, M. Kinoshita, and K.-S. s. party (2008), Characteristics of Sediment in Iheya North Knoll and the acoustic blanking layer, paper presented at Japan Geosciences Union Meeting 2008, Chiba, http://www2.jpgu.org/meeting/2008/program/pdf/J164/J164-P013_e.pdf.

Takai, K., Mottl, M. J., Nielsen, S. H., and the Expedition 331 Scientists, 2011. Proceedings of IODP, 331: Tokyo (Integrated Ocean Drilling Program Management International, Inc.). doi:10.2204/iodp.proc.331.2011.

Yokose, H., J.-i. Ishibashi, Y. Sano, and S.-M. K. L. s. s. party (2014), Active submarine volcanoes of the Tokara Islands: new tools to explore seafloor hydrothermal vent systems in *Annual meeting Volcanological Society of Japan 2014* edited by Volcanological Society of Japan, Volcanological Society of Japan, Fukuoka.

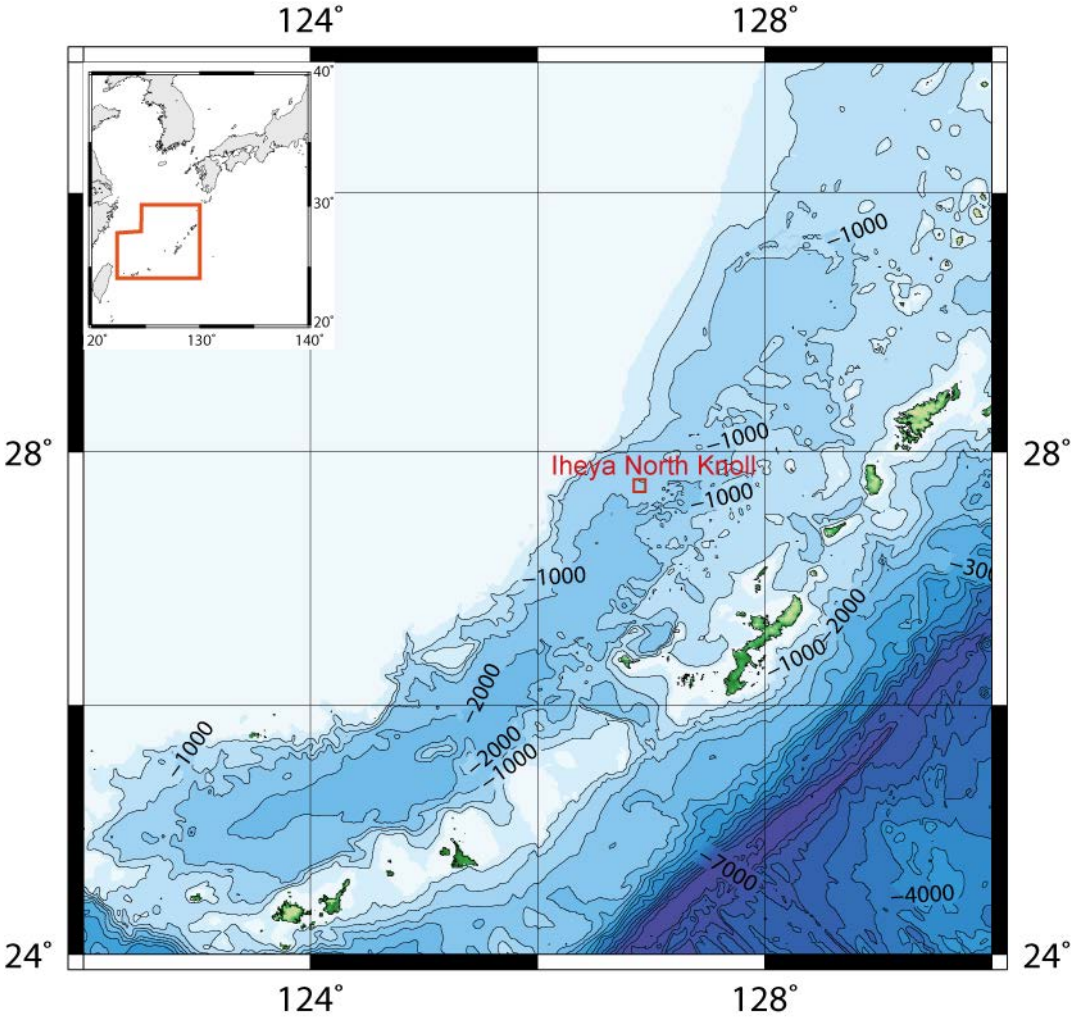

Figure 1-2-1: Topographic Map of Okinawa Trough. Iheya North Knoll is at an area indicated small red rectangular in main panel, of which area is magnified in Figure 1-2-2.

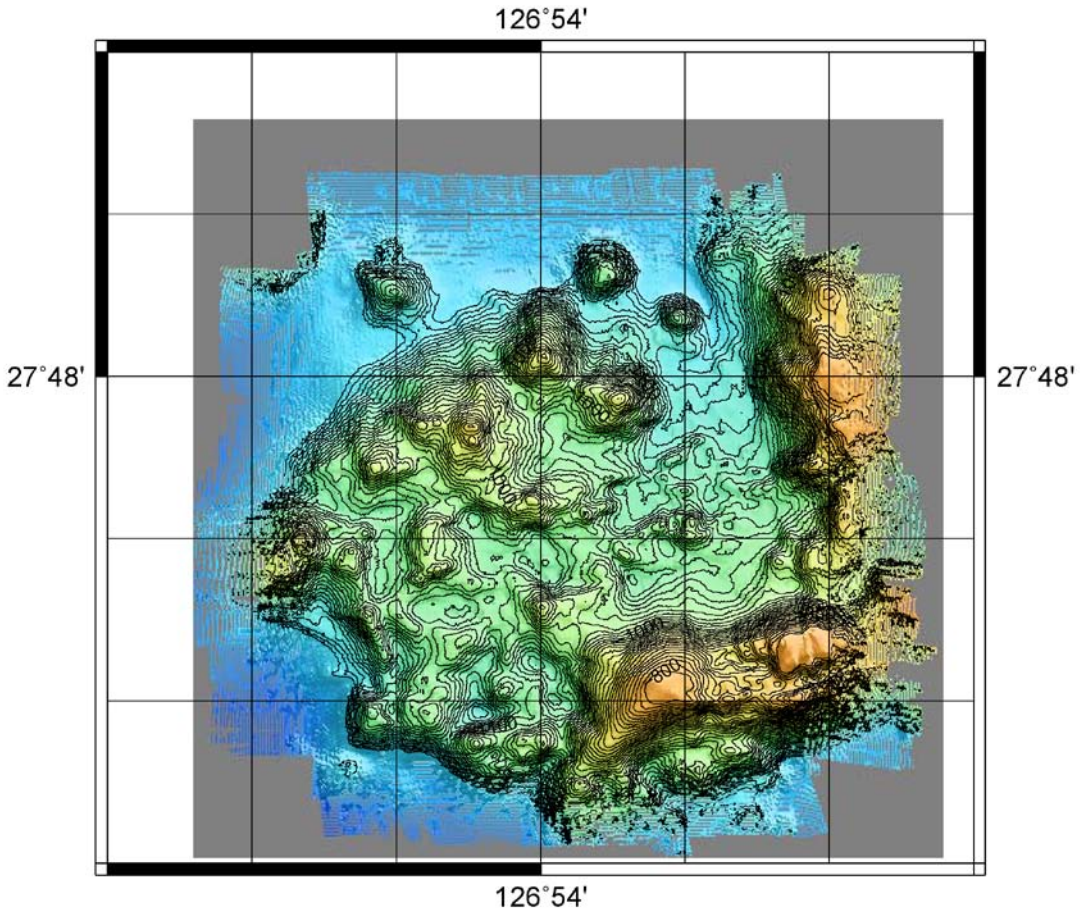

Figure 1-2-2: bathymetric map of Iheya North Knoll. Data were taken by R/V "Natsushima" at NT13-22 cruise.

1.3. Site Survey

H.Kumagai

A grid of multichannel seismic (MCS) and single-channel seismic (SCS) profiles has been completed for the Iheya North Knoll region prior to the IODP Exp.331 (Figure 1-3-1; Takai et al., 2011). The seismic profiles of the area reveal that numbers of patchy inversely polarized reflectors widely existed beneath the Iheya North Knoll (Figure 1-3-2). Such reflectors indicate that sharp and significant decrease of the acoustic impedance at the depth. Within some possible lithological conditions resulting such reflectors, formation fluids at the depth creates most clear ones because both density and sound velocity dramatically decreases at the top boundary. If it is the case, the inversely polarized reflectors may provide a good criterion to recognize or locate the distribution of hydrothermal reservoir. This is one of the targets to be investigated in this expedition.

The detailed bathymetry taken by the AUV Urashima mostly covers over the studied area of Iheya North Knoll of much better than 1 m resolution: SeaBat7126 Multi-Beam Echo Sounder (MBES, Figures 1-3-3, 1-3-4 and 1-3-5). Outside of the coverage of the Urashima MBES, bathymetric data taken by a ship-hulled MBES of R/V Natsushima also covers better than 2 m resolution. Using these ultra high resolution bathymetries, detailed distribution of hydrothermal mounds is well mapped even in the newly recognized two hydrothermal fields.

Iheya North (Original) Site

The Iheya North (Original) Site was found in 1995 by a deep-tow survey (Momma et al., 1996). Its vents and mounds were located in elongated area trending NNW-SSE including approximately 10 active vents or mounds on eastern frank of one of the peak of the knoll between 960-1000m WD. Although the entire distribution is on the area, however, active and inactive vents align NNE-SSW locally (Figure 3-3).

Iheya North Natsu Site

This site was newly found in January 2014 by a suite of MBES survey and ROV dives. One very limited sea-floor survey of ROV were conducted, however, an active chimney and several dead chimneys were located (Figure 1-3-4). This site is in a small depression at the almost the center of the knoll where sediment covers significantly.

Iheya North Aki Site

This site was also newly found in January 2014 by a suite of MBES survey and ROV dives. Rather limited two-day sea-floor survey of ROV was available; however, numerous active and dead chimneys, benthic colonies, bacterial mats, and crusts of native sulfur were well located (Figure 1-3-5). In comparison with the other two sites, this Aki-site is the largest hydrothermal field on Iheya North Knoll. This site also develops in a small depression near the edge the knoll where sediment covers significantly.

References

Momma, H., R. Iwase, K. Mitsuzawa, Y. Kaiho, Y. Fujiwara, Y. Amitani, and M. Aoki (1996), Deep tow survey in nanseisyoto Region (K95-07-NSS), *Jamstec J. Deepsea Research*, *12*, 195-210.

Takai, K., Mottl, M. J., Nielsen, S. H., and the Expedition 331 Scientists, 2011. Proceedings of IODP, 331: Tokyo (Integrated Ocean Drilling Program Management International, Inc.). doi:10.2204/iodp.proc.331.2011.

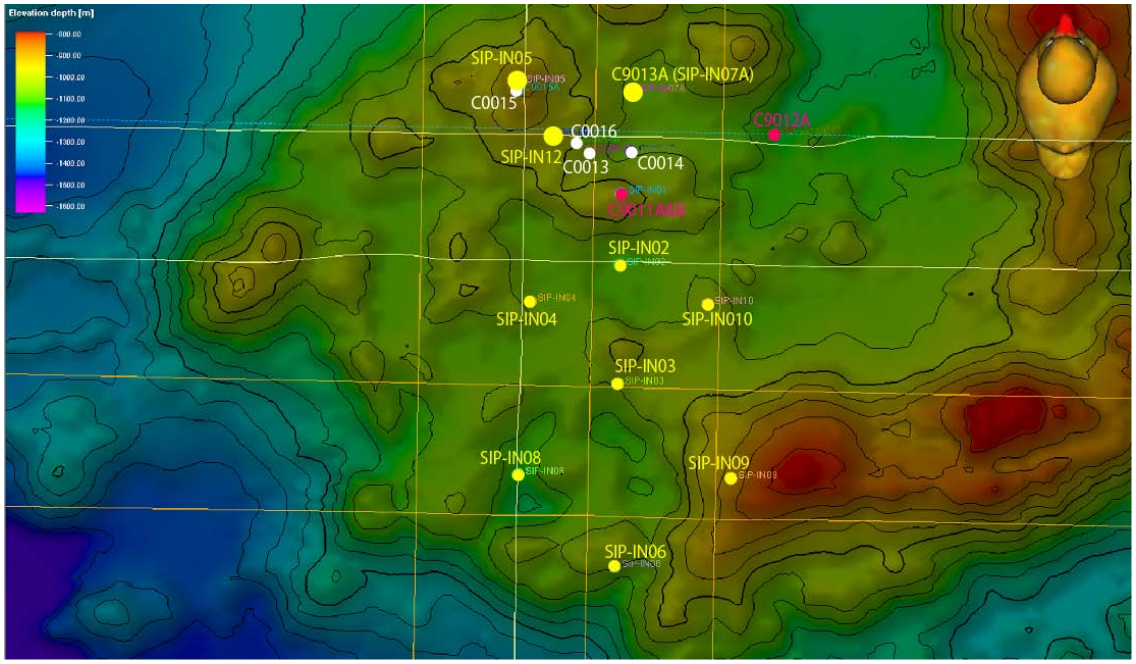

Figure 1-3-1 : Pre-survey grid on Iheya-North Knoll prior to IODP Exp. 331 and proposed sites in this expedition (Exp. 907) with the positions of IODP holes (filled white circles).

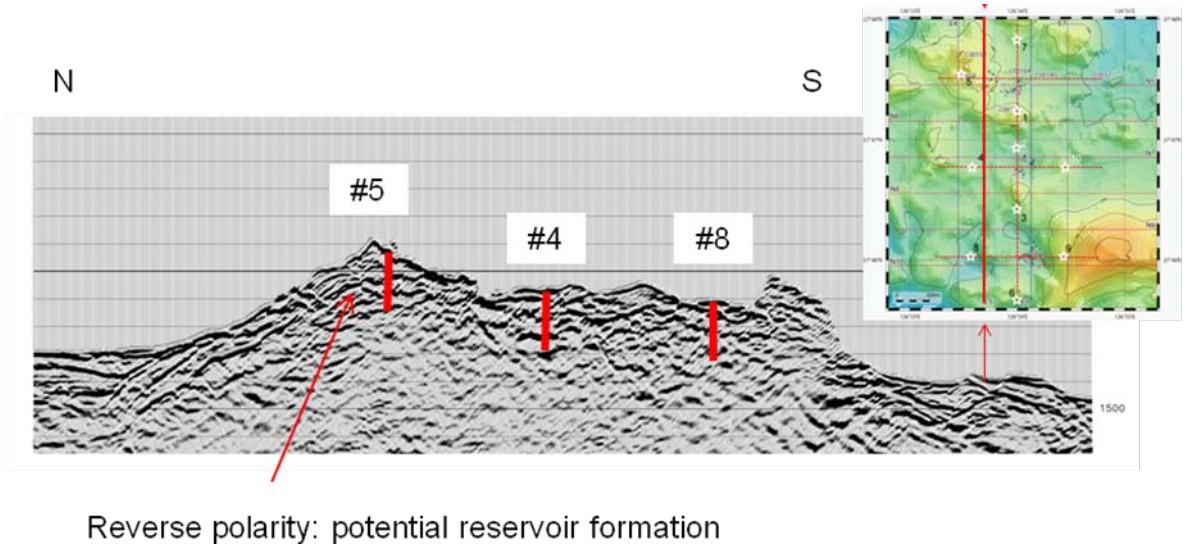

Figure 1-3-2 : An example of seismic reflection survey of which position is shown as red line in the inset. Below the summits of the knoll, some reflectors with reverse polarity were widely recognized (courtesy by K. Aoike).

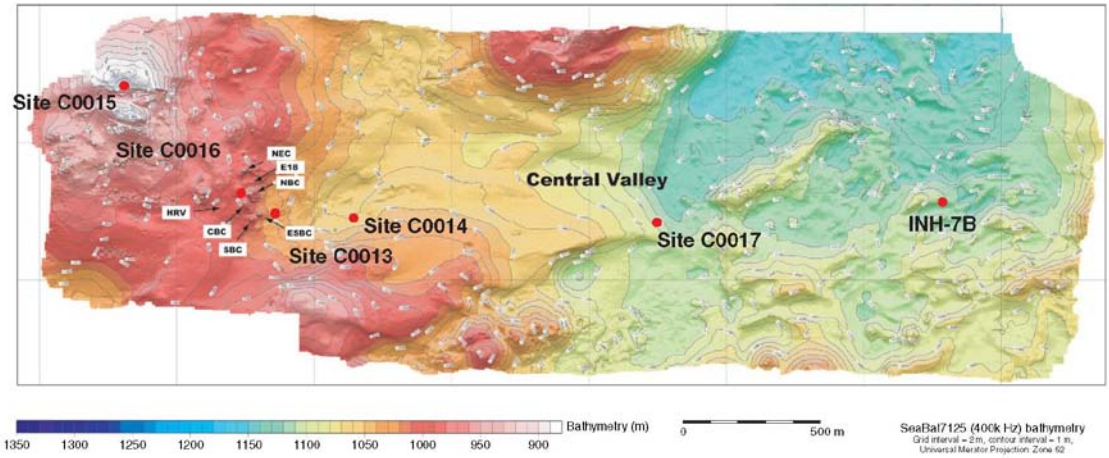

Figure 1-3-3 : Detailed bathymetric map of Iheya-North Original Site (Takai et al., 2011). Data were taken by AUV Urashima, YK07-07.

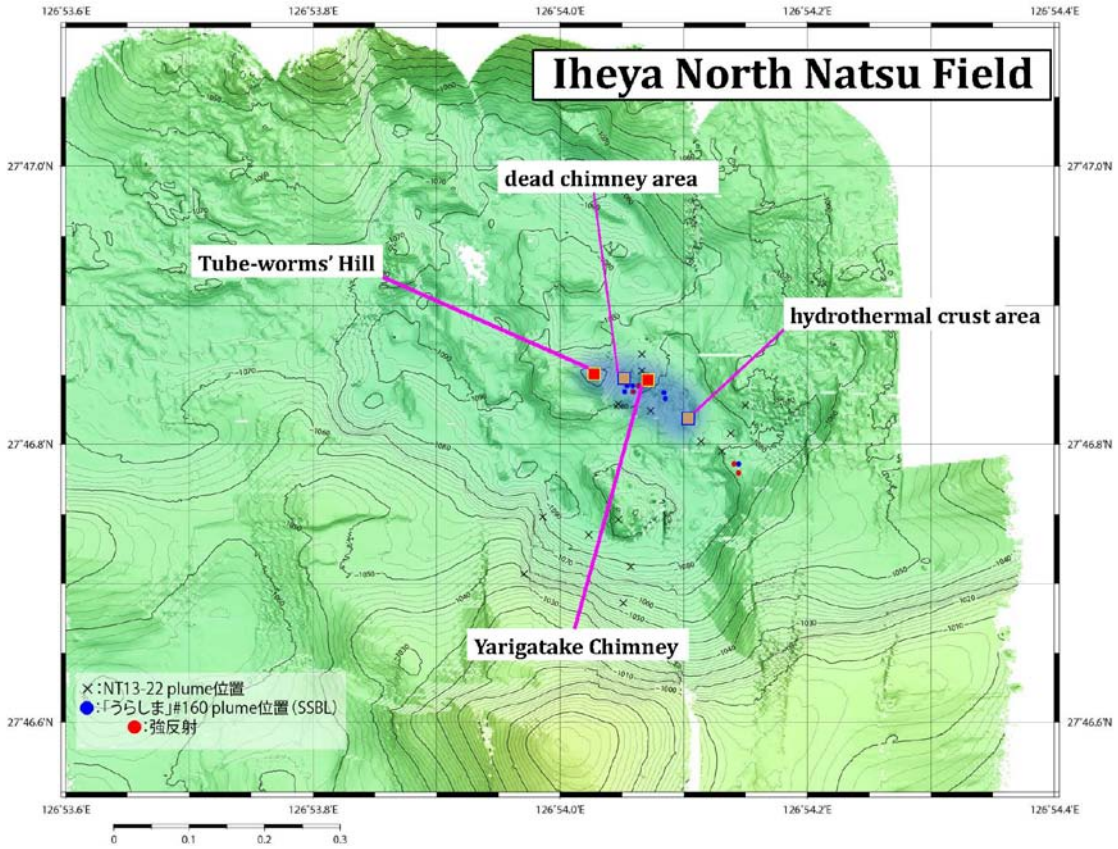

Figure 1-3-4: Detailed bathymetric of Iheya-North Natsu-site. Data were taken by AUV Urashima, YK13-14.

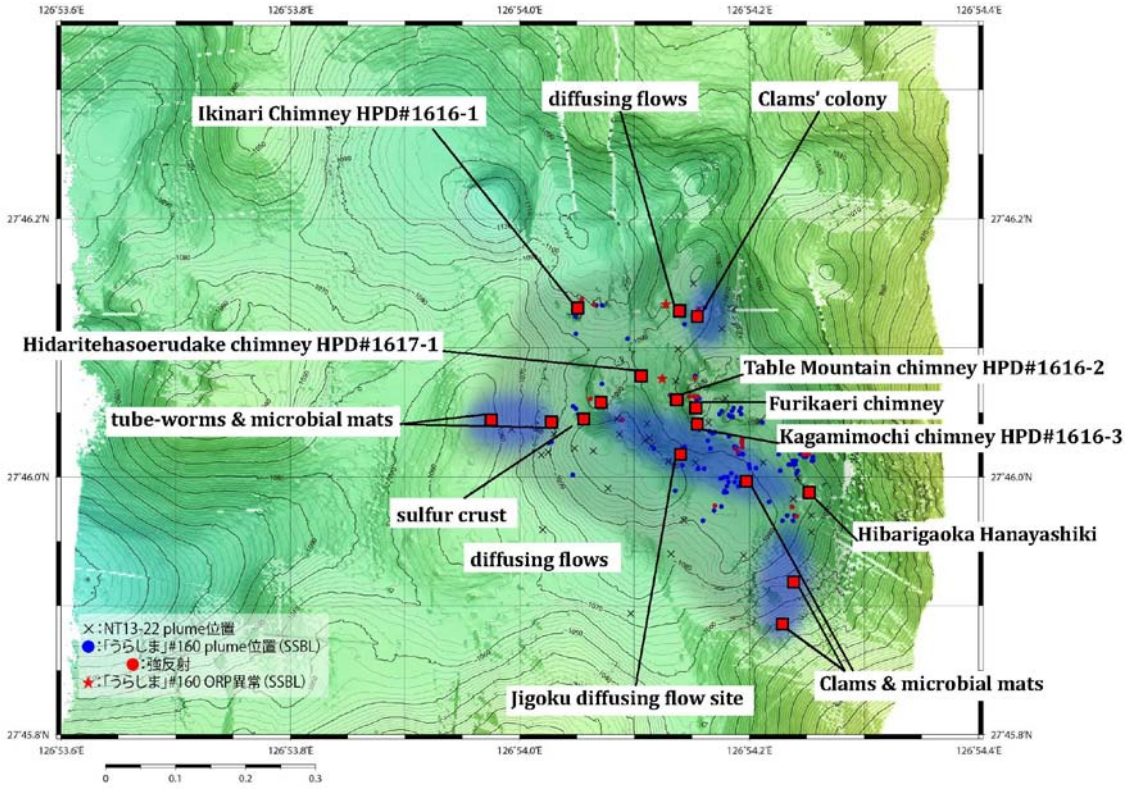

Figure 1-3-5: Detailed bathymetric of Iheya-North Aki-site. Data were taken by AUV Urashima, YK13-14.

1.4. Drilling Strategy

H.Kumagai

We drilled six sites during CK14-04: five were in/around Iheya-North original site (C9011-9015); one was in Iheya-North Aki site (C9016; Figure 1-4-1). The aims of the drilling were,

1) Locate the areas of hydrothermal fluid reservoir beneath the Iheya-North Knoll,
2) Investigate association between hydrothermal mineralization and fluid reservoir,
3) Form additional artificial vent by penetration to reservoir.

Concerning for the very poor core-recovery as in the case of IODP Exp.331, we prioritize a logging-while drilling operation (LWD-operation) than sample coring, especially to solve item 2).

At Site C9011 was chosen at the top of the hill colonized by tube warm, which indicate simmering of hydrothermal fluid. A complete penetration to westward extension from the located fluid reservoir during IODP Exp.331, Site C9012 was set very vicinity of C0017 of IODP. The deepest penetration at Site C0017 was 144.73 mbsf where further temperature increase anticipated, eventually reaching the discharged hydrothermal fluid temperature. Regardless of the anticipation of formation artificial vent by penetrating through the hydrothermal reservoir, preceding two cites, no clear discharges of the hydrothermal fluid at the polling out of the drill strings. Then, on-board science party estimated that rather low excess fluid pressure at the edge of the fluid reservoir. According to the result of these two site, C9013 was adjusted to much vicinity of the transect of IODP consisted by the holes discharging hydrothermal fluid after the drilling end. Alternatively, C9014 was planned to the top of local topographic high that seems to be a recent center of magmatic activity at the vicinity of C0015. Even such 4 holes were chosen carefully, they could not provide clear discharges of hydrothermal fluids neither during nor after the drilling. Thus, the final hole in the "original" site, C9015A, was set at the foot of an active mound where very high radioactivity was recorded in 1998, 1000th dive of Shinkai2000 (Okano unpublished data).

Above described five sites were in and around well-known Iheya-North original site, the final site was chosen at the center of a newly discovered hydrothermal site, Ihyea-North Aki site. C9016 was set between the two active mounds in Aki Field.

Regardless of these adjustment, still obvious discharge of hydrothermal fluid

was not observed, the scientific party tried to recover the massive sulphide in order to obtain physical properties of ore blocks; especially electric conductivity and p-wave velocities were desired by geophysical exploration technique. For this purpose, three holes, one at the Site 9016 (Hole C9016B), two at the Site 9015 (Holes C9015B and C) were drilled.

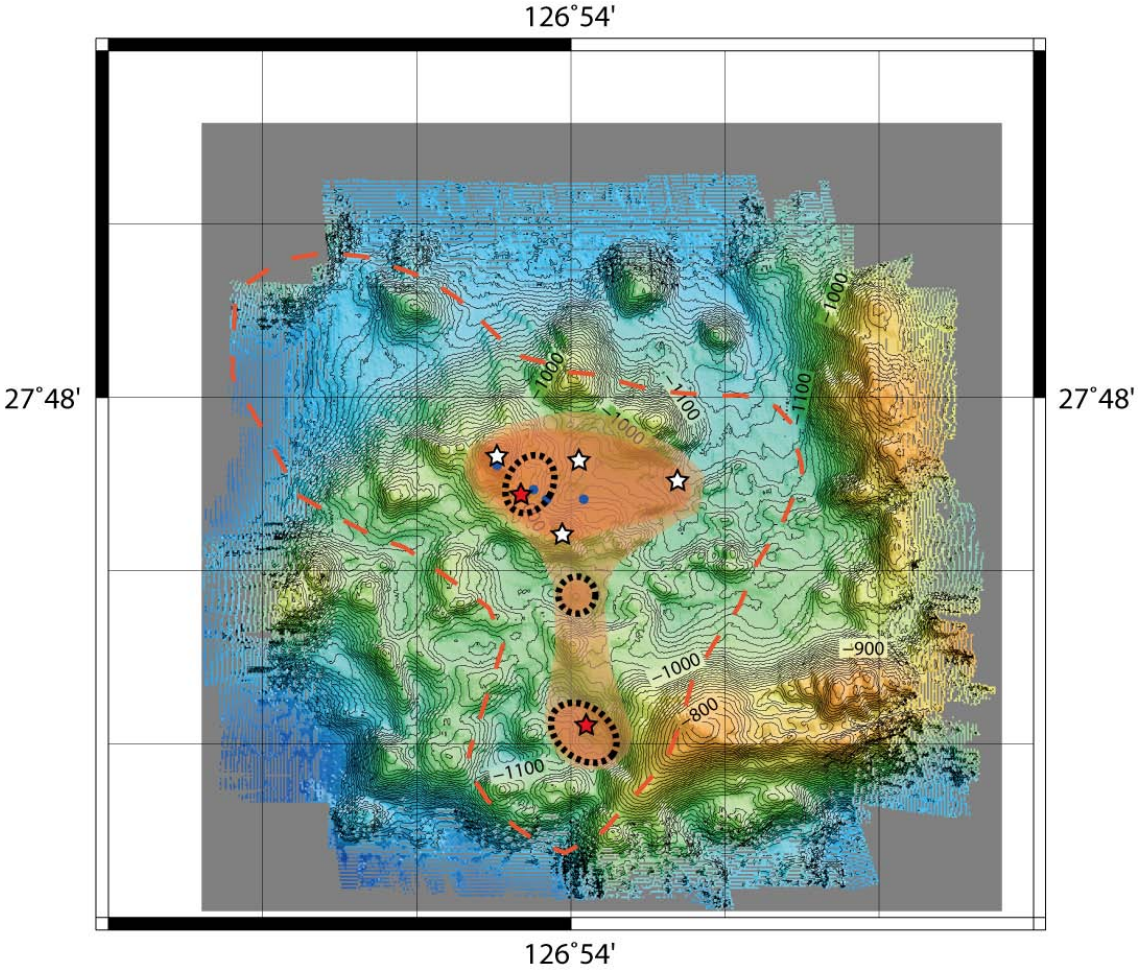

Figure 1-4-1: Location of drilled sites during CK14-04(Exp.907) and IODP Exp.331. Open star: LWD site at CK14-04. Red filled star: LWD site followed by coring. Blue dot: coring site at Exp.331. Broken circles: active vent area. Shaded area: estimated area of fluid reservoir beneath seafloor. Thin red-broken line: potential area of fluid reservoir beneath seafloor.

Chapter 2. Logging-while-drilling/Downhole Measurements

2.1 Tools description of LWD

K. Moe, S. Saito, Y. Sanada and Y. Kido

Logging while drilling (LWD) tools are supplemented by a measurement-while-drilling (MWD) tool that is located above of the LWD tools in the Bottom-hole-assembly (BHA) and measures downhole drilling parameters and well bore direction. The MWD tool also transmits a limited LWD data set by mud pulse telemetry to the surface for realtime monitoring. Complete LWD data are recorded into downhole computer memory and retrieved when the tools are brought to the surface. LWD tools are usually powered by batteries or a drilling fluid turbine in MWD. But, we did not use litium batteries for safety reason in this cruise, because high temperature is expected. The tools take measurements at regular time intervals and are synchronized with an acquisition system on the drilling rig that matches time with drilling depth. Drilling depth is determined using a drawworks encoder that measures the vertical motion of the top drive. After drilling, the LWD tools are retrieved and their data downloaded. The Schlumberger Maxwell logging system merges time and depth data (from the surface system) and the downhole time-measurement data (from the tools) into depth-measurement data files. Data files are then transferred to onboard log data processing and analysis team led by the logging staff scientists (LSS) for further processing using the Schlumberger's TechLog software and then passed to the hands of logging scientists for further interpretation. Expedition logging scientists tied these logs to core measurements and seismic data to help define lithofacies, structure, and physical properties (Expedition 314 Scientists, 2009a; Expedition 338 Scientists, 2013). LWD and MWD data acquisition was conducted under contract by Schlumberger Drilling and Measurements Services.

The LWD and MWD tools used in this expedition were Schlumberger's arcVISION 675 with Annular Pressure Whole Drilling (APWD) (annular borehole temperature and pressure, resistivity, and NGR [natural gamma-ray]), and the MWD TeleScope 675 with APWD (annular borehole temperature and pressure, drilling mechanics data and real-time telemetry). All of these tools had a 6¾ inch (17.1 cm) diameter and were located above an 8½ inch (21.6 cm) drill bit. BHA had stabilizers to

centralize the collars and keep measurement sensors near the borehole wall. **Figure 2-1** shows the configuration of the LWD BHA, with the depth of the measurements relative to the bit, and **Table 2-1** list the parameters of principal measurements recorded by each tool.

The measurement principles of these LWD tools are described below. LWD and MWD data were obtained to provide a wide range of in situ measurements and drilling parameters, including gamma ray, electromagnetic propagation resistivity, annular pressure and temperature. The advantage of LWD/MWD over wire line logging is that measurements are taken soon after the borehole is drilled, thus minimizing the effects of disturbance and invasion of drilling mud into the formation. As target of this expedition is hydrothermal formations, LWD-MWD is only measurement can do while drilling under continuous circulation using non-stop driller (NSD) system. TeleScope and arcVISION were modified for 175degC temperature proof from 150 deg_C standard. Key measurement, temperature from APWD is taken by two sensors from arcVISION and TeleScope from different positions. Combining these measurements with surface drilling parameters allows for improved real-time monitoring of drilling progress and assessment of data quality.

arcVISION tool

The arcVISION tool (array resistivity compensated) measures propagation resistivities. Electromagnetic waves are attenuated and phase-shifted when they propagate in an electrically conductive medium, and the degree of attenuation and phase shift depends on the resistivity of the formation (Bonner et al., 1995, 1996). Phase-shift resistivity has relatively high vertical resolution and a shallow depth of investigation, whereas attenuation resistivity has lower vertical resolution and a greater depth of investigation. The dual-frequency (2 MHz and 400 kHz) array of coils in the arcVISION makes 10 phase-shift and 10 attenuation measurements at five transmitter-receiver separations of 16, 22, 28, 34, and 40 inches (40.6, 55.9, 71.1, 86.4, and 101.6 cm), which correspond to several depths of investigation. The measurement range, accuracy, depth of investigation, are vertical resolution are shown in **Table 2-2, 3, and 4**, respectively. The arcVISION also measures the NGR of the formation.

TeleScope tool

The TeleScope MWD tool transmits data uphole through the fluid in the drill pipe in a

process known as “mud-pulse telemetry.” A modulator in the tool generates a continuous 12 Hz pressure wave within the drilling fluid and changes the phase of this signal to transmit bit words encoding various measurements made by the MWD tool or by other LWD tools in the BHA. Three pressure transducers attached to the standpipe. The first on at the active standpipe, the second is at the manihold next to the junction box, and the third is at the horizontal mud line on the rig floor to acquire the pressure signal that is then decoded by the Schlumberger surface software. (2 sensors are standard when without NSD). The MWD real-time data transmission rate is adjustable, depending primarily on water depth and drilling fluid density, and was 3 bits/s during Expedition 907.

In addition to transmitting uphole, selected measurements from the other LWD tools, the TeleScope acquires operational and drilling mechanics data, including collar rotation per minute, drilling fluid turbine rotation per minute, stick and slip, and axial and torsional vibration. The TeleScope also contains a turbine that powers the entire LWD string when drilling fluid is circulated at a sufficient flow rate (~400-750 gal/min, or 25.2-47.3 L/s, in the TeleScope tool used during Expedition 907).

APWD

APWD can be mounted in TeleScope and arcVISION. APWD measures temperature and pressure of the borehole fluid in the annulus (the space between the drill string and the borehole wall). Annular pressure data were used to calculate the equivalent circulating density (ECD), which is the density of the drilling fluid during pumping. Changes in downhole pressure can reveal flow from or into the formation. Such pressure changes and flows are related to formation pressure and permeability and may indicate the presence of fractures. Measurement specifications of APWD is shown in **Table 2-5**.

2.2 Preliminary data description of LWD

K. Moe, S. Saito, Y. Sanada and Y. Kido

2.2.1 Site C9011

Logging data quality control

Data quality control was performed by monitoring real time data, short repeat log, during data processing, and final processed data. LSS and logging scientists assessed real time drilling parameters and data from the downhole tools in terms of realistic values for the lithology of drilling interval. Mud line was confirmed by Gamma Ray curve at 979.0 mBRT. The overall quality of the processed logging data was good. We could not observe temperature anomaly in both arcVISION and TeleScope sensors which showed less than 20 degC constant. Temperature profile by TeleScope is almost flat and lower value than arcVISION. Both sensors are completely the same specification. Small temperature and pressue anomalis are observed when the pipe connection (**Fig 2-2**). Gamma Ray and Resistivity curves seemed in good response to lithological unit. Good repeatability was observed in the repeat session.

Log characterization

Hole C9011B logging units were characterized from visual inspection of gamma ray and resistivity log responses (**Fig 2-3**). Three logging units were defined based on variations in trend lines and log character (**Table 2-6**).

Logging Unit I (0–103.3 mbsf)

Gamma ray log exhibits variable values (30-70 gAPI) from mudline to 19 mbsf, then gradual increase (35-70 gAPI) with a sharp gamma ray spike up to 150 gAPI at 79 mbsf. Resistivity log shows gradual increase (~0.3 to 1 Ωm) at the upper interval (0-50 mbsf), decrease (~1 to 0.15 Ωm), then maintain lower values around 0.1 Ωm at the lower interval (83-103 mbsf).

Logging Unit II (103.3-172 mbsf)

Gamma ray log exhibits gradual decrease from 150 to 50 gAPI. Resistivity log shows variable values between ~0.2 and 3. Gamma ray and resistivity logs indicate similar response in this unit.

Logging Unit III (172 mbsf -TD)

Gamma ray log exhibits higher values from 100 to 190 gAPI. Resistivity log maintains constant value around ~0.8 Ωm.

Temperature and pressure

A baseline of the Annular temperature measured by ArcVISION increased with depth from 12°C at the mudline to 17°C (TD). A minor temperature anomaly (18°C) was measured at 83-87 mbsf. No significant annular temperature anomalies were measured by Telescope.

2.2.2 Site C9012

Logging data quality control

Data quality control was performed by monitoring real time data, short repeat log, during data processing, and final processed data. LSS and logging scientists assessed real time drilling parameters and data from the downhole tools in terms of realistic values for the lithology of drilling interval. Mud line was confirmed by Gamma Ray curve at 1160.5 mBRT. Gamma Ray and Resistivity curves matched well with some cyclic swells with GR range of 0-100 GAPI and Resistivity range of 0.1 – 10 ohm.m. Temperature anomaly observed at 1388.0 mBRT (227.5 mbsf) to maximum 84 degC recorded by arcVISION, 18 degC by TeleScope APWD sensors. Small temperature and pressure anomalies are observed when the pipe connection (**Fig 2-4**). APWD temperature at this time is much lower than estimation curve by APCT3 obtained Exp.331. Temperature anomaly could not observe by repeat session. Other LWD data repeatability was observed.

Log characterization

Hole C9012A logging units were characterized from visual inspection of gamma ray and resistivity log responses (**Fig 2-5**). Six logging units were defined based on variations in trend lines and log character (**Table 2-6**).

Logging Unit I (0–95.5 mbsf)

Logging Unit I exhibits an initial increase in gamma ray up to 75 gAPI from the mudline to 8 mbsf. Then the values maintain a constant baseline around 30 gAPI with local high peaks up to 80 gAPI. Resistivity log shows a constant baseline around 0.8 ohm-m with minor fluctuations. The resistivity log shows two sharp excursions at 8 mbsf (5 ohm-m) and 36 mbsf (3 ohm-m).

Logging Unit II (95.5-201.3 mbsf)

Gamma Ray log displays a high gamma ray interval (70-100 gAPI) at 95.5 to 128 mbsf. Then the gamma ray baseline gradually decreases from 50 to 30 gAPI. Resistivity values are highly fluctuated between 0.5 and 9 ohm-m in the interval 105-143 mbsf. Then the values gradually decrease with depth from 1 to 0.15 ohm-m. A gamma ray excursion (~105 gAPI) locates at 170-173 mbsf corresponding to a resistive spike (1 ohm-m).

Logging Unit III (201.3-270.9 mbsf)

Gamma Ray log displays a high gamma ray interval (70-110 gAPI) at 213 to 222 mbsf. Then the gamma ray baseline maintain a constant trend around 50 gAPI. Resistivity values are highly fluctuated between 0.2 and 8 ohm-m and the values exhibits a gentle increasing baseline with depth. A resistivity excursion (~1 ohm-m) at 214-222 mbsf corresponds to a gamma ray excursion (~110 gAPI). Other resistivity excursions (~8 ohm-m) around 250 mbsf corresponds to a negative gamma ray excursion (~30 gAPI).

Logging Unit IV (270.9 mbsf to TD)

Gamma Ray log displays a high gamma ray interval (70-110 gAPI) at 270 to 280 mbsf. Then the gamma ray baseline maintain a constant trend around 25 gAPI. The gamma ray log displays three spikes at 301 mbsf (~100 gAPI), 307 mbsf (~75 gAPI), and 324 mbsf (~118 gAPI). Resistivity values maintain a constant trend around 0.6 ohm-m.

Temperature and pressure

A baseline of the Annular temperature measured by ArcVISION increased with depth from 7°C (mudilne) to 16°C (TD). A major temperature anomaly up to 84°C was observed in a narrow interval around 234 mbsf. The temperature anomaly started at 233 mbsf (15°C) and ended at 234 mbsf (17°C) (Figure X). The initiation of temperature anomaly was detected when the bit reached to within a resistive layer at ~248 mbsf. A minor anomaly up to 22°C were observed above at ~226 mbsf. A small anomaly of annular temperature (18°C) was measured by Telescop at 230 mbsf.

2.2.3 Site C9013

Logging data quality control

Data quality control was performed by monitoring real time data, short repeat log, during data processing, and final processed data. LSS and logging scientists assessed real time drilling parameters and data from the downhole tools in terms of realistic values for the lithology of drilling interval. Mud line was confirmed by Gamma Ray curve at 1093.5 mBRT. In this site, resistivity in the seawater indicated conductive than general seawater with 0.3 ohm.m constant. They suddenly decreased 0.3 to 0.2 at the mud line. Temperature and pressure anomaly were observed around 1128.5 – 1130.0 mBRT (35.0 – 36.5 mbsf), the reason would be that telemetry signal was disturbed by the drilling break with suddenly ROP down. The other interval of logging data quality was good. Temperature started 5 degC at mud line gradually increasing upto 12 degC at 1111.0 mBRT (8.4 mbsf). There were some temperature anomaly swells from baseline of 11 degC to 12.5 degC at 1113.8 mBRT (20.3 mbsf), upto 16 degC at 1172.2 mBRT (78.7 mbsf) and 1217.5 mBRT (124 mbsf), 15 degC at 1240.8 mBRT (147.3 mbsf),19.3 degC at 1248.5 mBRT (155 mbsf). TeleScope sensor response 10 to 13 degC from baseline 9 to 11 degC following arcVISION sensor with 5 meter sensor offset. Small temperature and pressure anomalies were observed when the pipe connection (**Fig 2-6**).

Log characterization

Hole C9013A logging units were characterized from visual inspection of gamma ray and resistivity log responses (**Fig 2-7**). Three primary logging units were defined based on variations in trend lines and log character (**Table 2-6**).

Logging Unit I (0–48.7 mbsf)

Logging Unit I exhibits an initial increase in gamma ray up to 130 gAPI from the mudline to 12 mbsf. Then the values maintain a constant trend around 75 gAPI with large fluctuation between 50 and 100 gAPI. Resistivity log shows gradual increase from 0.3 to 3 ohm-m. The resistivity log shows a sharp negative excursion (~0.4 ohm-m) at the base of the unit.

Logging Unit II (48.7-88.8 mbsf)

Gamma ray log displays a gradual decreasing trend with large fluctuation between 30 and 190 gAPI. Resistivity log also displays a gradual decreasing trend with large fluctuation between 0.3 and 6 ohm-m. Gamma ray and resistivity logs exhibit positive correlation throughout the unit.

Logging Unit III (88.8-131.7 mbsf)

Gamma ray log exhibits a constant trend around 70 gAPI. Resistivity log exhibits a very low value around 0.2-0.3 ohm-m. A resistive spike (5 ohm-m) occurred at 102 mbsf, corresponding to a minor gamma ray spike.

Logging Unit IV (131.7 mbsf to TD)

Gamma ray log shows variable value between 15 and 145 gAPI. Resistivity values also large variation between 0.3 to 4 ohm-m.

Temperature and pressure

A baseline of the annular temperature measured by ArcVISION increased with depth from 7°C (mudilne) to 11°C (2 mbsf), maintained a constant baseline at 11°C, and variable between 12 and 15°C to the bottom of the hole. Minor temperature anomalies were observed at 78 mbsf (16°C), 124 mbsf (16°C), and 155 mbsf (19°C).

2.2.4 **Site C9014**

Logging data quality control

Data quality control was performed by monitoring real time data, short repeat log, during data processing, and final processed data. LSS and logging scientists assessed real time drilling parameters and data from the downhole tools in terms of realistic values for the lithology of drilling interval. Mud line was confirmed by Gamma Ray curve at 915.0 mBRT. All resistivity curves were also sharply increasing at the mud line. The responses of Gamma Ray and Resistivity curves were showing generally similar trend. The arcVISION mounted on transmitter and receivers with 5 different spacing would be shown separated values to indicate fluid invasion effect at 915 - 918, 928 - 932, 945 – 994, 1015 – 1041, 1045 – 1107, and 1112 – 1115 mBRT (0 – 3, 13 – 17, 30 – 79, 100 – 126, 130 – 192, and 197 – 200 mbsf). It occurred packed off at 1016.0 mBRT (101.0 mbsf) and immediately released then we conducted controlled drilling speed, WOB, Torque, Flow Rate and stroke, therefore, temperature and pressure data showed stepwise responses. Small temperature and pressure anomalies were observed when the pipe connection (**Fig 2-8**). This site is located 100 km south of IDOP_Exp.331_Site_C0015 on the hydrothermal active mount. Temperature baseline (13 degC) obviously seemed to be increasing from 6 degC at mud line to 13 degC at 919 mBRT (4.7 mbsf). Temperature anomaly were observed upto 15 degC at 935, 952, 1050, 1077, 1081, 1097, 1105, 1126 and 1129 mBRT (20, 37, 135, 162, 166, 182, 190, 211, and 214 mbsf).

Log characterization

Hole C9014A logging units were characterized from visual inspection of gamma ray and resistivity log responses (**Fig 2-9**). Two logging units were defined based on variations in trend lines and log character. Logging Unit (**Table 2-6).**

Logging Unit I (0–75.8 mbsf)

Gamma ray log shows variable values (23-82) gAPI. There is a higher gamma ray interval (up to 80 gAPI) at 17-37 mbsf. Resistivity log indicates initial increasing up to 3 ohm-m. Then the values are fluctuated (0.4-7 ohm-m) at 0-48.5 mbsf and constant resistivity (1-2 ohm-m) at the lower part of the unit (48.5-75 mbsf). Many of conductive spikes (e.g. at 14 and 75 mbsf) correspond to negative gamma ray spikes in this unit.

Logging Unit II (75.8–192.5 mbsf)

Gamma ray log shows variable values (30-85) gAPI. There is a higher gamma ray interval (up to 78 gAPI) at 75-100 mbsf. From the top of the unit, resistivity value increase with depth from 0.3 to 8 ohm-m (91 mbsf). Then the values gradually decrease with strong fluctuation (0.4-6 ohm-m) to the bottom of the unit. Many of conductive spikes correspond (eg. at 101, 116, 139, 169 and 186 mbsf) to negative gamma ray spikes in this unit.

Logging Unit III (192.5 mbsf-TD)

Gamma ray log exhibits higher values and large fluctuation between 50 and 80 gAPI, There is large excursion of resistivity value up to 5 ohm-m.

Temperature and Pressure

A baseline of the annular temperature measured by ArcVISION and telescope increased with depth from 6°C (mudilne) to 13°C (25 mbsf), then maintain constant baseline at 13°C to TD. A minor temperature anomaly up to 16°C was observed at 20 mbsf.

2.2.5 **Site C9015**

Logging data quality control

Data quality control was performed by monitoring real time data, short repeat log, during data processing, and final processed data. LSS and logging scientists assessed real time drilling parameters and data from the downhole tools in terms of realistic values for the lithology of drilling interval. Mud line was confirmed by Gamma Ray and resistivity curves at 1017.0 mBRT. We observed large Gamma Ray anomaly with 342.6 GAPI maximum and resistivity curves decreasing at 1025.8 mBRT (8.8 mbsf) for 10 m interval. Resistivity in 1027.0 – 1032.0 mBRT (10.0 – 15.0 mbsf) are less than 0.1 Ohm.m that is out of specification (range from 0.1 to 3000 ohm.m). In this period, resistivity responses were too low and conductible, consequently the resistivity transformation was noisy and unreliable. We observed a sequence of high-Gamma Ray – low-resistivity – low ROP (stiff formation) from mud line to 1028 and 1111 – 1126 mBRT (0 – 11 and 94 – 109 mbsf). Small temperature and pressure anomalies were observed when the pipe connection conducted (Figure. 10). Annular Temperature by arcVISION measured from 5 degC at mud line to 15 degC at 1019 mBRT (2 mbsf). There are temperature swell from 13 degC baseline upto 17 degC at 1019 – 1032 mBRT (2 – 15 mbsf), upto 19 degC from 1042 – 1045 mBRT (25 – 28 mbsf), upto 18 degC from 1057 – 1063 mBRT (30 – 36 mbsf). Cyclic temperature swells were observed from 14 – 17 degC at 1133 – 1190 mBRT (116 – 173 mbsf). Relog was obtained at Gamma Ray and resistivity large anomaly zone at top section. Gamma ray and resistivity in measurement range were good repeatability but resistivity values were not repeatedly observed from 1027 - 1032 mBRT (10 – 15 mbsf) in the repeat session (**Fig 2-10**).

Log characterization

Hole C9015A logging units were characterized from visual inspection of gamma ray and resistivity log responses (**Fig 2-11**). Two logging units were defined based on variations in trend lines and log character. Logging Unit (**Table 2-6**).

Logging Unit I (0–95.5 mbsf)

Logging I exhibits an initial increase in gamma ray up to 340 gAPI from the mudline to 8 mbsf. The gamma ray log shows sharp decrease to ~100 gAPI at 10 mbsf, gradual decrease to ~40 gAPI, then gradual increase of baseline from 40 to 100 gAPI with minor

fluctuations in the interval 24-94 mbsf. Resistivity log exhibits decrease with depth at the mudline, then show extremely low values (~0.1 ohm-m, that is significantly lower than sea water resistivity) from the 9 to 16 mbsf. The resistivity value sharply increases up to 2 ohm-m at 16-17 mbsf. Then resistivity log shows variable values ranges from 0.3 to 3 ohm-m.

Logging Unit II (95.5 mbsf – TD)

Logging Unit II exhibits high gamma ray (~250 gAPI) at the top of the unit (95-106 mbsf). Then, the gamma ray log shows constant baseline (40-70 gAPI at 113-133 mbsf, around 70 gAPI at 133-174 mbsf). Resistivity log shows variable values ranges from 0.4 to 2 ohm-m. A minor conductive interval (~0.4 ohm-m) occurs at 110-113 mbsf, that corresponds to a peak of gamma ray (~120 gAPI).

Temperature and Pressure

A baseline of the Annular temperature measured by ArcVISION increased with depth from 13°C at the mudline to 16°C (TD). No major temperature anomaly was observed in the hole. Several minor anomalies 3-5°C higher than the baseline were observed throughout the section. No significant annular temperature anomalies (more than 2°C) were measured by Telescope.

2.2.6 **Site C9016**

Logging data quality control

Data quality control was performed by monitoring real time data, short repeat log, during data processing, and final processed data. LSS and logging scientists assessed real time drilling parameters and data from the downhole tools in terms of realistic values for the lithology of drilling interval. Mud line was confirmed by Gamma Ray and resistivity curves at 1124.0 mBRT. There are abruptly large Gamma ray anomaly with 670 GAPI at 1133.6 - 1141.3 mBRT (9.6 ~ 17.3 mbsf). Annulus temperature profile was 5 degC at mud line and gradually increasing to 16 degC at 1129 mBRT (5 mbsf). Small temperature and pressure anomalies were observed when the pipe connection conducted (**Fig 2-12**). The overall quality of the processed logging data was good. We observed temperature anomaly upto 40 degC at 1202 – 1209 mBRT (78 - 85 mbsf). Considering sensor distance from the bit, a hydrothermal layer which causes this temperature anomaly came from 1214 mBRT. Temperature profile by TeleScope is almost flat and lower value than 20 degC.

Log characterization

Hole C9016A logging units were characterized from visual inspection of gamma ray and resistivity log responses (**Fig 2-13**). Two logging units were defined based on variations in trend lines and log character. Logging Unit are also shown in **Table 2-6**.

Logging Unit I (0–121.0 mbsf)

Logging Unit I exhibits two sequences of large variation in gamma ray and resistivity values. This unit are divided into two logging subunits (Logging Units IA and IB) for the upper and lower sequences.

Logging Subunit IA (0-47.7 mbsf)

Logging Subunit IA exhibits an initial increase in gamma ray from the mudline, then the gamma ray log show sharp increase (~100 to 670 gAPI). Two intervals of extremely high gamma ray value (~250 to 870 gAPI) are identified at 7-18 mbsf and 22-31 mbsf. Below the sharp decrease in gamma ray the values show around 100 gAPI at the interval of 31-40 mbsf. The gamma ray log show lower values around 50 gAPI at the base of this subunit. Resistivity log exhibits fluctuated values between 0.2 and 2 ohm-m. There are

conductive (0.2-0.3 ohm-m) and resistive (1-10 ohm-m) intervals at 34-40 mbsf and 41-48 respectively. The resistive interval (41-48 mbsf) corresponds to low gamma ray (~40 gAPI) and low ROP (~20 m/h) interval.

Logging Subunit 1B (47.7-121.0 mbsf)

Logging Subunit IB exhibits a similar log response as Logging Subunit IA. Gamma ray log shows a gradual increase (~30 to 90 gAPI), then abrupt increase up to 400 gAPI at 74 mbsf. An interval of extremely high gamma ray value (~250 to 550 gAPI) is identified at 74-92 mbsf. Below the sharp decrease in gamma ray the values show around 150 gAPI at the interval of 95-109 mbsf. Then the gamma ray log shows lower values (~15 gAPI) at 111 mbsf. Resistivity log exhibits fluctuated values between 0.2 and 1 ohm-m. There are conductive (~0.3 ohm-m) and resistive (~4 ohm-m) intervals at 103-110 mbsf and 111-121 respectively. The top of resistive interval corresponds to low gamma ray (~20 gAPI) and low ROP (~20 m/h) interval.

Logging Unit II (121.0 mbsf to TD)

Logging Unit II exhibits constant gamma ray trend around 60 gAPI through the interval. Resistivity log shows constant trend with variation between (0.5-1 ohm-m).

Temperature and Pressure

A baseline of the Annular temperature measured by ArcVISION increased with depth from 13°C at the mudline to 19°C at TD). A major temperature anomaly up to 39°C was observed at 80 mbsf. The temperature anomaly started at 78 mbsf (17°C) and ended at 96 mbsf (15°C) (**Fig 2-14**). The initiation of temperature anomaly was detected when the bit reached to the lower boundary of the high gamma ray interval (92 mbsf). Other several minor anomalies up to 6°C higher than the baseline were observed above 60 mbsf. No significant annular temperature anomalies were measured by Telescope.

References

Bonner, S., Fredette, M., Lovell, J., Montaron, B., Rosthal, R., Tabanou, J., Wu, P., Clark, B., Mills, R., and Williams, R., 1996. Resistivity while drilling—images from the string. *Oilfield Rev.,* 8(1):4–19.

Bonner, S.D., Tabanou, J.R., Wu, P., Seydoux, J.P., Moriarty, K.A., Seal, B.K., Kwok, E.Y., and Kuchenbecker, M.W., 1995. New 2-MHz multi-array borehole-compensated resistivity tool developed for MWD in slim holes. *Proc.—SPE Annu. Tech. Conf.,* Pap. SPE 30547.

Expedition 314 Scientists, 2009a. Expedition 314 Site C0002. *In* Kinoshita, M., Tobin, H., Ashi, J., Kimura, G., Lallemant, S., Screaton, E.J., Curewitz, D., Masago, H., Moe, K.T., and the Expedition 314/315/316 Scientists, *Proc. IODP,* 314/315/316: Washington, DC (Integrated Ocean Drilling Program Management International, Inc.).
doi:10.2204/iodp.proc.314315316.114.2009

Expedition 334 Scientists, 2011. Costa Rica seismogenesis project (CRISP): sampling and quantifying input to the seismogenic zone and fluid output. IODP Prel. Rept., 334. doi:10.2204/iodp.pr.334.2011

2.3 Temperature measurement in the borehole at Iheya hydrothermal area

Junichi Miyazaki

Boreholes in the Iheya hydrothermal area were expected to the extremely hot environments (more than 310°C). Although to measure the temperature is important in such environments for mineralogy, fluid-chemistry, microbiology and so on, there are some difficulties. The most considerable problem was heat tolerance of electrical tools including memory for data recording and batteries. It is known that most stabilized electronic tool can even use less than 175°C. Therefore, there are no available distributed electronic tools against our targeted environments.

TRDT (Thermo-resistant downhole temperature recording logger) that was a downhole temperature logger was designed to use such extremely hot environments. Electrical tools in TRDT were protected from rapid temperature increasing by Dewar flask. Owe to the Dewar flask, we can use this temperature logger for 5.5 hour under 350°C environments. In this exp.907 cruise, by using TRDT we tried to measure the bottom temperature in the borehole through the drill pipe during the coring.

Methods

1. TRDT was set to the ESCS core barrel (TMD: Temperature measurement device, Fig. 2-14).
2. TMD was freely fallen into the drill pipe.
3. After arrival at the bottom, temperature has been measured for 10 minutes without circulating water.
4. Using wire line equipped in the Chikyu, TMD was recovered from the bottom.

Results and discussion

I opened the logger to download temperature data from the memory in TRDT, and then I found the disconnection of the wire to connect between electrical tool including memory and sensor. And also I found the damage in heat insulator which are made by heat stabilized plastic. It seemed that the breaking heat insulator was caused by strong vibration during the free-fall of the TMD and led the disconnection of the wire. Therefore, temperature was not recorded.

To the future cruise, I will repair and modify the TRDT to tolerate the strong vibration through the drill pipe.

Table 2-1 MWD-LWD tool acronyms, descriptions, and units.

Tool	Output	Description	Unit
Surface		**Drilling parameters**	
	BD	Bit Depth	m
	TD	Total Depth	m
	TVD	True Vertical Depth	m
	HKLD	Hookload	kkgf
	SPPA	Standpipe Pressure	kkgf
	ROP*5	5 feet average of Rate of Penetration	m/h
	SWOB	Surface weigth on bit	kkgf
MWD (TeleScope+APWD)		**Measurements while drilling**	
	CRPM	Average MWD collar RPM	rpm
	SHKR	Shock Rate	
	SHKRSK	Shock Risk	1/s
	STICK	Stick Slip Indicator	c/min
	DHAP	Downhole Annular Pressure	kPa
	DHAT	Downhole Annular Temperature	°C
	RGX	Rotating Axial Accelerometer	rpm
	RHX	Rotating Axial Magnetometer	rpm
arcVISION+APWD memory		**Array resistivity tool**	
	GR	Gamma Ray	gAPI
	AXXH, AXXL	Attenuation resistivity at source-receiver spacing XX, where XX=16, 22, 28, 34, and 40 inches. H: high frequency (2MHz). L: Low frequency (400kHz).	ohm-m
	PXXH, PXXL	Phase-shift resistivity at source-receiver spacing XX, where XX= 16, 22, 28, 34, and 40 inches. H: high frequency (2MHz). L: Low frequency (400kHz).	ohm-m
	SHKL	Tool Shock Level	
	SHKR	Shock Rate	1/s
	DHAP	Downhole Annular Pressure	kPa
	DHAT	Downhole Annular Temperature	°C
	ECD	Equivalent Circulating Density	g/cc
	TAB_RES	Resistivity Time After Bit	h

Table 2-2 arcVISION resistivity range and accuracy.

Measurement	Accuracy	Range
2 MHz phase-shift	+-2%	0.2-60 ohm.m
resistivity	+- 0.3 mS/m	60-3000 ohm.m
400 kHz phase-shift	+-2%	0.1-10 ohm.m
resistivity	+- 2 mS/m	10-100 ohm.m
2MHz attenuation	+-3%	0.2-25 ohm.m
resistivity	+- 1.5 mS/m	25-50 ohm.m
400kHz attenuation	+-3%	0.1-3 ohm.m
resistivity	+- 10 mS/m	3-10 ohm.m

Table 2-3 arcVISION resistivity depth of investigation.

Measurement	Spacing (in)				
	16	22	28	34	40
R = 1.0 ohm.m (depth of investigation in dadii and in)					
2 MHz phase-shift resistivity	13	14	15	17	18
400 kHz phase-shift resistivity	17	19	22	25	27
2 MHz attenuation resistivity	19	22	24	26	29
400 kHz attenuation resistivity	27	30	33	36	38
R = 10 ohm.m (depth of investigation in dadii and in)					
2 MHz phase-shift resistivity	18	22	25	28	30
2 MHz attenuation resistivity	31	34	36	38	40

Table 2-4 arcVISION resistivity vertical resolution.

Measurement	Spacing (in)				
	16	22	28	34	40
R = 1.0 ohm.m (vertical resolution values in ft)					
2 MHz phase-shift resistivity	0.7	0.7	0.7	0.7	0.7
400 kHz phase-shift resistivity	1.0	1.0	1.0	1.0	1.0
2 MHz attenuation resistivity	1.8	1.8	1.8	1.8	1.8
400 kHz attenuation resistivity	3.0	3.0	3.0	3.0	3.0
R = 10 ohm.m (vertical resolution values in ft)					
2 MHz phase-shift resistivity	1.0	1.0	1.0	1.0	1.0
2 MHz attenuation resistivity	4.0	5.0	6.0	6.0	6.0

Table 2-5 APWD sensor resolution and accuracy.

Resolution	1 psi
Accuracy	0 to 0.1% of fullscale
Available ranges	0 to 20,000 psi
Annular temperature resoolution	1 degC
Annular temperature accuracy	1 degC

Table 2-6 Logging units characterized from visual inspection of gamma ray and resistivity log responses.

Hole C0011B

	Top (mbsf)	Bottom (mbsf)	Log characteristics
Log Unit I	0	103.3	Variable GR (30-70 gAPI) from 0 to 19 mbsf, gradual increase (35-70 gAPI). Gradual increase resistivity (~0.3-1 Ωm) from 0-50 mbsf, decrease (~1-0.15 Ωm), lower values (~0.1 Ωm) at
Log Unit II	103.3	172	Gradual decrease of GR values from 190 to 50 gAPI. Variable resistivity values between 0.2 and 3 ohm-m.
Log Unit III	172	TD	Higher GR values (100-190 gAPI). Contrant resisticvity value around 0.8 ohm-m.

Hole C9012A

	Top (mbsf)	Bottom (mbsf)	Log characteristics
Log Unit I	0	95.5	Increase in GR up to 75 gAPI from 0 to 8 mbsf. Constant baseline around 30 gAPI. Constant resistivity baseline ~0.8
Log Unit II	95.5	201.3	High GR interval (70-100 gAPI) at 95.5-128 mbsf. GR baseline decreases from 50 to 30 gAPI. Fluctuated resistivity between 0.5-9 ohm-m at 105-143 mbsf, gradual decrease from 1 to
Log Unit III	201.3	270.9	High GR interval (70-110 gAPI) at 213-222 mbsf. GR baseline maintain a constant trend around 50 gAPI. Fluctuated resistivity between 0.2-8 ohm-m.
Log Unit VI	270	TD	High GR interval (70-110 gAPI) at 270-280 mbsf. Constant GR trend around 25 gAPI. Constant resistivity trend around 0.6

Hole C9013A

	Top (mbsf)	Bottom (mbsf)	Log characteristics
Log Unit I	0	48.7	Increase of GR from up to 170 gAPI, variable between 70 and 190 gAPI. Gradual increase of resistivity vvalue from 0.3 to 5
Log Unit II	48.7	88.8	Highly fluctuated GR values (40-200 gAPI). Higher resistivity values (1-8 ohm-m).
Log Unit III	88.8	131.7	GR baseline ranges between 70 and 100 gAPI. Lower resistivity baseline around 0.2 ohm-m.
Log Unit IV	131.7	TD	Variable GR values between 20 and 190 gAPI. Variable resistivity values between 0.3 and 6 ohm-m.

Hole C9014A

	Top (mbsf)	Bottom (mbsf)	Log characteristics
Log Unit I	0	75.8	Variable GR values (23-82 gAPI). Higher GR interval at 16.5-38.6 mbsf. Fluctiation of resistivity (0.4-7 ohm-m) at 0-48.5 mbsf. Constant resistivity (1-2 ohm-m) at 48.5-74.9 mbsf).
Log Unit II	75.8	192.5	Variable GR values (30-85 gAPI). High GR (up to 78 gAPI) interval at 75.8-100.4 mbsf. Increasing resistivity (1 to 8) down to 90.9 mbsf. Decreasing trend of resistivity (6 to 0.5 ohm-m).
Log Unit III	192.5	TD	Common negative excursion (down to 0.3 ohm-m) of High GR up to 80 gAPI. Increasing resistivity up to 5 ohm-m.

Hole C9015A

	Top (mbsf)	Bottom (mbsf)	Log characteristics
Log Unit I	0	95.5	GR increase up to 343 gAPI, decrease down to 53 gAPI, gradual GR baseline increase up to 170 gAPI. Very low resistivity (0.1-0.3 ohm-m) at the top interval (0-16 mbsf).
Log Unit II	95.5	TD	Decreasing trend from 2 to 0.1 ohm-m at 33.5 mbsf. Constamt Constant GR baseline (40-70 gAPI at 113-133 mbsf, around 70 gAPI at 133-174 mbsf).

Hole C9016A

	Top (mbsf)	Bottom (mbsf)	Log characteristics
Log Unit I	0	121	Two sequences of large variation of GR resistivity.
Log Subunit Ia	0	47.7	Increasing GR from mudline, very high GR zone (up to 870 gAPI) at 6-31 mbsf, high GR zone (100-200) at 31-40 mbsf, decreasing GR down to 33 gAPI. Valiable resistivity values
Log SubUnit Ib	47.7	121	Gradual increasing of GR from 47.7 to 48 mbsf, very high GR zone (up to 560 gAPI) at 74-92 mbsf, high GR zone (100-200) at 92-110 mbsf, decreasing GR down to 20 gAPI. Valiable resistivity values from 0.2 to 4 ohm-m.
Log Unit II	121	TD	Constant GR (50-70 gAPI) and resistivity (0.5-1 ohm-m)

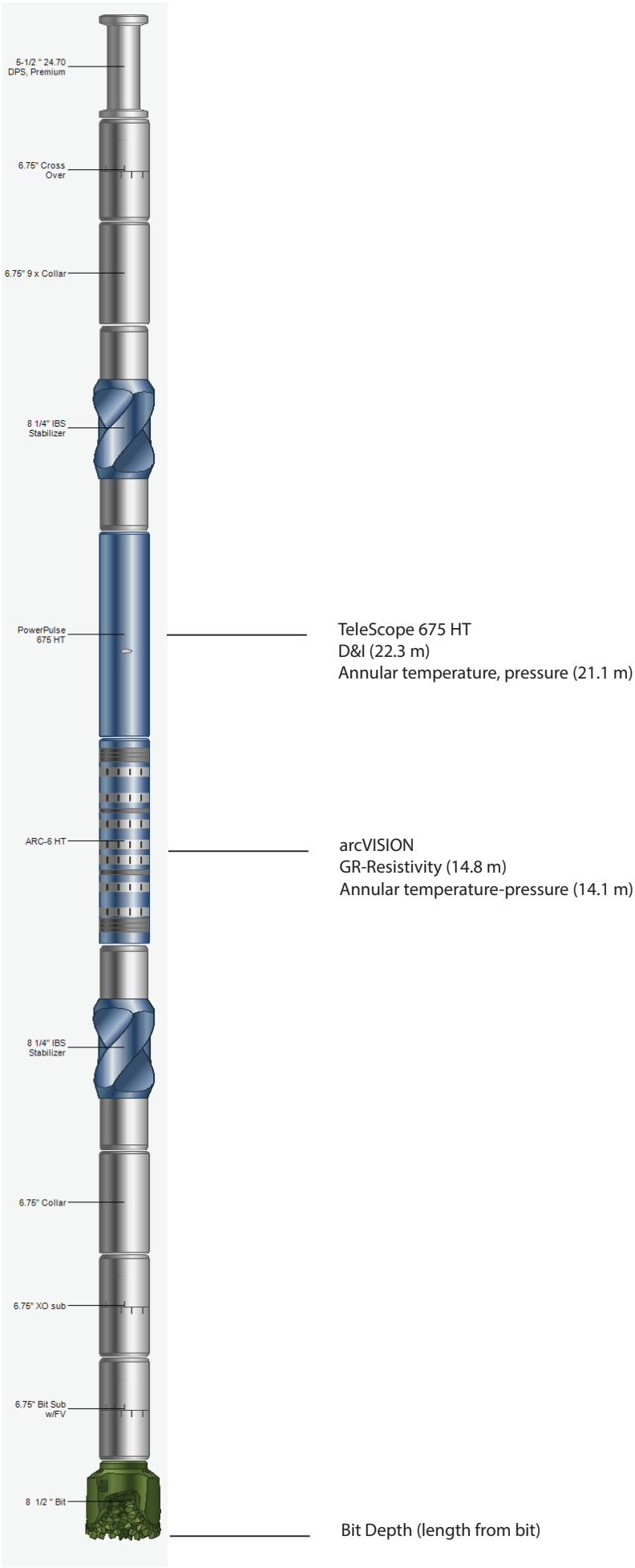

Fig. 2-1: Configuration of the LWD BHA.

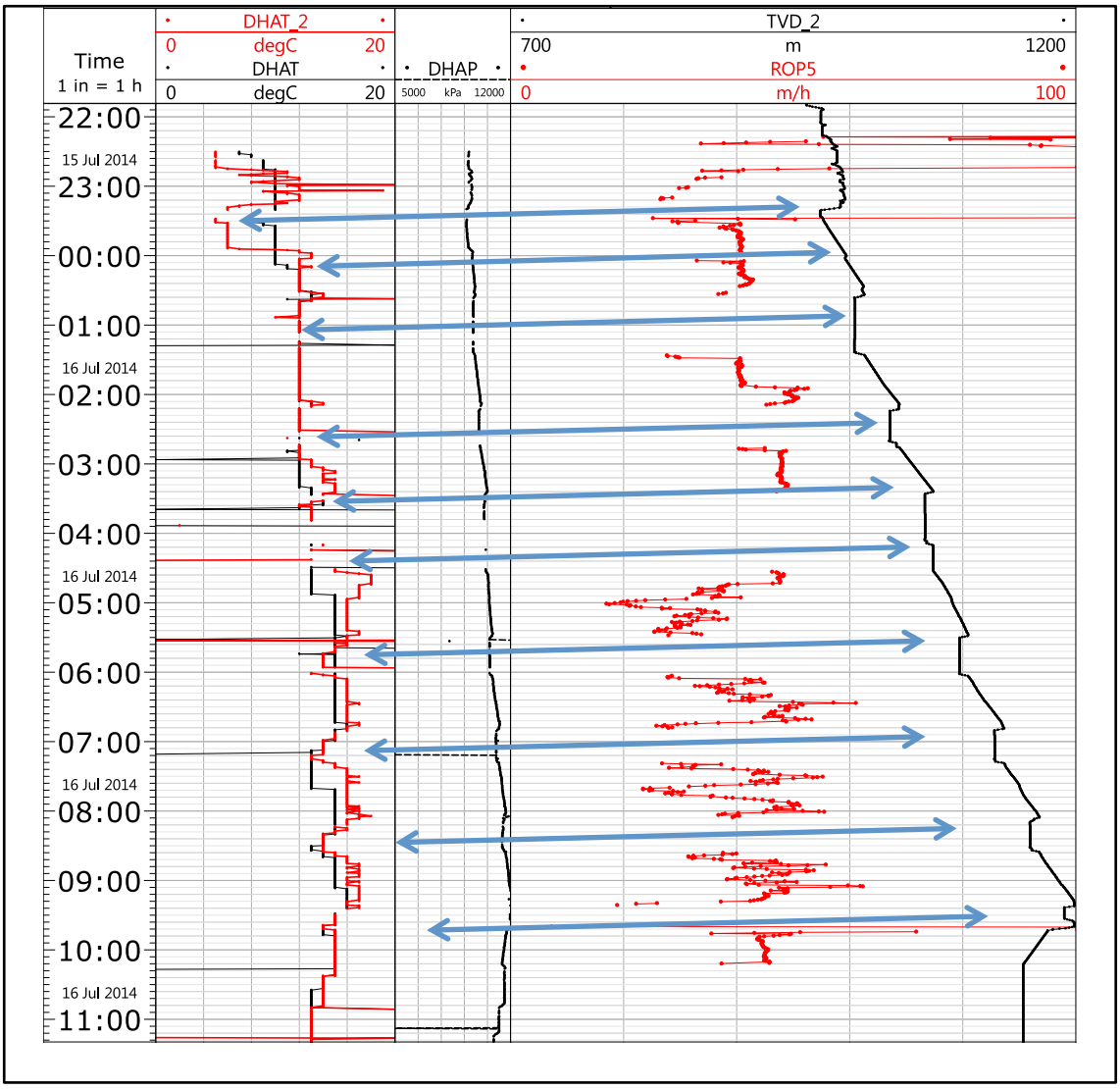

Fig. 2-2: Small temperature and pressure anomalies are observed when the pipe connection in holeC9011B.

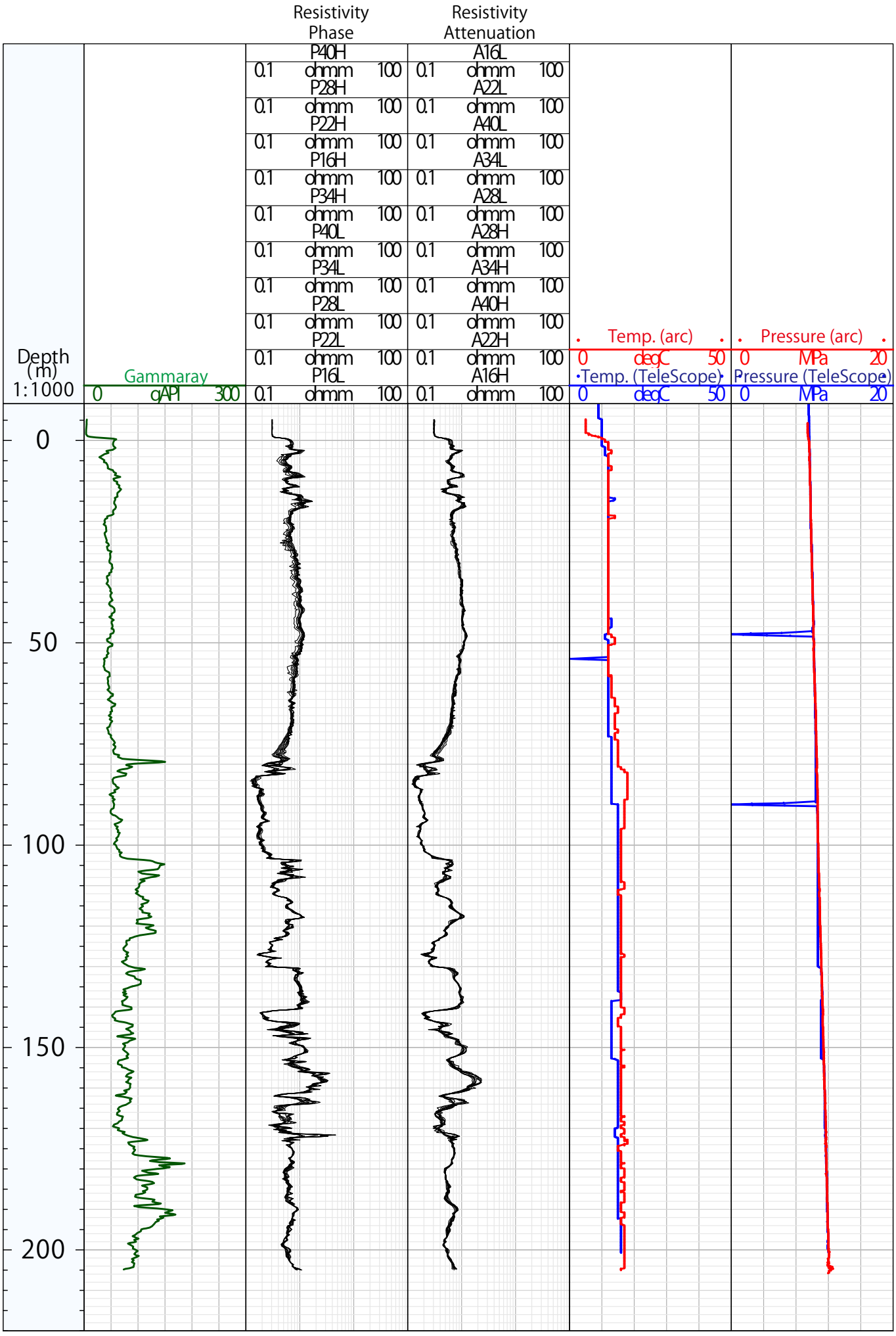

Fig. 2-3: Hole C9011B logging units were characterized from visual inspection of gamma ray and resistivity log responses.

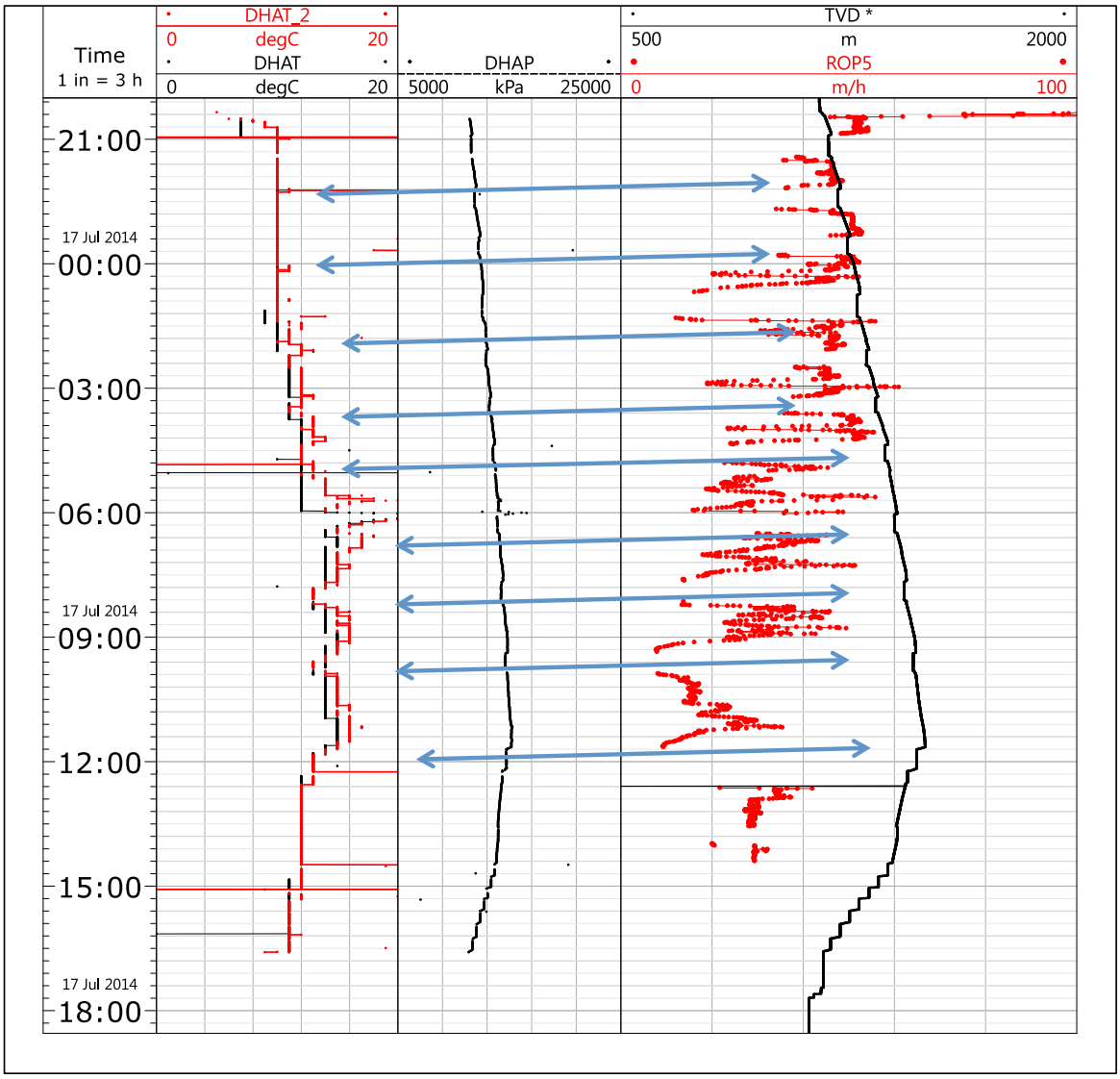

Fig. 2-4: Small temperature and pressure anomalies are observed when the pipe connection in holeC9012A.

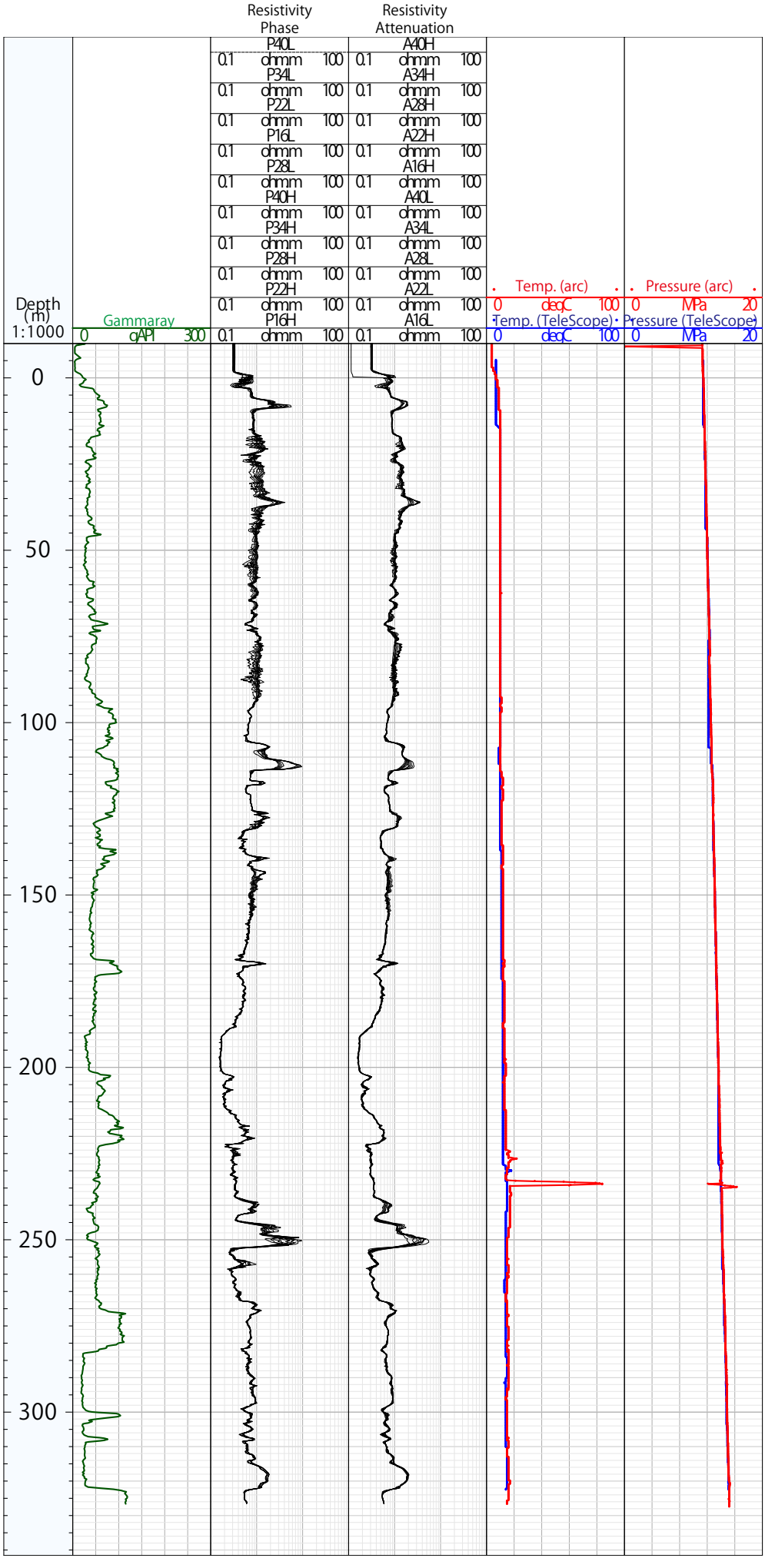

Fig. 2-5: Hole C9012A logging units were characterized from visual inspection of gamma ray and resistivity log responses.

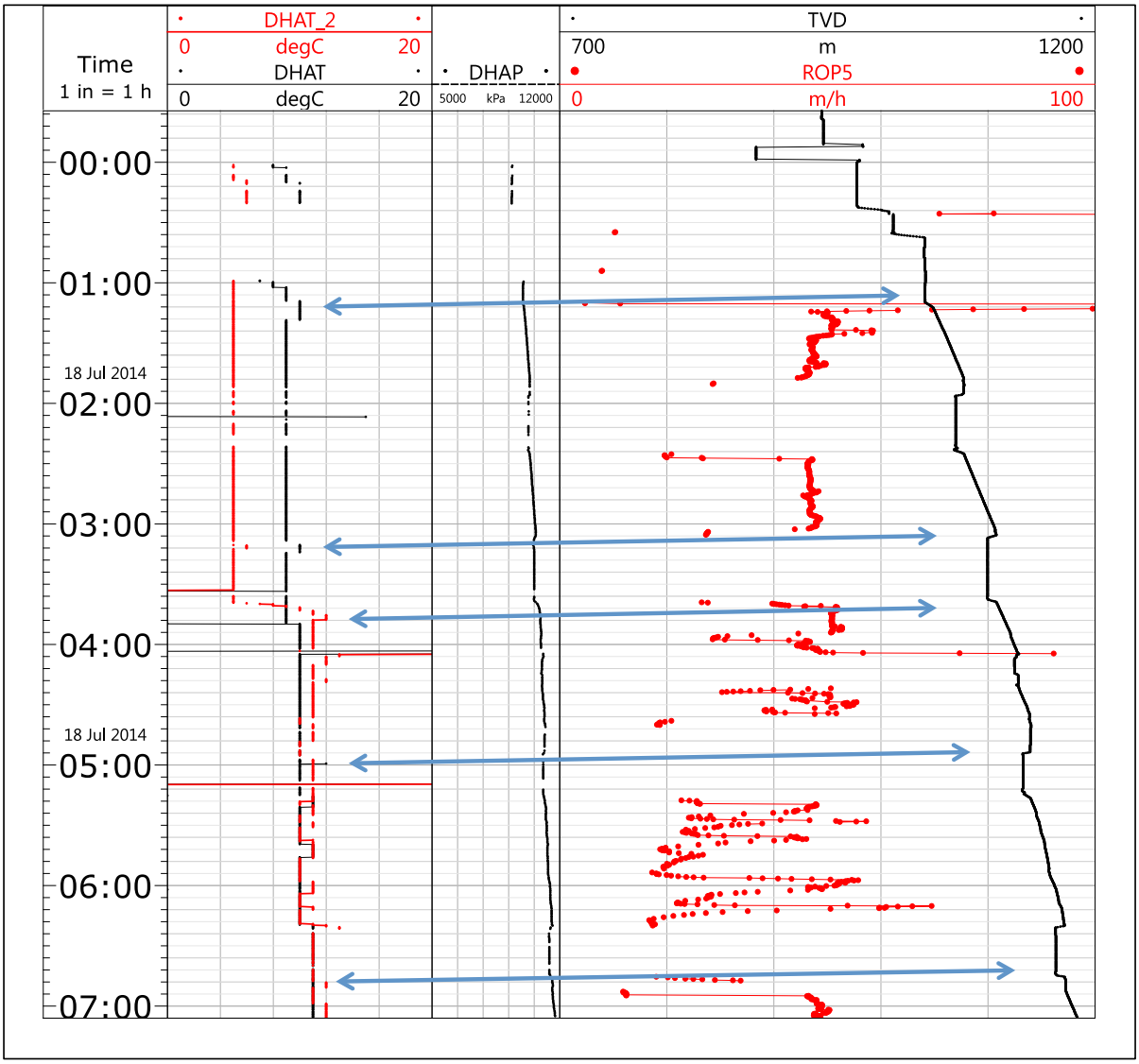

Fig. 2-6: Small temperature and pressure anomalies are observed when the pipe connection in holeC9013A.

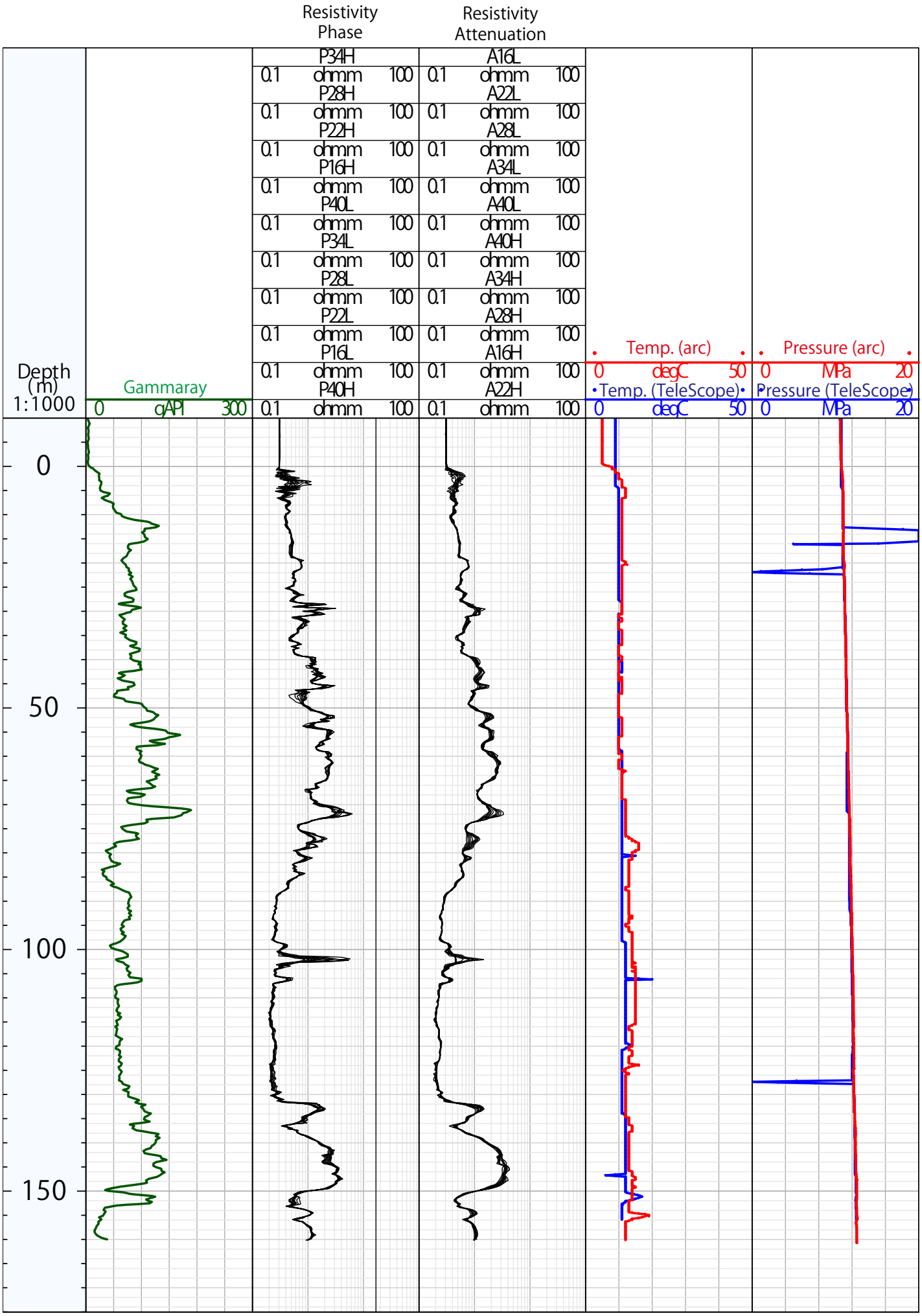

Fig. 2-7: Hole C9013A logging units were characterized from visual inspection of gamma ray and resistivity log responses.

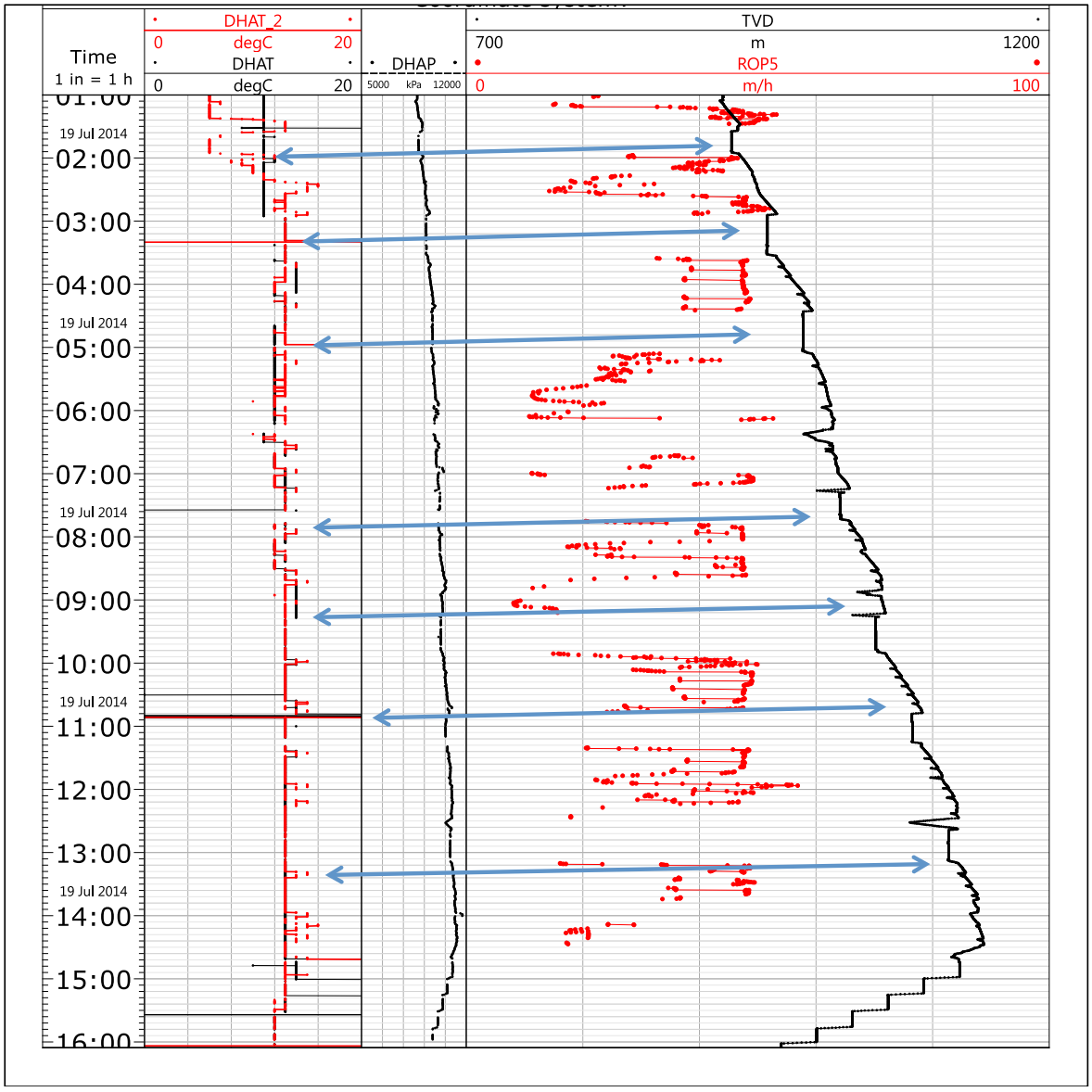

Fig. 2-8: Small temperature and pressure anomalies are observed when the pipe connection in holeC9014A.

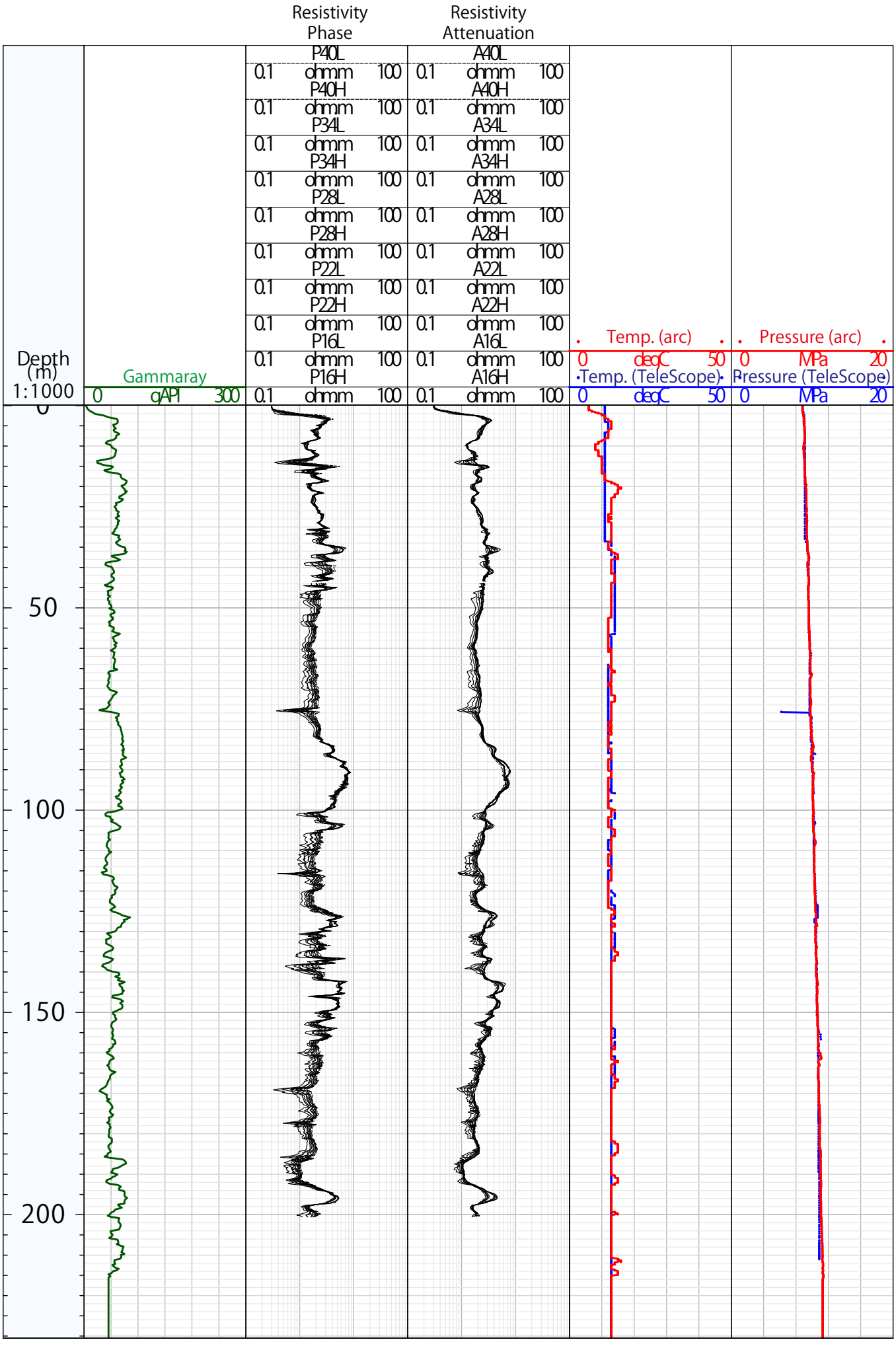

Fig. 2-9: Hole C9014A logging units were characterized from visual inspection of gamma ray and resistivity log responses.

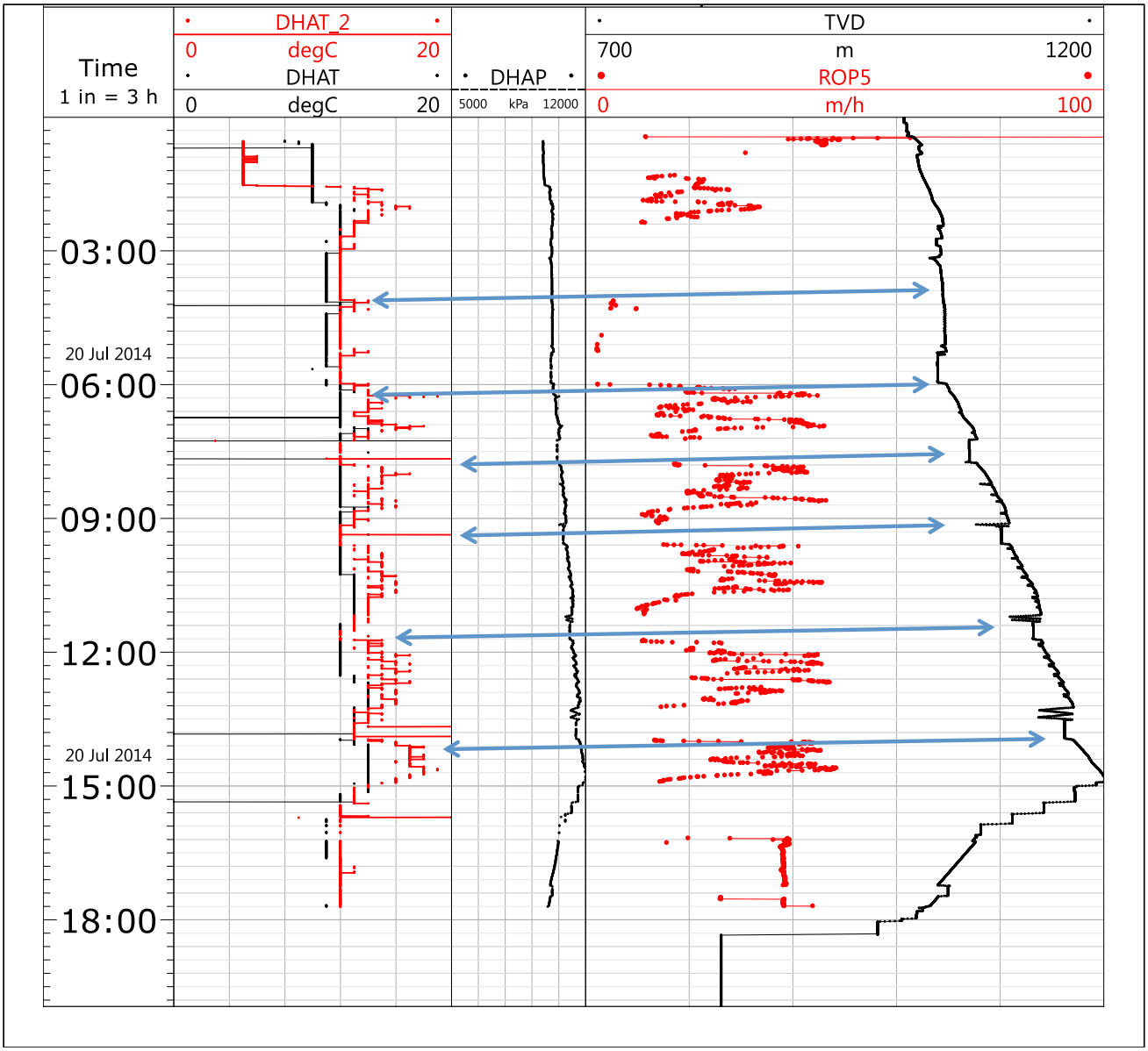

Fig. 2-10: Small temperature and pressure anomalies are observed when the pipe connection in holeC9015A.

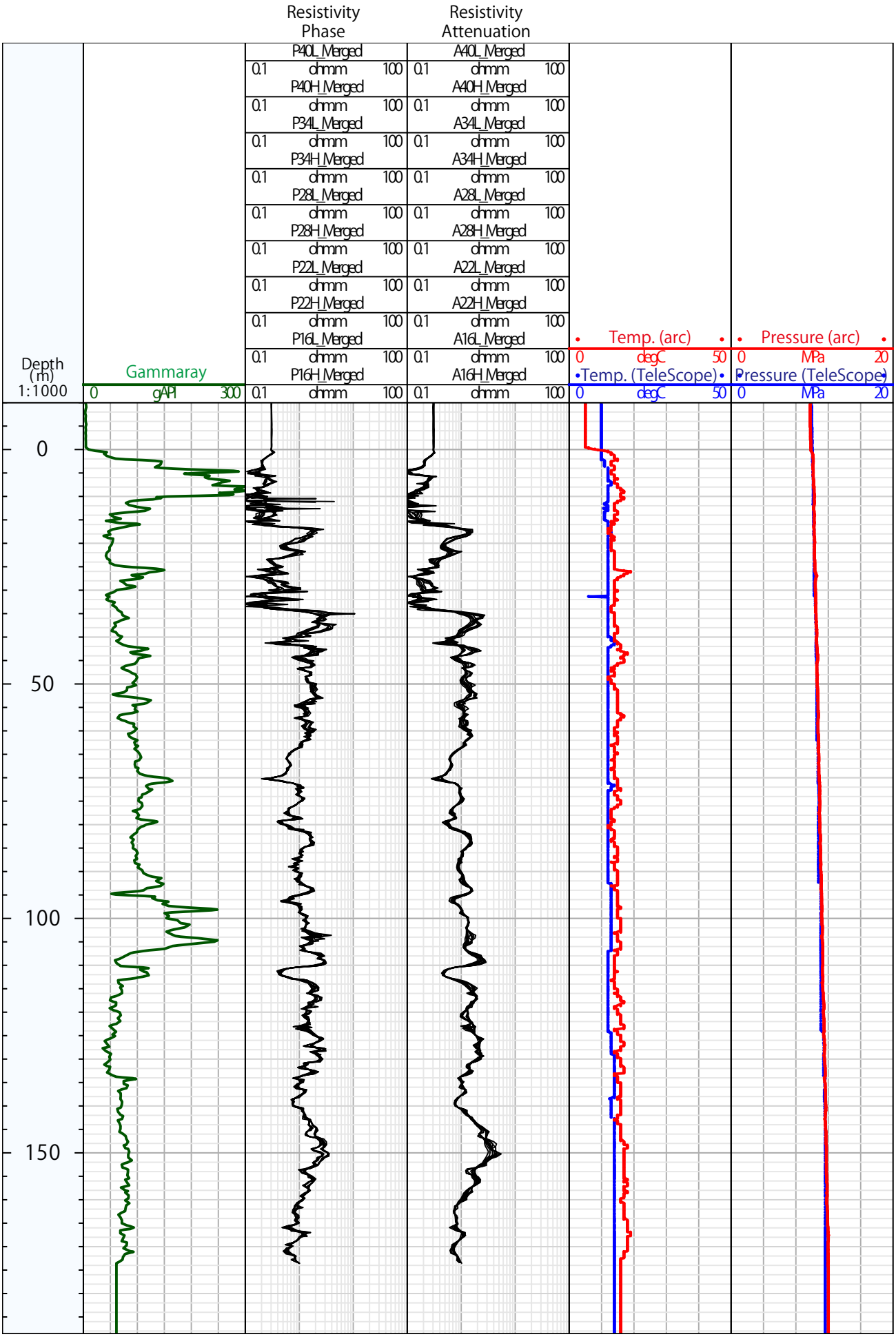

Fig. 2-11: Hole C9015A logging units were characterized from visual inspection of gamma ray and resistivity log responses.

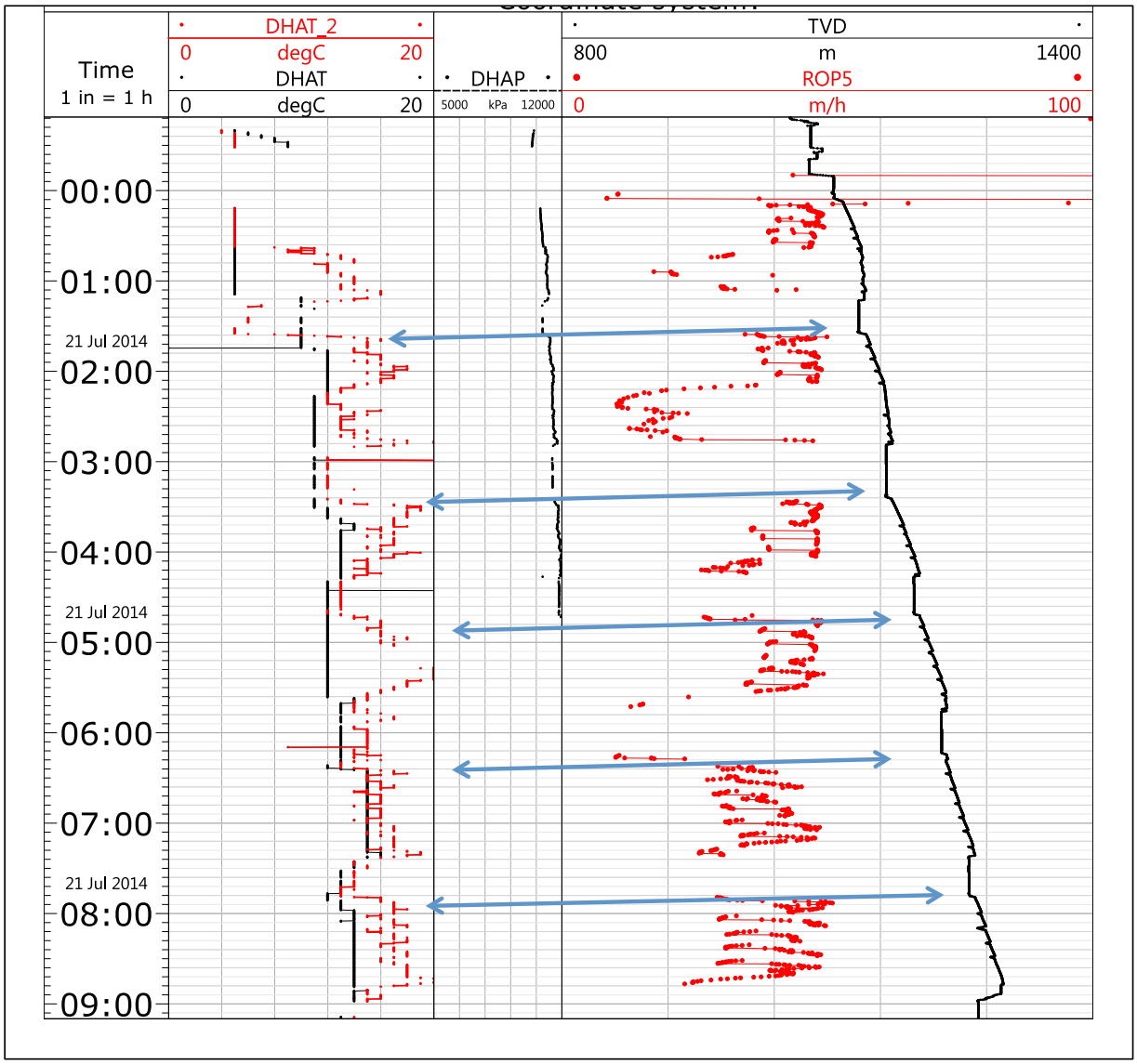

Fig. 2-12: Small temperature and pressure anomalies are observed when the pipe connection in holeC9016A.

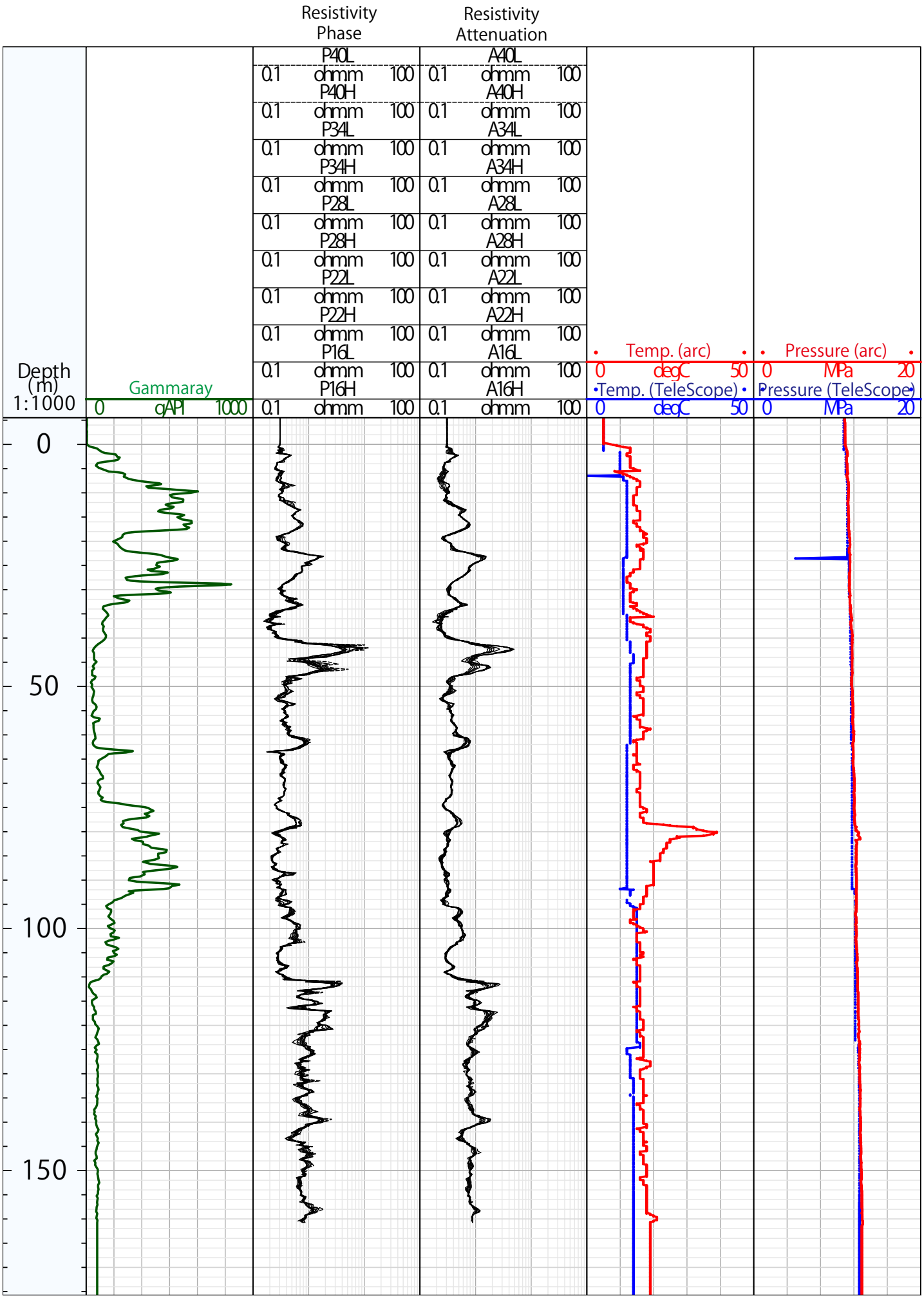

Fig. 2-13: Hole C9016A logging units were characterized from visual inspection of gamma ray and resistivity log responses.

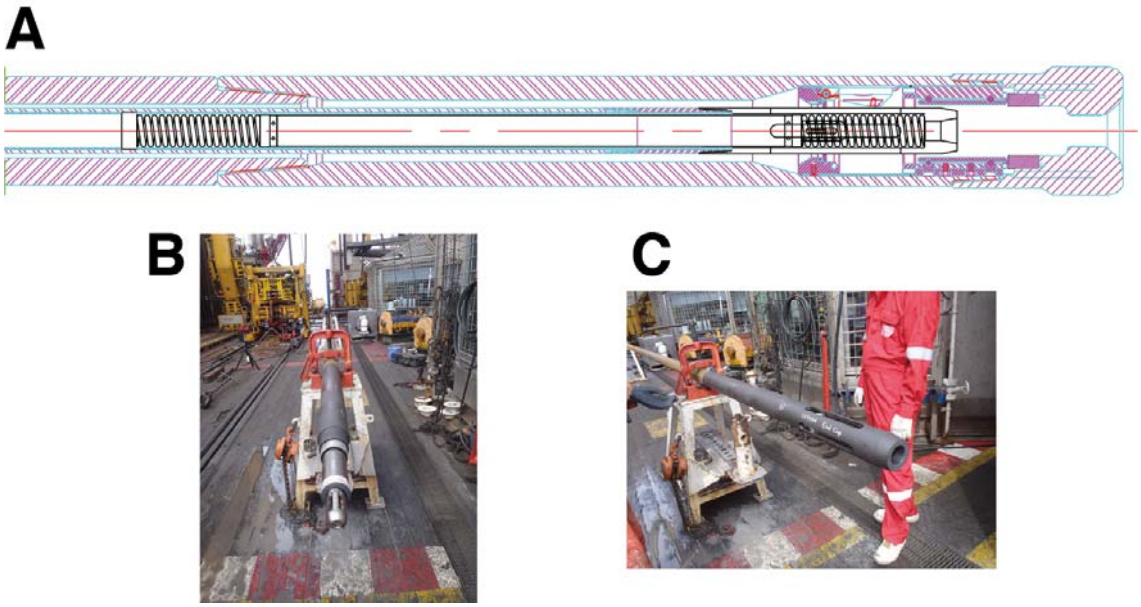

Figure 2-14: TMD (Temperature measurement device)

A: Schematic view of TMD with SD-RCB drill bit.

B&C: Picture of TRDT into ESCS core barel.

Chapter 3. Coring

T. Nozaki/ T. Yamasaki/ Y. Takaya/ S. Totsuka

In order to compare with physico-chemical parameters obtained by LWD and actual core lithologies, three holes were drilled in the expedition, Hole C9016B, C9015B and C.

Hole C9016B was cored with a Hydraulic Piston Corer System (HPCS)/Extended Shoe Coring System (ESCS) Bottom Hole Assembly (BHA). Coring target intervals were designed for recovering 14 intervals (11 cores) that show typical LWD signatures. First run was cored by HPCS with a normal plastic liner followed by ESCS coring with an aluminum liner. Due to the technical reasons, intervals between target intervals were also cored with a 9.5 m aluminum liner. Hydraulic piston coring and extended shoe coring proceeded for 35.5 hours, 16 cores including intervals between target intervals, and deepened to 150 m below seafloor (mbsf)[1].

Hole C9015B was cored using a Small-Diameter Rotary-Core Barrel (SD-RCB) BHA with an aluminum liner, in order to recover continuous hard-rock (hard-ore) cores. Coring target intervals were designed similar to that in Hole C9016B. Coring proceeded for ~13 hours and 5 cores were recovered on deck, and drilled to 31 mbsf.

Hole C9016B was cored using SD-RCB BHA with an aluminum liner. Coring proceeded for ~11.5 hours and 5 cores were recovered on deck, and drilled to 40 mbsf.

3.1 Lithology/Visual description

T. Yamasaki/ T. Nozaki

Visual Core Description (VCD) was conducted essentially the same procedures with that of Integrated Ocean Drilling Program (IODP) Expedition 331, and the results of VCD were generated via the shipboard J-CORES system. Descriptions and symbols on VCD sheets are followed by the definition of Expedition 331 Scientists (2010) with slight modifications/additions.

3.1.1 Hole C9016B

Cores recovered from Hole C9016B were divided into six major lithological units. 1) From seafloor to ~9.6 mbsf consists of pumiceous gravel, grit and silty clay

[1] A penetration depth in a particular hole was primarily recorded as the distance from rotary table on the rig floor (mBRT coordinate). The "mbsf" coordinate was calculated from the value in mBRT with the altitude of the rig floor from the sea level. See chapter 5.

sediments, 2) 9.6 - 29.5 mbsf consists of hydrothermally altered clay with sulfide and sulfate minerals, 3) 29.5 - 35.0 mbsf consists mainly of disseminated to massive sulfide ore (including kuroko-ore), 4) 35.0 - 38.2 mbsf consists of hydrothermally altered clay, 5) 38.2 - 40.0 mbsf consists of semi-massive sulfide ore, and 6) 40.0 - 150.0 mbsf consists mainly of silicified volcanic rocks including keiko-ore and minor hydrothermally altered clay layers.

Unit 1:

From seafloor to ~9.6 mbsf, pale brownish-yellow to pale gray clast-supported pumiceous gravel is dominantly distributed. The gravel contains ~2 cm pumice (normally polymodal) within a gritty pumiceous matrix (Fig. 3-1). Fine-grained (<1.0 mm) oxidized fragments and quartzo-feldspathic white fragments (fragments of rhyolitic volcanic rocks?) are also sparsely distributed. Intervals between ~3.0 mbsf to 5.0 mbsf, dark gray sility clay are intercalated (Fig. 3-2). The clay includes sparse fragments of 0.5 - 1.0 cm subangular pumice and 1.0 - 2.0 cm pumiceous gritty patches. Below this clay interval, pale gray to dark gray pumiceous grits are recovered. Matrix of the grits is silty. Apparent dips of boundary of grit layers are generally 40˚ - 50˚. The grits commonly contain ~0.5 mm volcaniclastic fragments. Several intervals show high-H_2 gas concentrations corresponding to the part of organic-carbon rich matrix. Sparse distribution of fine-grained sulfide mineral grains is also confirmed by XCT images. Interval between ~9.0 mbsf and 9.5 mbsf are composed of weakly altered dark gray clay.

Unit 2:

Interval between 9.6 mbsf to 29.5 mbsf consists of hydrothermally altered clay with lenticular- and/or layer-shaped anhydrite, and discrete sugary coarse anhydrite crystals and sulfide minerals. From ~9.6 mbsf to ~10.3 mbsf pale-colored hydrothermal altered clay is observed (Fig. 3-3). Below this interval dark gray hydrothermally altered clay is distributed (Fig. 3-4). This dark gray clay contains various amount of anhydrite showing mm-scale lenticular-shaped thin layer of white anhydrite. Transparent (apparently dark-colored) sugary (euhedral) coarse grains of anhydrites are also commonly observed. Hard black massive sulfides (typically, 80% sphalerite, 15% anhydrite, 5% galena network vein and pyrite) are occasionally observed (※1).

Unit 3:

From 29.5 mbsf to 35.0 mbsf, the gray ~ light gray disseminated sulfide ore is

dominantly distributed (※2). In the interval between 29.5 mbsf to 29.65 mbsf, black hard semi-massive or massive sulfide ore mainly composed of fine-grained sphalerite together with anhydrite and minor pyrite occur (※1). Below this interval, the mode of occurrence of silicified black hard ore fragment with fine-grained sulfide minerals and anhydrite white patched or veins increased more than the 2nd lithological unit (9.6 - 29.5 mbsf) (Fig. 3-5). Sulfide minerals in the black hard rock fragment are typically composed of fine-grained 95% sphalerite and 5% pyrite. These disseminated sulfide ores are intercalated with gray ~ light gray hydrothermal altered clay with anhydrite white patches, veins and transparent coarse-grained (~3 mm) euhedral sugary anhydrite crystals.

Unit 4:

The interval between 35.0 mbsf to 38.2 mbsf is dominated by gray ~ light gray hydrothermal altered clay with fine-grained white anhydrite aggregates (~2 mm), patches, veins and transparent coarse -grained (~ 1cm) euhedral sugary anhydrite crystals together with very minor fine-grained sphalerite, pyrite and galena (Fig. 3-6). The fraction of black hard ore fragment with sulfide minerals much more decreased than that of the 3rd lithological unit (29.5 - 35.0 mbsf) (※2). In the bottom part of Core 5X-4 (38.05 - 38.2 mbsf), gray hydrothermal altered clay contains dark gray clastic portions (1 - 2 cm) which is mainly composed of fine-grained sulfide minerals.

Unit 5:

From 38.2 mbsf to 40.0 mbsf, dark gray semi-massive sulfide ore composed of 85% fine-grained sphalerite and 15% whitish anhydrite with minor amounts of fine-grained pyrite and galena is dominated (Fig. 3-7) (※1). Matrix part is gray hydrothermal altered clay whose component is similar to that of the 4th lithological unit (35.0 - 38.2 mbsf). The size of the maximum semi-massive sulfide ore fragment is up to 6 cm.

Unit 6:

Below 40.0 mbsf to the end part (150.0 mbsf), gray ~ whitish gray highly silicified volcanic breccia or volcanic rock supported by gray ~ light gray hydrothermal altered clay mainly occur. From 40.0 mbsf to 50.0 mbsf, gray highly altered brecciated volcanic rock fragments are partly (15 %) replaced by fine-grained sphalerite, chalcopyrite (or pyrite?) and galena (Fig. 3-8). Below this interval to 85.0 mbsf, gray ~ whitish gray highly silicified volcanic breccia or volcanic rock supported by gray ~ light gray

hydrothermal altered clay still continued but the mode of occurrence of sulfide minerals replacing volcanic fragment becomes much more minor than that of the interval between 40.0 and 50.0 mbsf (Fig. 3-9). From 85.0 mbsf to 95.0 mbsf (Cores 11X and 12X), gray highly silicified volcanic rock became more massive (Fig. 3-9) than above interval (40.0 - 85.0 mbsf) and recovery rates of these two cores are 28.4% and 53.6%, respectively, which are much higher than those of Cores 7X, 8X, 9X and 10X (6.8 - 11.7%). Below 95.0 mbsf to the end part (150.0 mbsf), gray highly silicified volcanic rock is brecciated again (Fig. 3-10) and the core recovery rate is lower than 7%. In Core 15X (115.0 - 140.0 mbsf), highly silicified volcanic breccia contains a pale greenish metamorphic mineral (chlorite?).

※1: Mode of occurrence of sulfide minerals in the ore fragment; Based on the preliminary XRD analysis just after the CK14-04 cruise, it has been turned out that the black hard semi-massive or massive sulfide ore contains many quartz. Since these quartz crystals are fine-grained and exhibit dark gray color, we have misidentified as sphalerite instead of quartz. Thus, the mode of occurrence of sulfide minerals in the ore fragment of Hole 9016B was possibly overestimated.

※2: Difference between hydrothermal altered clay and disseminated sulfide ore; Two lithologies of hydrothermal altered clay and disseminated sulfide ore are fundamentally composed of same materials, but the mode of occurrence of black hard silicified ore fragments with sulfide minerals and anhydrite exceeds 25% in the disseminated sulfide ore.

3.1.2. Hole C9015B

Cores recovered from Hole C9015B were divided into 4 major lithological units. 1) From seafloor to ~18 mbsf consists of volcaniclastic drilling breccia of dacite-rhyolite fragments and sulfide grains, 2) 18.0 - 23.1 mbsf, highly silicified gray quartz-rich ore, 3) 23.1 - 23.39 mbsf, highly silicified grade quartz-rich ore and disseminated or semi-massive sulfide ore where the mode of occurrence of sulfide minerals increased than that of upper unit in the former, 4) 23.39 mbsf to the bottom of the hole, highly silicified angular volcanic rock.

Unit 1:

From seafloor to ~18 mbsf consists of volcaniclastic drilling breccia of dacite-rhyolite fragments and sulfide grains (sphalerite, pyrite and As-S minerals

(realger and orpiment); 20-30% of total amount of the recovered core) (Fig. 3-11). The volcanic rocks are relatively fresh and show degassed cavity without cavity-filling minerals.

Unit 2:

From 18.0 mbsf to 23.1 mbsf, highly silicified gray quartz-rich ore (keiko-ore (※3)) occurs, which is composed of 98 % fine-grained quartz, 2 % fine-grained pyrite, chalcopyrite and low-Fe sphalerite (Fig. 3-12).

Unit 3:

In the interval between 23.1 and 23.39 mbsf, the mode of occurrence of sulfide minerals in the highly silicified grade quartz-rich ore increased more than above the keiko-ore zone (18.0 - 23.1 mbsf) and disseminated or semi-massive sulfide ore dominantly occurs (Fig. 3-13). This unit could be sub-divided into three. From 23.1 mbsf to 23.14 mbsf, there is one fragment of hard semi-massive sulfide ore composed of 60 % fine-grained sphalerite, 30 % quartz and 10 % fine-grained chalcopyrite, pyrite and galena. Below this fragment to 23.26 mbsf, there are three pieces of disseminated sulfide ore composed of 80 % quartz, 15% fine-grained sphalerite and 5 % fine-grained chalcopyrite, pyrite and galena. From 23.26 mbsf to 23.39 mbsf, there is one fragment of black hard semi-massive sulfide ore composed of 70 % quartz, 25% fine-grained sphalerite and 5 % fine-grained chalcopyrite, pyrite and galena.

Unit 4:

Below the lower end of unit 3 (23.39 mbsf) to the bottom part (31.0 mbsf), the recovered core is dominated by highly silicified angular volcanic rock (keiko-ore (※3)) with 3% fine-grained sulfide minerals (chalcopyrite and sphalerite) (Fig. 3-14).

※3 Definition of keiko-ore; In this description, the term of keiko-ore is used as highly silicified gray quartz-rich rock with less than 5% sulfide minerals for the sake of simplicity and does not include metallogenic meanings.

3.1.3 Hole C9015C

Cores recovered from Hole C9015C consist of 3 major lithological units. 1) From seafloor to 10.0 mbsf (Core 1R) consists of dark gray soupy silt with ~1 cm pumiceous fragments, 2) 10.0 - 20.0 mbsf, allochthonous disseminated and semi-massive sulfide ore fragment, 3) . 20.0 - 25.0 mbsf, only one fragment of dark greenish gray highly

silicified volcanic rock was recovered.

Unit 1:

From seafloor to 10.0 mbsf (Core 1R) consists of dark gray soupy silt with ~1 cm pumiceous fragments (Fig. 3-15). Some white rounded grains, possibly sulfide minerals are also confirmed by XCT images, but visually not confirmed due to covering by soupy silt.

Unit 2:

From 10.0 mbsf to 20.0 mbsf, allochthonous disseminated and semi-massive sulfide ore fragment derived from peripheral chimney or mound (?) is dominated (Fig. 3-16). This unit was also sub-divided into two. From 10.0 mbsf to 15.0 mbsf, there are four fragments of allochthonous mound observed as disseminated sulfide ore fragments composed of 85 % fine-grained quartz, 10 % fine-grained pyrite and 5 % fine-grained sphalerite, galena and undetermined dark brownish sulfide mineral. In the two intervals from 10.04 to 10.06 mbsf and 10.10 to 10.13 mbsf, there is one piece of fine-grained marcasite(?)-rich colloform aggregate in the above interval (10.04 to 10.06 mbsf) and one allochthonous chimney or mound fragment (?) composed of 80 % sphalerite, galena, pyrite and quartz, and 20 % dark yellowish brown barite with As-S mineral occurs. From 15.0 mbsf to 20.0 mbsf, there is one fragment of sulfide ore composed of 60% fine-grained sphalerite, 35 % fine-grained quartz and 5 % fine-grained pyrite and undetermined brownish sulfide mineral.

Unit 3:

Below the sulfide ore fragments zone to 25.0 mbsf, one fragment of dark greenish gray highly silicified volcanic rock containing 5 % fine-grained pyrite was recovered. In the last core of this cruise (25.0 - 30.0 mbsf, C9015C 5R-CC), Several pieces of dark greenish gray highly silicified volcanic rock containing 5 % fine-grained pyrite which are same materials of the above layer (20.0 - 25.0 mbsf) were recovered (Fig. 3-17).

3.2 XCT data

Y. Takaya/ T. Nozaki

Prior to split cores into working and archive halves, X-ray computed tomography (XCT) image consists of many axial (cross-section) radiographic images taken for every 0.65 mm (about 1,600 images for 1 m-length section). Whole 3D image is generated by combination of these 2D axial (cross-section) images. X-ray absorption number (CT number) of each target material reflects to brightness (whiteness) of the radiographic image. Since brightness of each point on the CT image basically indicates density of the scanned point, it is possible to interpret the lithological structure, density, consolidation degree and permeability of target material from the CT image in a qualitative manner. In this expedition, all core sections (72 sections) were scanned by X-ray CT in order to obtain the lithological information and to choose whole-round samples for microbiological researches and interstitial water squeezing. In the following part, the interpretation of characteristic CT image is explained based on the photograph and visual core description of each hole. Below identified units are not the same described in the previous section in some cases.

3.2.1 Hole C9016B

Lithology of Hole C9016B is explained by 7 characteristic lithological features; pumice, silty clay, hydrothermal altered clay, hydrothermal altered and anhydrite clay, clay with kuroko-like ore fragments, structure remained silicified volcanic rock, and highly silicified volcanic rock with sulfide minerals.

Typical pumice section is Core 1H-2 (Fig. 3-1). Aggregation of ~1.5 cm gray fragments is observed in the CT image. These fragments correspond to pumiceous gravels. Some light gray small fragments and bright white patches in the CT image may be quartz and feldspathic fragments.

Silty clay layer is observed in Core 1H-4 (Fig. 3-2). Whole section CT image shows homogeneous gray ~ light gray in color (slightly brighter (higher CT number) than pumiceous gravels). The 1 - 10 mm gray fragments correspond to pumiceous gritty patches.

Hydrothermal altered clay is typically observed in Core 2X-1 (Fig. 3-3). Clay layers show slightly lighter color than the overlying pumiceous gravels in the CT image. In the actual photograph, hydrothermal altered clay shows white, light gray, gray, brownish gray and greenish gray along with the change in the chemical composition and/or constituent minerals. It is possible to determine moderate changes of the mud component in the CT image. Several cm-sized spherical white patches in the CT image

correspond to the spherical aggregates of low-Fe fine-grained sphalerite, and scattered mm-sized white patches correspond to feldspathic grains and disseminated sulfide minerals.

Typical anhydrite clay layer (hydrothermal altered clay with thin anhydrite-rich layers and patches) is observed in the lower part (30.0 - 40.5 cm) of Core 2X-CC (Fig. 3-4). 1 mm-width anhydrite laminations can be easily identified as white ~ light gray veins in the CT image.

Kuroko-like sulfide ore fragments (semi-massive sulfide ore), which are mainly composed of fine-grained sphalerite (85%) and anhydrite (15%) and minor amounts of pyrite and galena, are often distributed in Core 5X-4 and 5X-CC (Fig. 3-7). Since the most of sulfide minerals are fine-grained and coexist with hydrothermal altered clay, the kuroko-like sulfide ore fragments are detected basically as homogeneous light gray part and mm-sized anhydrite and sulfide minerals are clearly distinguished as white patches in the CT image. However, it is impossible to distinguish these anhydrite and sulfide minerals without contrast tuning because the CT number of these fragments exceed the threshold and both anhydrite and sulfide fragments are represented as similar white patches in the CT image.

Typical structure-remained silicified volcanic rock is observed in Core 6X-1 (Fig. 3-8). Matrix part composed of hydrothermal altered clay is represented as homogeneous gray color in the CT image similar to the above interval. Since the structure-remained silicified volcanic rocks observed in this section are poorly-lithified, these rocks are represented as gray similar color to the hydrothermal altered clay part. Then, it is difficult to distinguish these rocks from hydrothermal altered clay in the CT image. On the other hand, sulfide grains are shown as bright white patches and are clearly separated from both volcanic rock and hydrothermal altered clay.

Highly silicified volcanic rock with sulfide minerals, which corresponds to “keiko-ore” in the typical lithological sequence in the kuroko-type VMS deposit on land, is typically observed in Core 15-CC. The highly silicified volcanic rock with sulfide minerals exhibits homogeneous light gray color with black veins in the CT image. The white oval fragment in ca. 23.0 cm of this section is an artificial material (metal material derived from the core catcher), and the white lines extending radially around the fragment is also artificial (halation made by too high X-ray absorption number).

3.2.2 Hole C9015B

Hole C9015B is explained by 3 characteristic lithological features; volcanic (including pumice) rock rubble, volcaniclastic breccia (drilling breccia?), semi-massive

sulfide ore, disseminated sulfide ore, and hydrothermal altered clay.

Volcanic rock rubble occurs in Core 1-CC. Since the volcanic rock rubbles likely moved around in the core during the core cutting operation, we cannot determine the exact relationship between the CT image (taken before the cutting operation) and core actual image (taken after cutting operation). Based on the results of the visual core description (VCD), the pumice rubbles correspond to gray fragments (middle CT number) and dense volcanic fragments correspond to whitish (high CT number) in the CT image, respectively.

Volcaniclastic breccia is typically observed in Core 2R-1 (Fig. 3-11). Volcanic breccia mainly consists of less than 5 mm-sized dacite - rhyolite fragments which are represented as whitish small fragments in the CT image. It is difficult to distinguish from these rock fragments, but, native sulfur and sulfide grains are also represented as whitish fragments in the CT image. On the other hand, some pumice fragments are clearly detected as gray color zone in the CT image.

Semi-massive sulfide ore and disseminated sulfide ore are observed in Core 5R-1 (Fig. 3-13). Typical semi-massive sulfide ore occurs in the center part of the core (10.0 - 15.0 cm in the core photo) and disseminated ore is located at the bottom part of this core. Semi-massive sulfide ore is mainly composed of sulfide minerals (70%) and quartz (30%). In the CT image, this sulfide ore fragment is fogged by halation due to the sulfide grains with very high CT number. The change of brightness in the rock fragment may correspond to the fractions of sulfide and silicate (quartz) minerals. Meanwhile, the disseminated sulfide ore is represented as whitish gray zone in the CT image reflecting the lower sulfide mineral fraction than that of the semi-massive sulfide ore. It is possible to detect the small change of sulfide/silicate fraction and to separate the semi-massive sulfide ore and disseminated sulfide ore in the CT image.

3.2.3 Hole C9015C

Hole C9015C is explained by 4 characteristic lithological features; soupy silt, disseminated sulfide ore, semi-massive sulfide ore, and greenish gray highly silicified volcanic rock.

Soupy silt is observed from Core 1R-1 to Core 1R-CC (Fig. 3-15). In the CT image, the soupy silt is represented as homogeneous dark gray ~ gray zone. Scattered white patches in the CT image may correspond to small volcanic rock fragments.

Typical disseminated sulfide ore occurs in the bottom part of Core 2R-CC and is observed as a white fragment with some halation in the CT image (Fig. 3-16). Some dark gray zones in the CT image represent the pore space in the ore fragment.

Semi-massive sulfide ore is observed in Core 3R-CC. In the CT image, this sulfide ore is represented as a white fragment with some halation which is very similar to the disseminated sulfide ore in Core 2R-CC.

Typical greenish gray highly silicified volcanic rock is located in Core 4R-CC and 5R-CC (Fig. 3-17). This greenish silicified rock corresponds to a whitish gray area in the CT image. Some white patches in the CT image correspond to pyrite grains.

3.3 Physical property measurement

Yuka Masaki, Ryota Nakajima, Tomohiko Fukushima, Wataru Arai

Continuous physical property measurements provide basic information to assist characterization of lithologic units and states of consolidation and deformation. During this Expedition, we obtained thermal conductivity data and MSCL-W data as a physical property.

THERMAL CONDUCTIVITY

Thermal conductivity measurements were conducted on whole-round core samples using a needle probe method (VLQ probe) and/or on split cores using a half-space method (HLQ probe) and a TeKa TK04 thermal conductivity meter.

The TK04 determines thermal conductivity based on a transient heat flow method. The heating wire and a temperature sensor are incorporated in a needle probe. When the wire is heated, the surface temperature of the probe is recorded simultaneously. The thermal conductivity of the surrounding material can be calculated from the temperature versus time measurement curve based on the simple calculation of the thermal conductivity coefficient.

$$k_a(t) = (q/4\pi)\{\ln(t_2) - \ln(t_1)\}/(T(t_2) - T(t_1)),$$

where

q = the heat input per unit length unit length and unit time,

$k_a(t)$ = the apparent thermal conductivity,

t_1, and t_2 = picking times,

and

$T(t_1)$, and $T(t_2)$ = the corresponding source temperatures,

respectively.

Since $k_a(t)$ is not constant but depends on the time interval used for calculation of thermal conductivity, the real thermal conductivity is approached only for sufficiently large heating times. A special approximation method (SAM) in the TK04 software automatically detects disturbances and determines the optimal time interval of the heating curve for evaluation. Heating power and evaluation parameters are changed depending on the specific sample.

During this Expedition, thermal conductivity measurements are made once in each

core section. For the whole-round cores and half cores of each section. A 2 mm diameter temperature probe (VLQ) was inserted into the working half of the core section. At the beginning of each measurement, temperature in the samples was monitored automatically without applying a heater current until the background thermal drift was determined to be <0.2 m K h^{-1}. The heater circuit closed automatically and the temperature increase in the probe was recorded.

For cores that were too consolidated to permit use of the needle probe, we used a half-space method measurement. The HLQ probe was placed on a flat surface of the sample with the line probe oriented parallel to the core axis, and heating and measurements were conducted automatically. The core and the probe were placed in a cooler, wrapped in a soft cloth and covered with a piece of bubble-wrap to maintain the ambient temperature. The measurement of temperature drift and conductivity was conducted in the same way as with the VLQ probe.

During each 24h period, the TK04 must be calibrated with standard blocks; the blocks have nominal conductivities of 1.623 ± 2% $Wm^{-1}K^{-1}$ for the VLQ probe and 1.652 ± 2% $Wm^{-1}K^{-1}$ for the HLQ probe, respectively. Measurement results for the standard block were then plotted against the true values, and the slope of the linear regression obtained was used to calibrate core sample measurements.

3.4 Personal sampling and methods

3.4.1 Tatsuo Nozaki and Yutaro Takaya (907TN)

Whole-rock geochemical analysis of hydrothermal altered sediment and sulfide/sulfate ores:

(1) Whole-rock geochemical compositions of sulfide/sulfate ore samples will be determined by ICP-MS to understand sulfide mineralization and ore grade. Combined these data with ore petrologic depictions (see 3.4.4 section), the depth profile of sulfide/sulfate mineralization in this area will be clarified. These powder samples will be also used for XRD analysis to identify constituent minerals. These samples were picked up as ore/rock fragments.

(2) Whole-rock geochemistry of sediment will be determined by ICP-MS analysis. These samples were collected next to the 907SAKI samples (see 3.4.5 section). Combined with whole-rock geochemical data and depictions of constituent clay minerals, we aim to understand depletion and enrichment of various elements by hydrothermal alteration. These samples were collected from 2-cm width whole part of working-halves.

(3) Whole-rock Pb, Hg, Fe, Zn, Ag and Re-Os isotope compositions of sulfide ores will be measured by collaborating with co-requestors. Compared with the data obtained from seafloor chimney/mound and sub-seafloor ore body, isotope fractionation system of these elements will be understood. Moreover, by comprehending the Pb, S and Os isotope compositions in the unaltered sediment and volcanic rock (wallrock) together with sulfide/sulfate ore, we aim to understand the metal source of the sulfide/sulfate ore.

(4) Several cm-sized low-Fe fine-grained sphalerite aggregates sparsely occur in the drilled core and these are used for petrologic and chemical study by using polished section, XRD, EPMA and ICP-MS analyses.

Our samples are taken from C9016B (50 samples) and C9015B (7 samples).

3.4.2 Toru Yamasaki (907TY)

Petrological observation and chemical analysis of volcanic rock:

In order to understand igneous processes and petrologic and geochemical features of igneous basement rocks in the Iheya-North Knoll, pumices, volcanic rock fragments and altered volcanogenetic clay are sampled. All samples are taken as half-round core from working-halves.

Pumices and pumiceous gravel in Hole C9016B, 1H (5 samples) will be used for description and bulk chemical composition analyses (XRF, ICP-MS). Highly altered and/or silicified volcanogenetic rocks in Hole C9016B, 7X-2, 8X-CC, 10X-CC, 11X-1,

13X-CC and 15X-CC will be used for description and bulk chemical composition analyses, in order to compare with pumices in interval above. Volcanic rock fragments (probably fragments of lava) in Hole C9015B, 2R-CC, 3R-1 and 4R-CC are the freshest volcanic rocks samples recovered in this expedition. Thus, these samples will be used for petrological description and several bulk rock geochemical analyses to understand petrologic and geochemical features of basement rocks. Highly silicified sample from Hole C9015B, 4R-CC will be used for description and bulk chemical composition analyses, in order to compare with fresh rocks in interval above.

3.4.3 Yutaro Takaya and Shinsuke Kawagucci (907TAK)

Water content and dry density:

In order to measure water (H_2O) content and dry density, the 7 cc-cubic sampling often used for paleomagnetic study was conducted for Hole C9016B (65 samples) and 9015B (4 samples). The hard rock part was avoided at sampling and these samples were collected in the interval of ca. 50 cm.

3.4.4 Syuhei Totsuka (907SYU)

Petrologic study of sulfide and sulfate ore:

Disseminated and semi-massive sulfide ores or volcanic rocks containing sulfide/sulfate minerals are preferentially collected from Hole C9016B (37 samples), Hole C9015B (5 samples) and Hole C9015C (2 samples). Thin sections on the slide glass and polished sections in a 1-inch diameter resin will be made for microscopic observation to identify sulfide, sulfate and gangue silicate minerals. Besides the microscopic observations, these thin and polished sections will be utilized for EPMA analysis to understand the chemical composition of constituent minerals. Based on these experiments, the depth profile of sulfide/sulfate mineralization will be clarified. Combined with the depiction of altered clay minerals (see 3.3.5 section), sulfide mineralization style and hydrothermal alteration will be compared with those of the kuroko-type VMS deposit on land. These thin and polished sections will be also used for the collaborative study of Cu, Pb and S isotope analysis by LA-ICP-MS at Tsukuba University and JAMSTEC together with co-requestors.

3.4.5 Saki Tsutsumi (907SAKI)

Hydrothermal alteration focusing on clay minerals:

Sedimentary samples including hydrothermal altered clay minerals are preferentially collected from Hole 9016B (37 samples) and Hole 9015B (1 sample). The

samples corrected from Hole 9016B cover the range of Core 1H-4 to 14X-CC and composed of unaltered silty clay sediment, pale greenish glauconite(?)-rich sediment, hydrothermal altered gray ~ light gray clay layer with anhydrite, hydrothermal altered gray ~ light gray clay layer intercalated with dark greenish highly silicified volcanic rock. Two samples collected from Hole 9016B 15X-1 and Hole 9015B 5X-CC are light greenish highly silicified volcanic rock fragment including dark greenish metamorphic mineral (chlorite?). These sediments were collected from the 2 - 4 cm width whole parts (34 - 68 cc) of the working-halves. Clay minerals will be determined by XRD and EPMA analyses and TEM observation via elutriation of clay minerals, aiming to understand the depth profiled of clay mineral component and hydrothermal alteration zoning. Thin sections will be made for two highly silicified volcanic rock fragments for microscopic observation to comprehend metamorphic mineral assemblage.

3.4.6 Hidenori Kumagai (907HK)

Outreach activity:

Typical samples of representative lithological unit drilled in this expedition were selected and collected for outreach activity such as press release and exhibition. These samples were collected from Hole 9016B 2X-CC, 5X-CC, 8X-CC, 10X-CC, Hole 9015B 5R-1, Hole C9015C 2R-CC and4R-CC, which cover hydrothermal altered clay, semi-massive sulfide ore, highly silicified volcanic breccia, highly silicified fine-grained quartz-rich rock with less than 5% sulfide minerals, allochthonous semi-massive sulfide ore fragment derived from peripheral mound (?) and dark greenish gray highly silicified volcanic rock containing 5% fine-grained pyrite. These samples were preferentially selected from the core capture part because these samples are not used for analytical research after the expedition.

3.4.7 Masanobu Kawachi (907KAW)

Elution of heavy metal components from core specimen and the impact on phytoplankton community:

Oceanic phytoplankton is generally sensitive for particular heavy metal elements. Core specimens will be used for the elution experiments targeting heavy metals under the different conditions. After confirming chemical component of the eluted solution with inductively-coupled plasma mass spectrometry (ICP-MS), we apply the solution and the particular heavy metal components to growth experiment of phytoplankton, monitoring of biodiversity with metagenomics and/or particular gene expressions. Effects of heavy metals on phytoplankton community will be assessed in detail. These

samples were collected from Hole 9016B 1H-1, 1H-4, 1H-8, 2X-3 and 4X-CC as the 3 or 4 cm-width whole part (51 or 68 cc) of the working-halves.

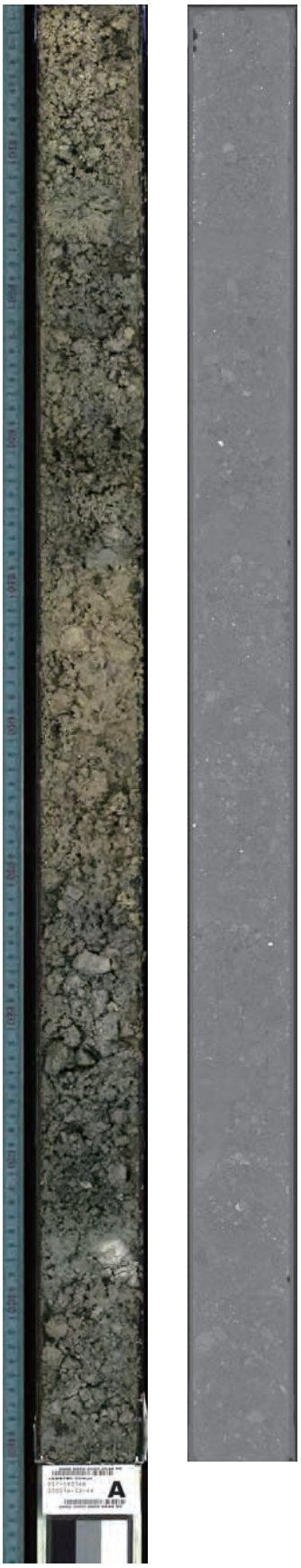

Fig. 3-1 Scanned color image and XCT image of Core9016B 1H-2

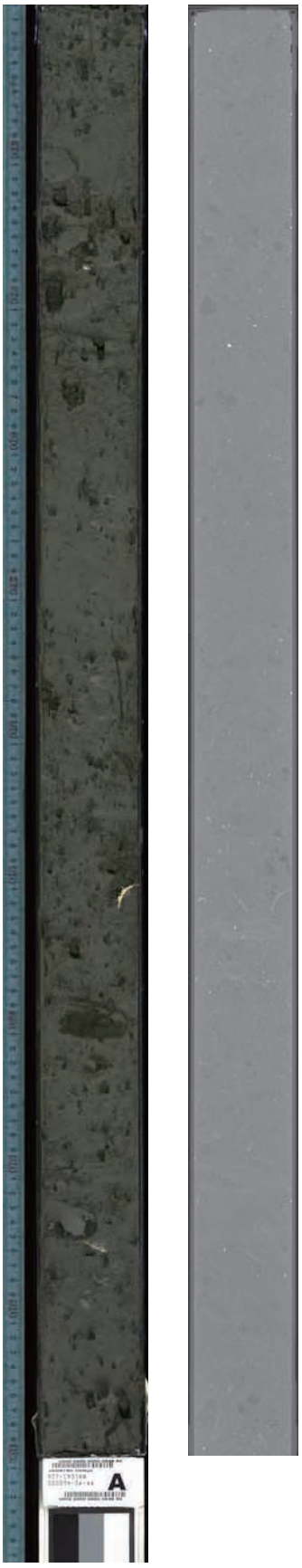

Fig. 3-2 Scanned color image and XCT image of Core9016B 1H-4

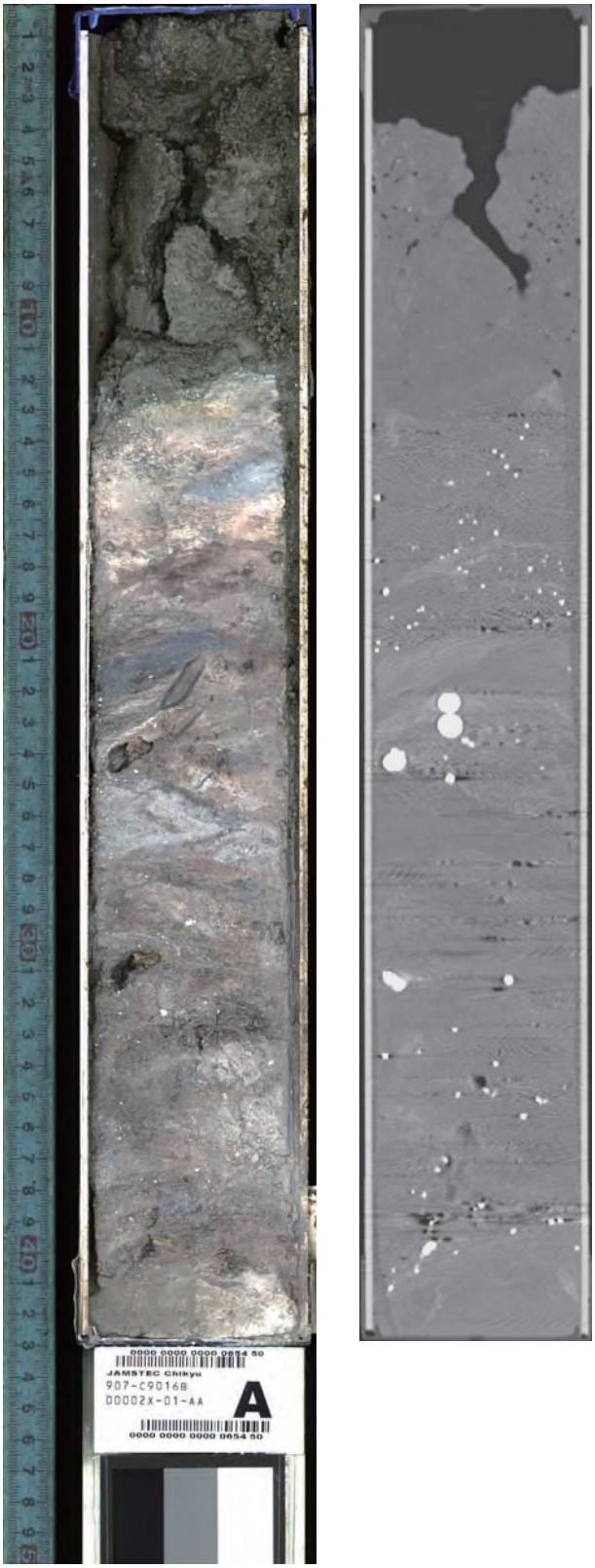

Fig. 3-3 Scanned color image and XCT image of Core9016B 2X-1

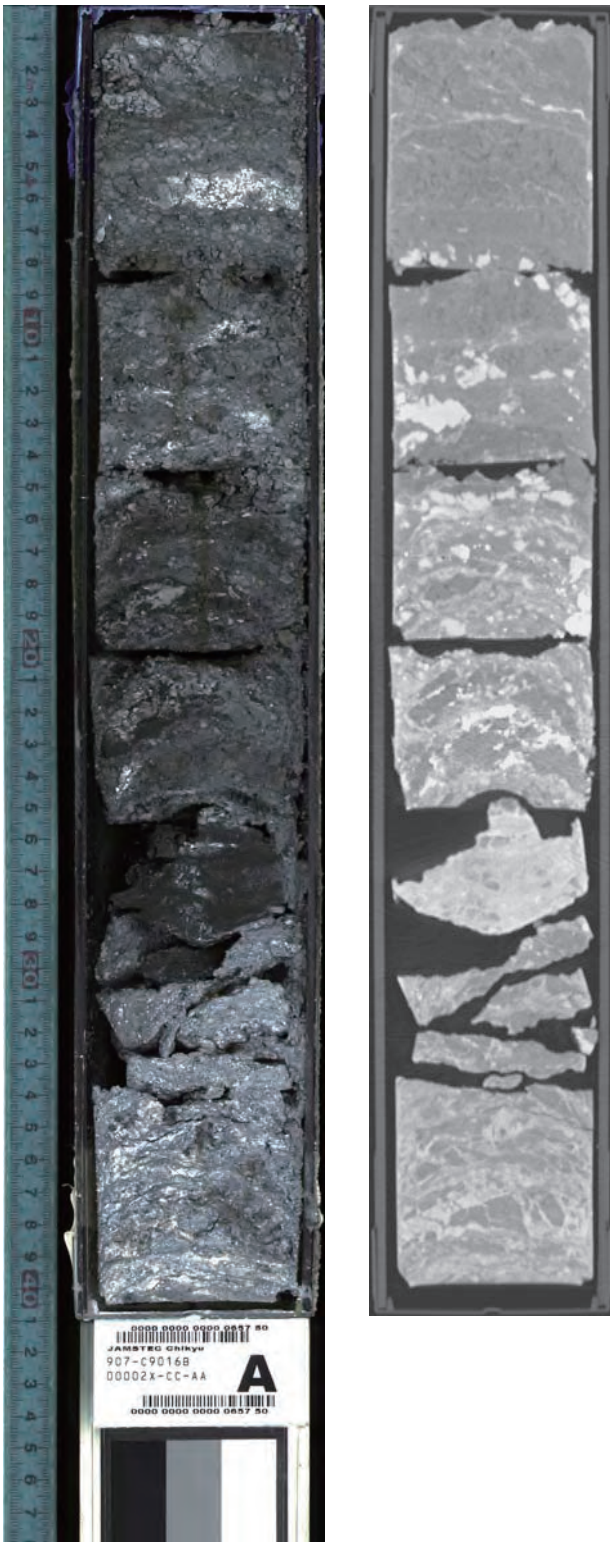

Fig. 3-4 Scanned color image and XCT image of Core9016B 2X-CC

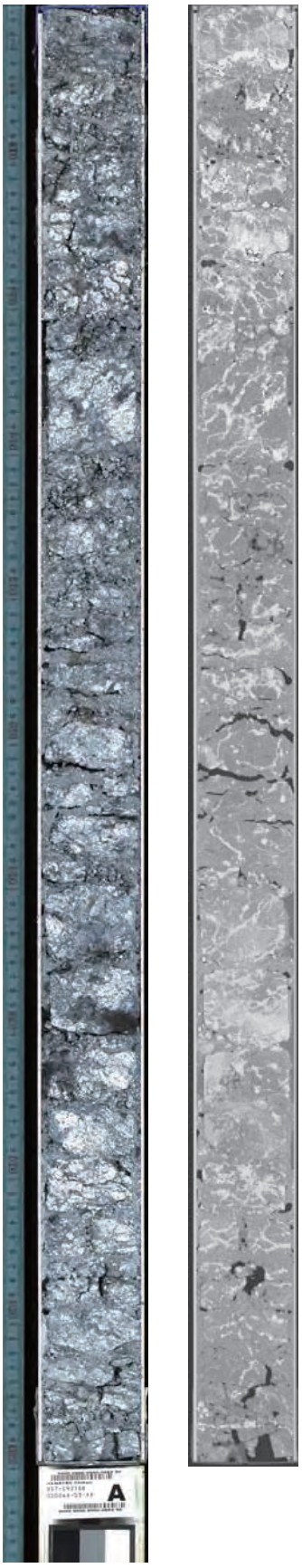

Fig. 3-5 Scanned color image and XCT image of Core9016B 4X-3

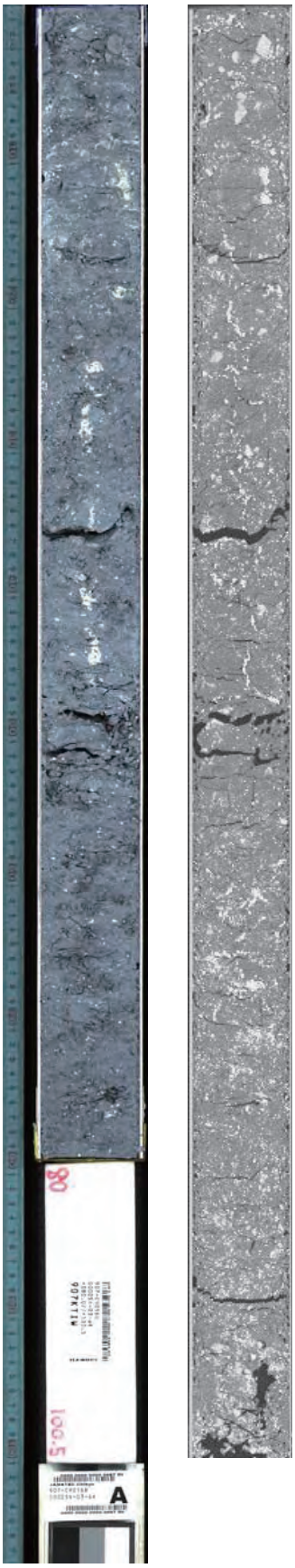

Fig. 3-6 Scanned color image and XCT image of Core9016B 5X-3

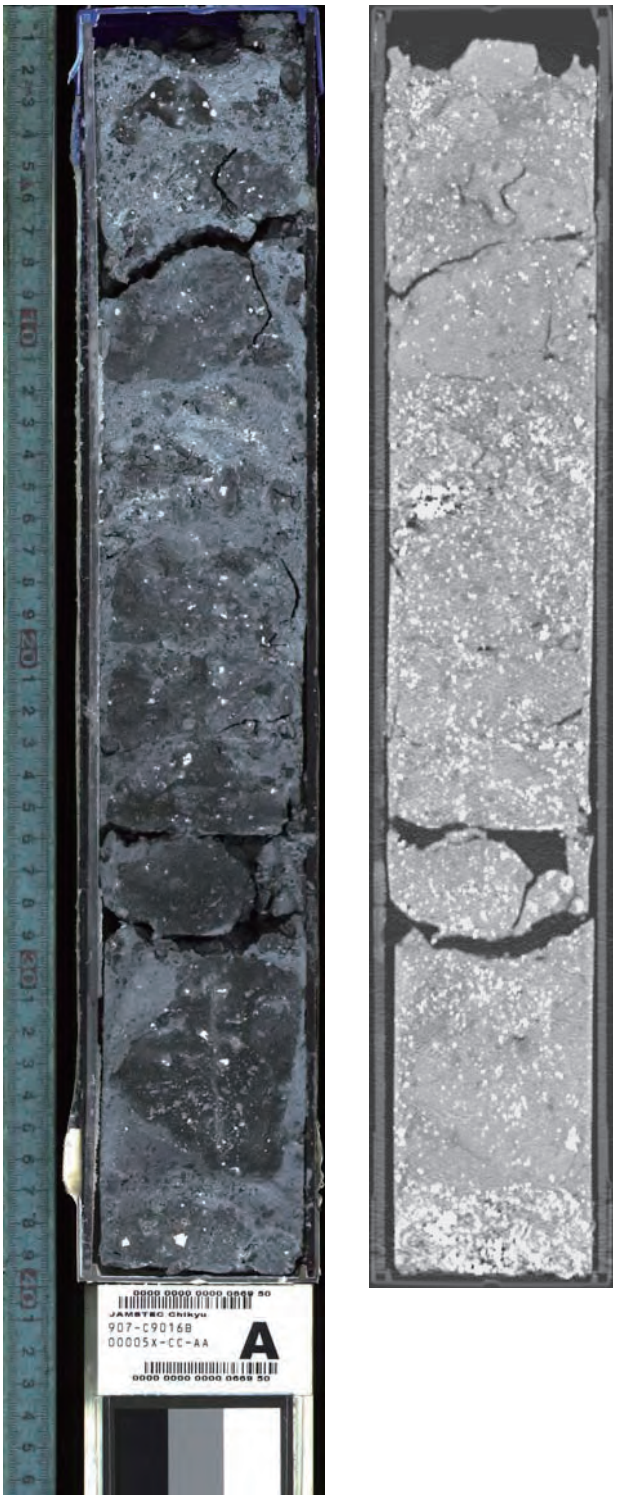

Fig. 3-7 Scanned color image and XCT image of Core9016B 5X-CC

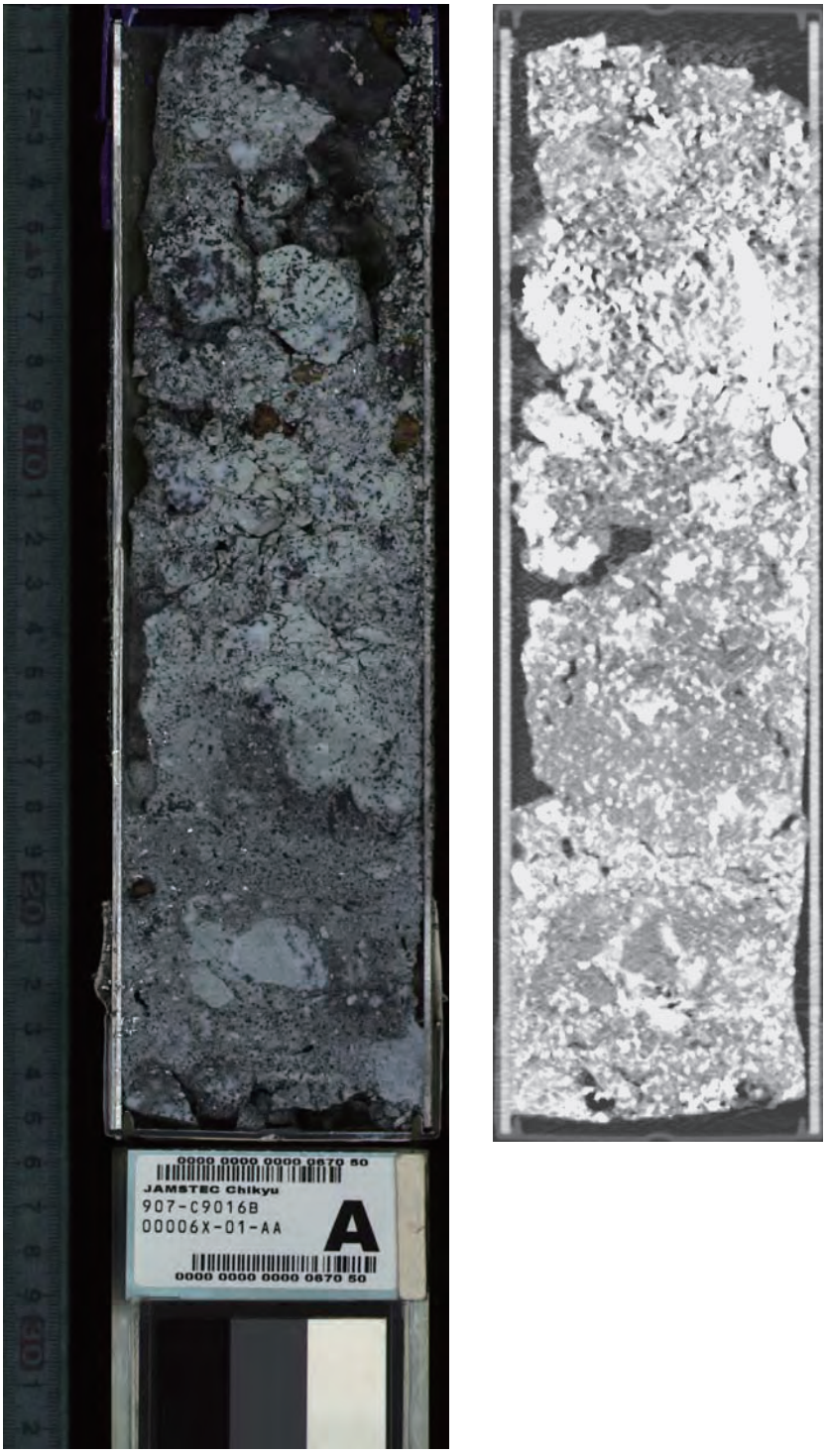

Fig. 3-8 Scanned color image and XCT image of Core9016B 6X-1

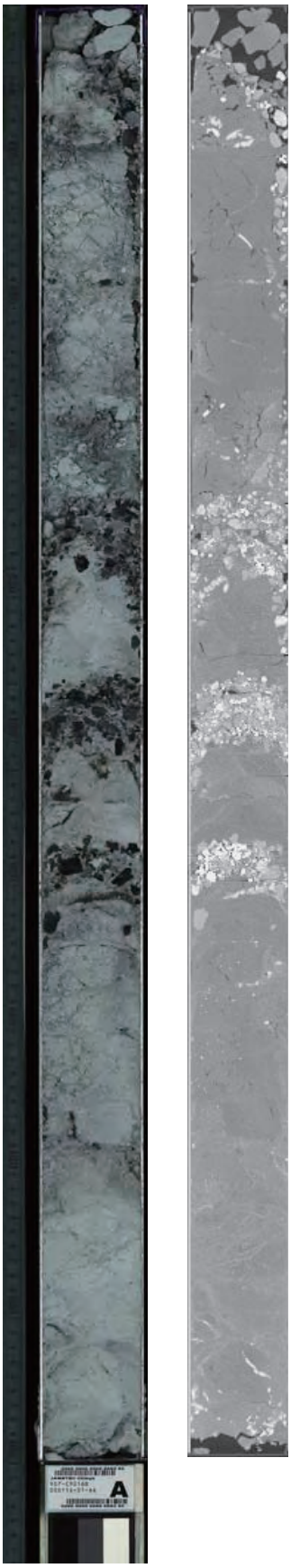

Fig. 3-9 Scanned color image and XCT image of Core9016B 11X-1

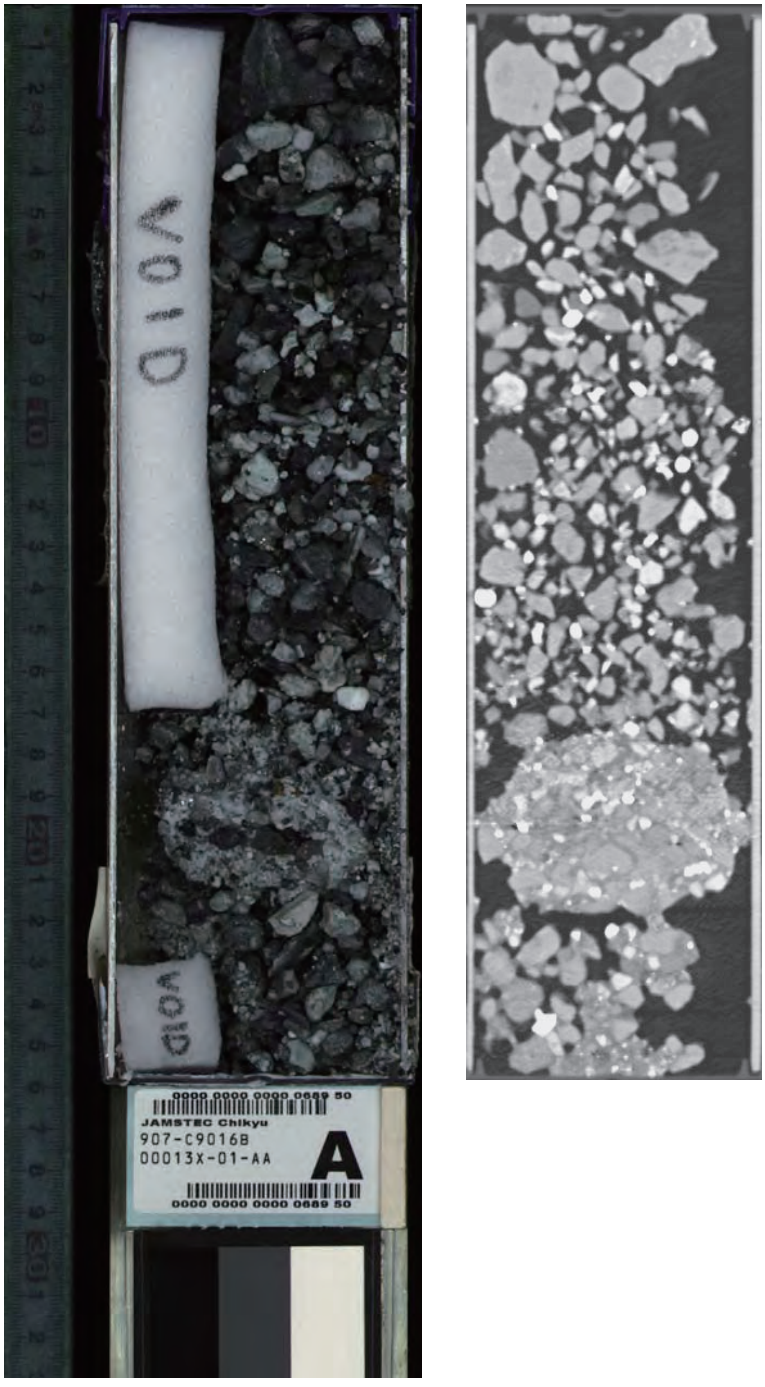

Fig. 3-10 Scanned color image and XCT image of Core9016B 13X-1

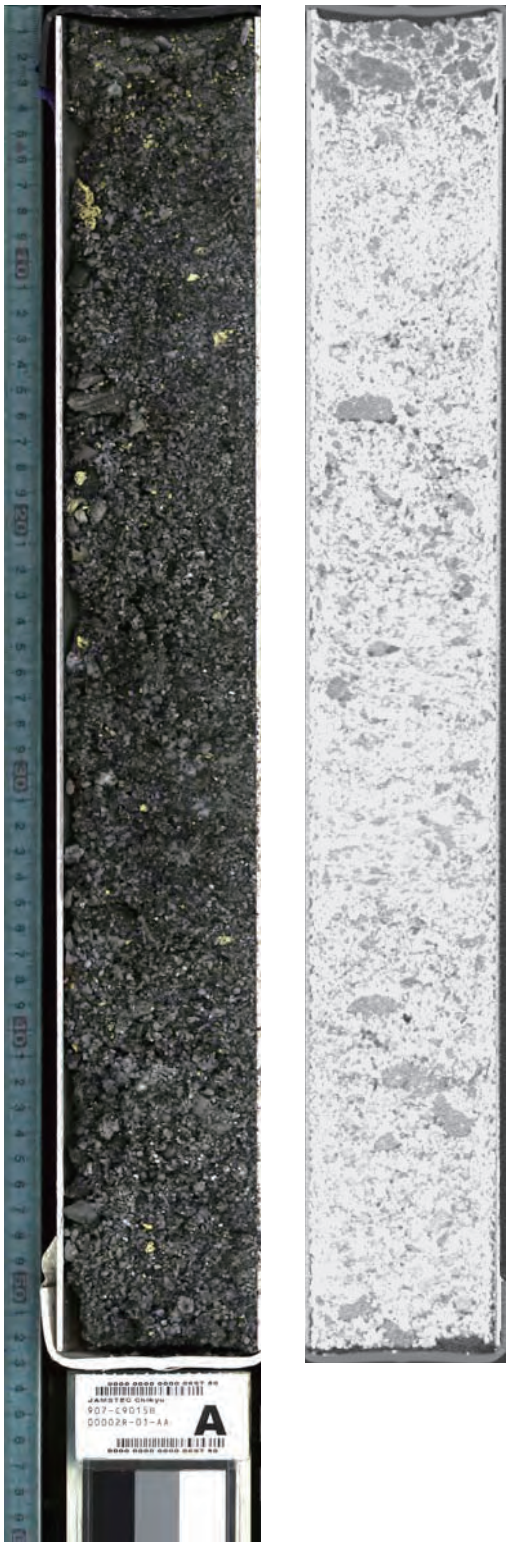

Fig. 3-11 Scanned color image and XCT image of Core9015B 2R-1

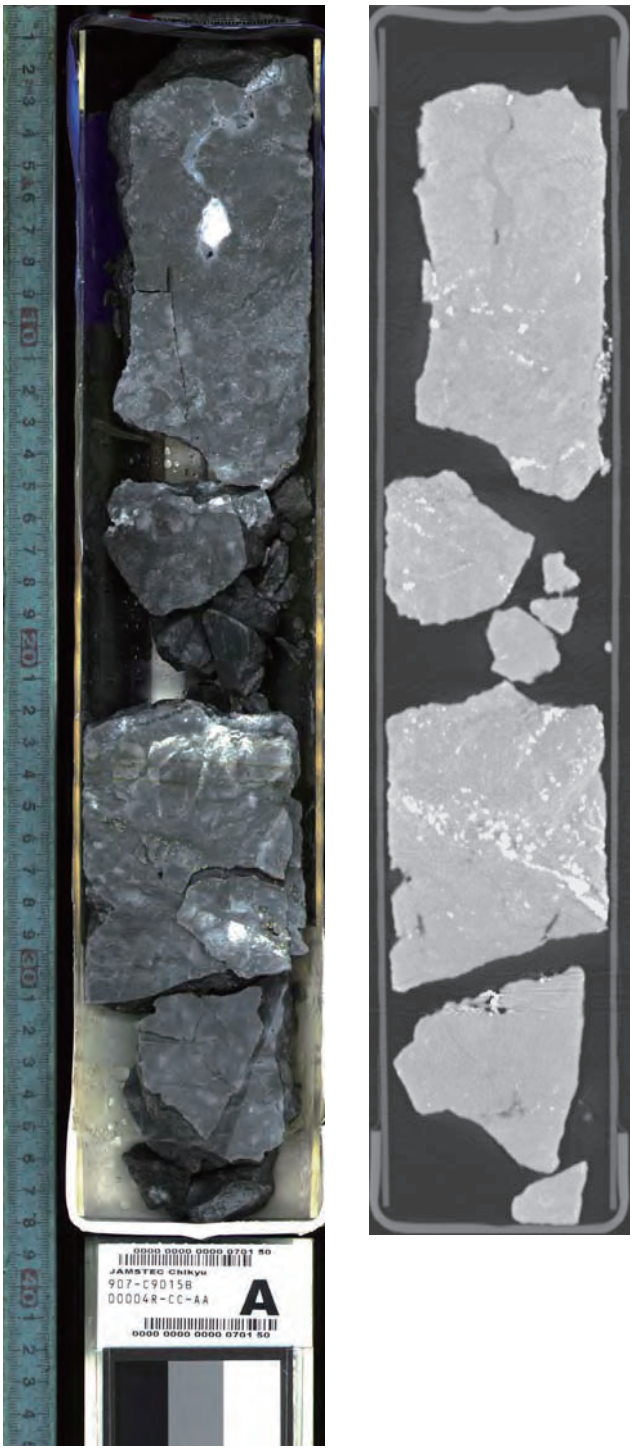

Fig. 3-12 Scanned color image and XCT image of Core9015B 4R-CC

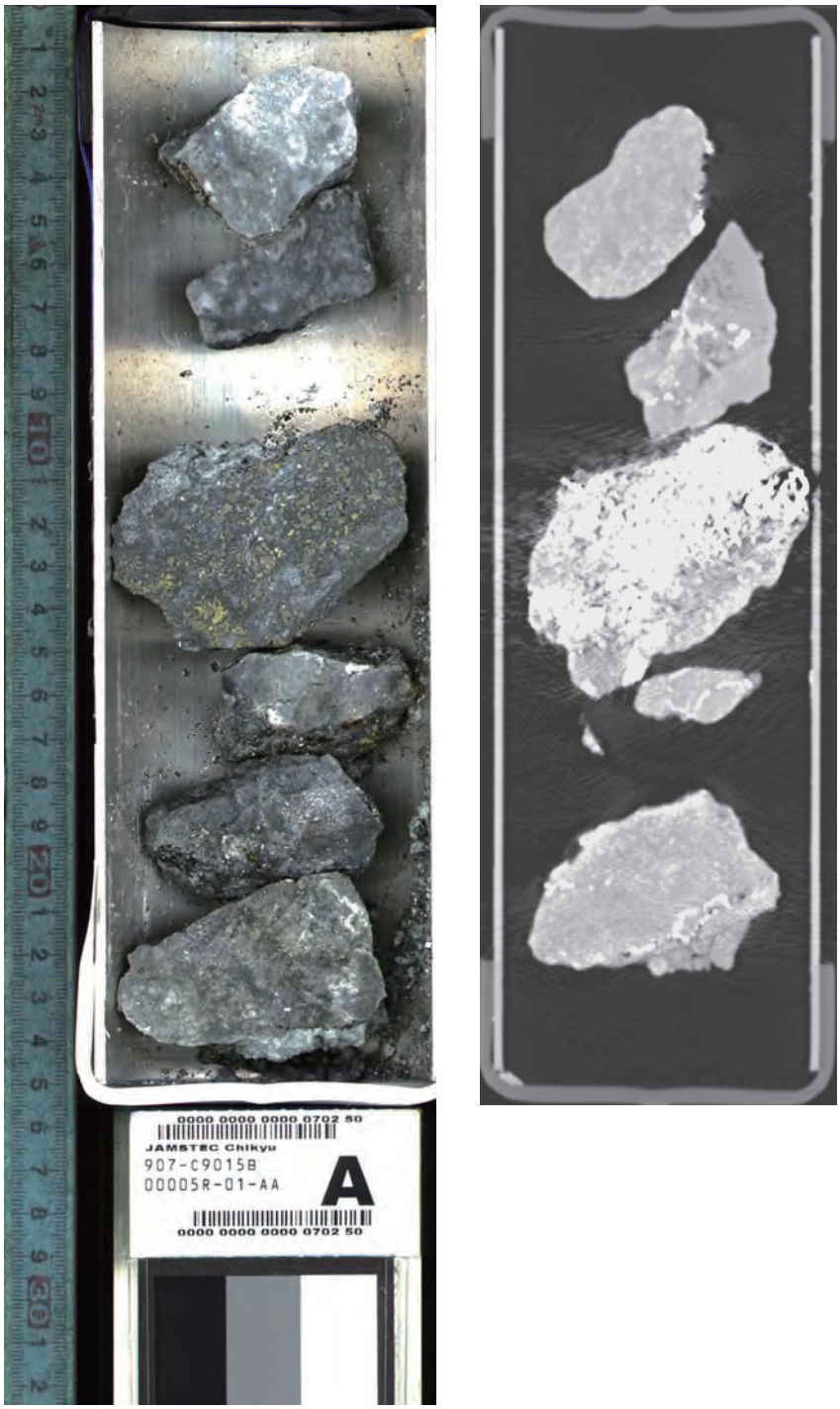

Fig. 3-13 Scanned color image and XCT image of Core9015B 5R-1

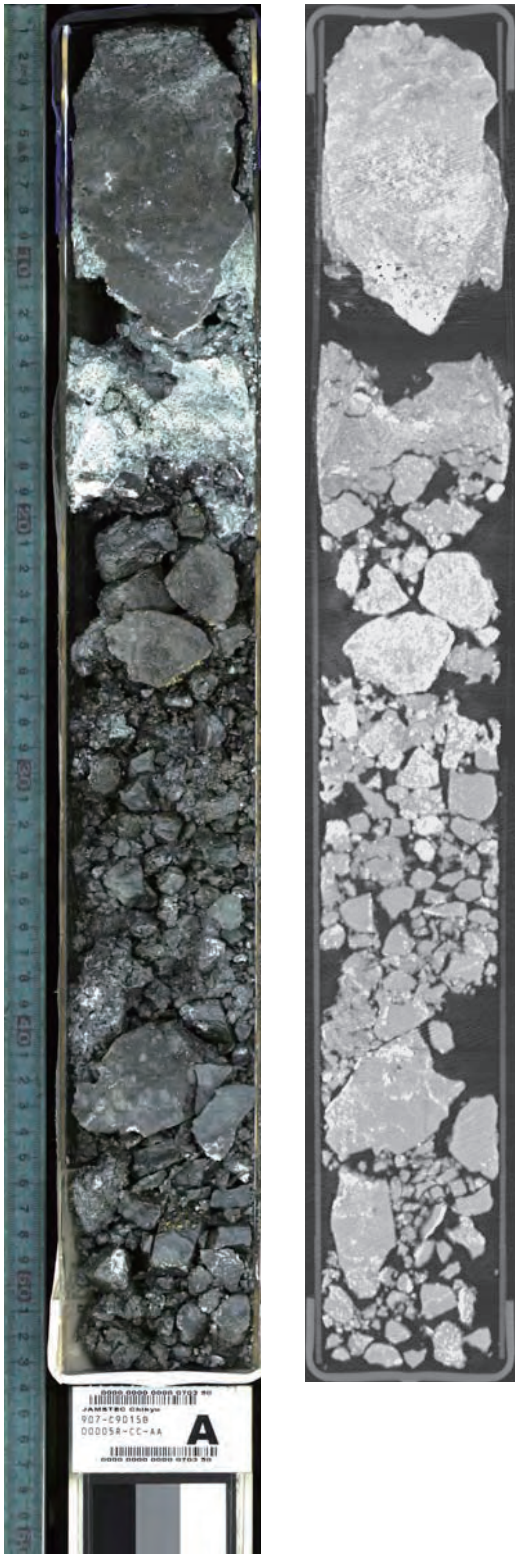

Fig. 3-14 Scanned color image and XCT image of Core9015B 5R-CC

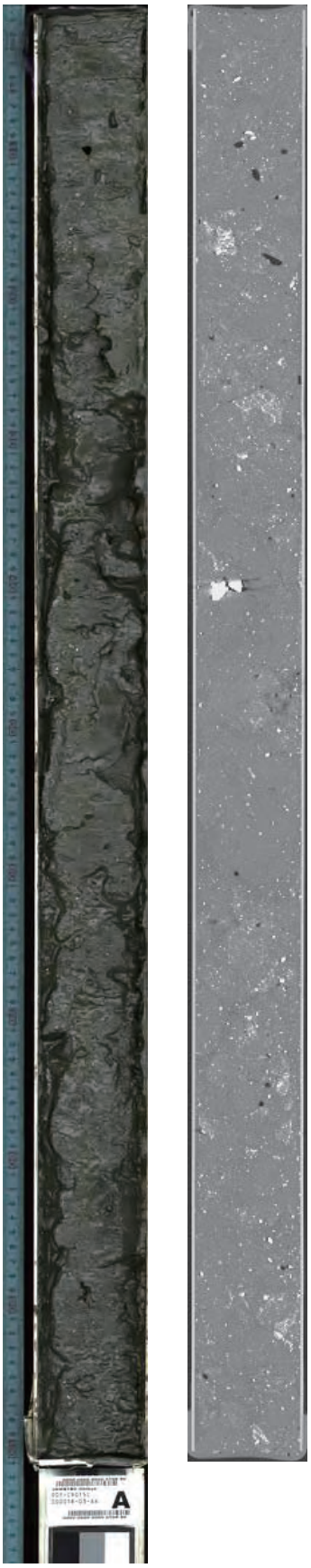

Fig. 3-15 Scanned color image and XCT image of Core9015C 1R-3

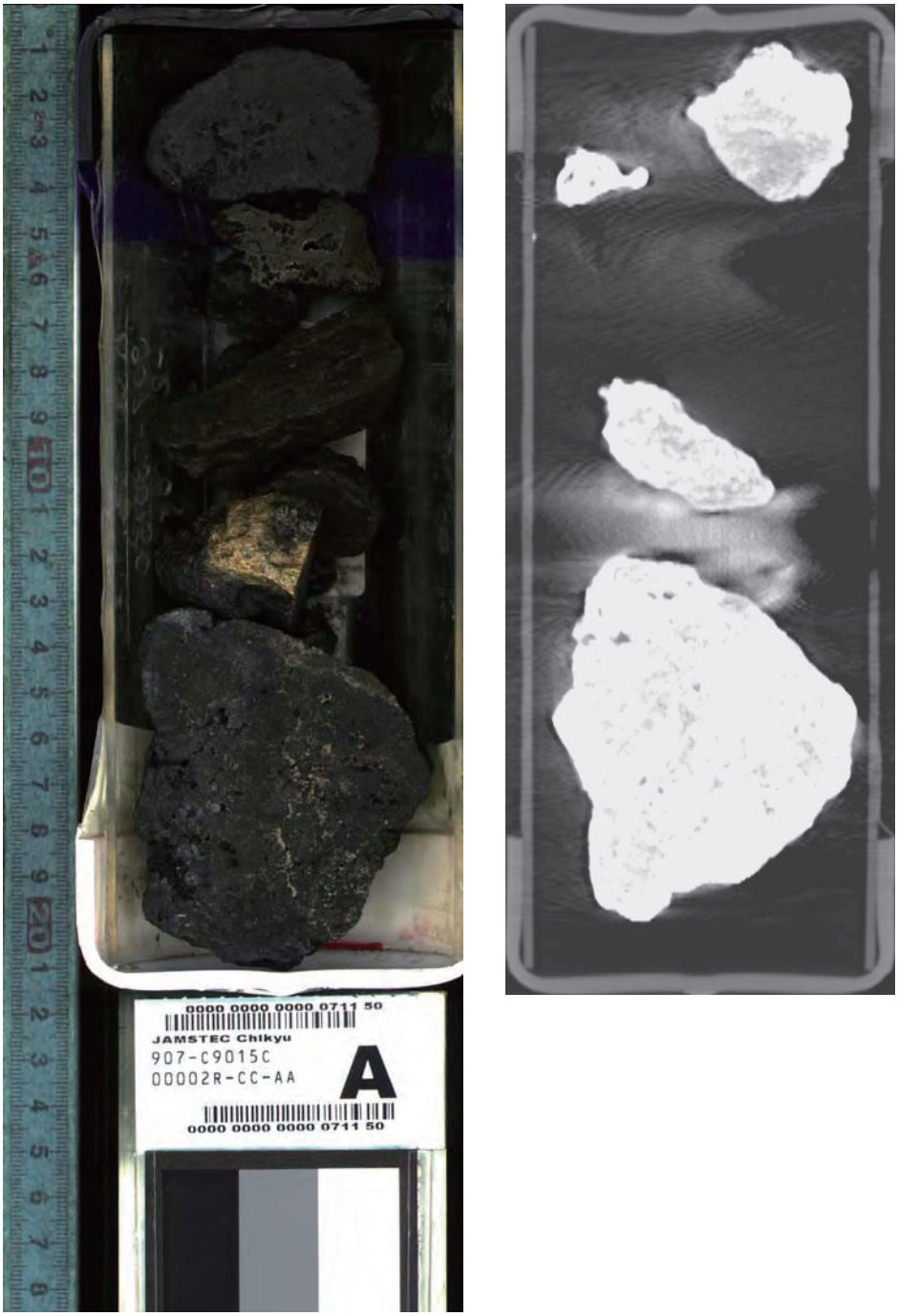

Fig. 3-16 Scanned color image and XCT image of Core9015C 2R-CC

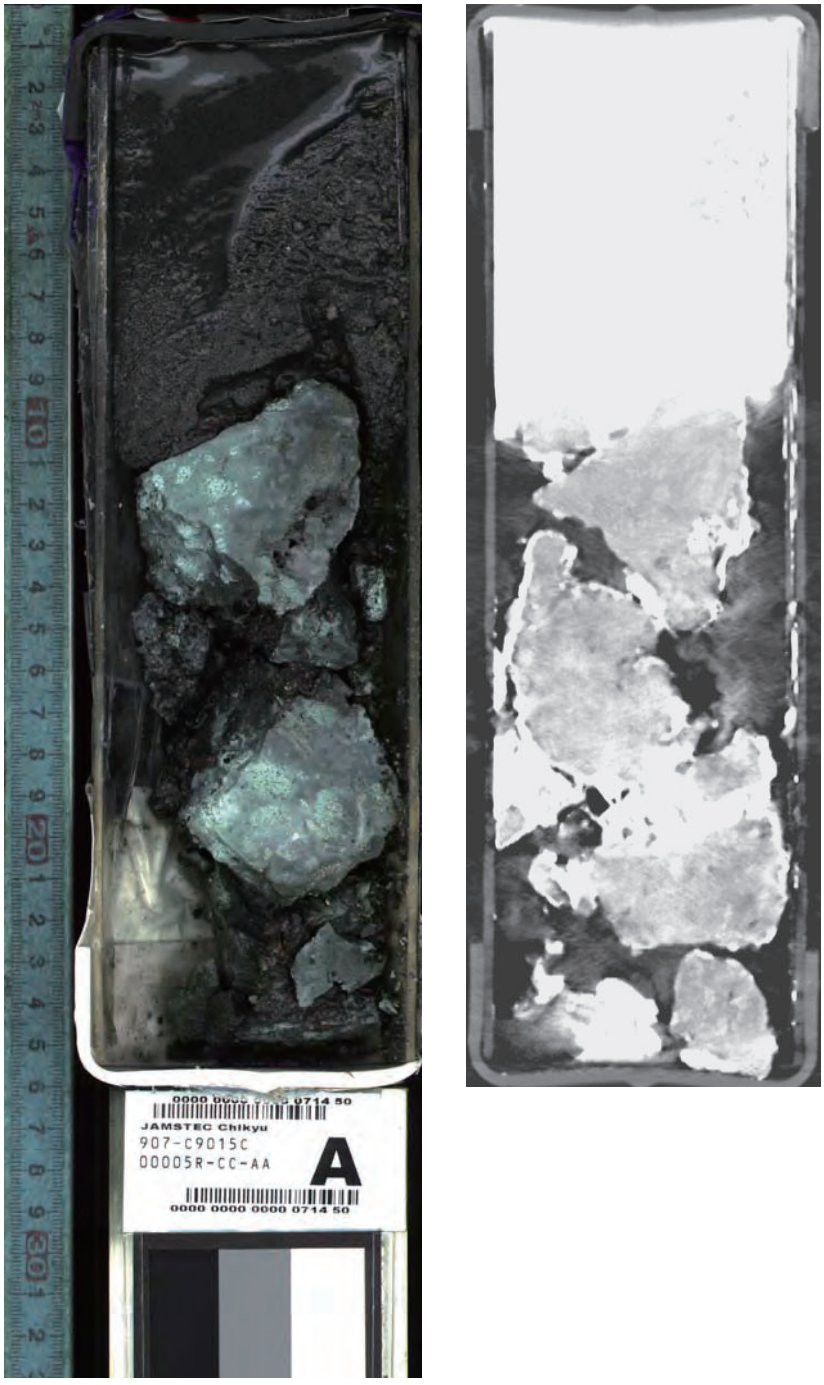

Fig. 3-17 Scanned color image and XCT image of Core9015C 5R-CC

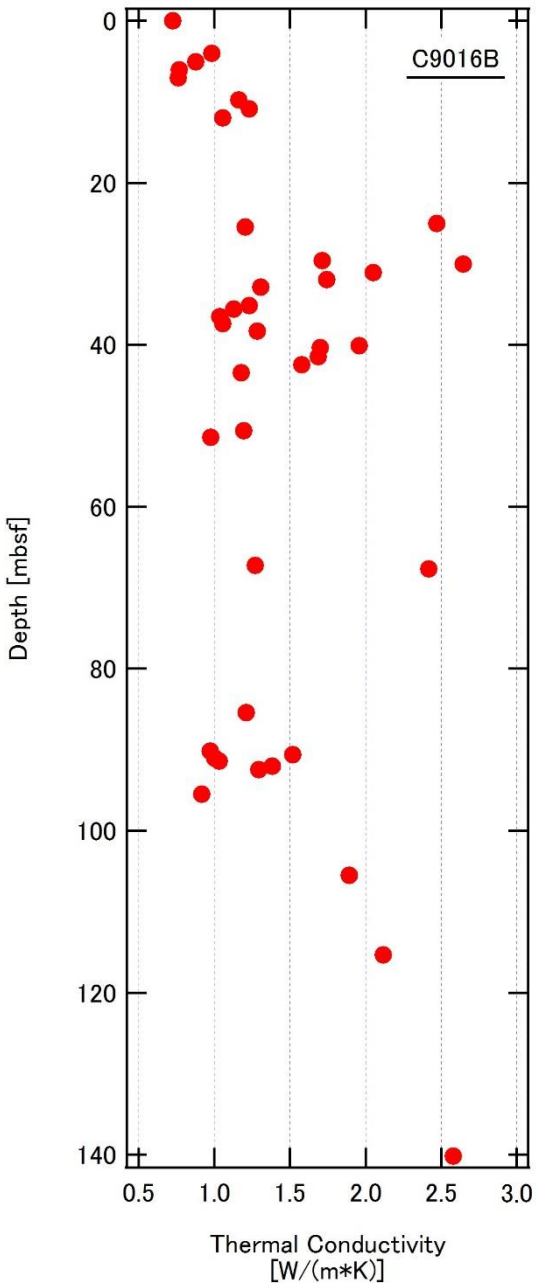

Fig. 3-18 : Depth profile of thermal conductivity at Hole C9016B

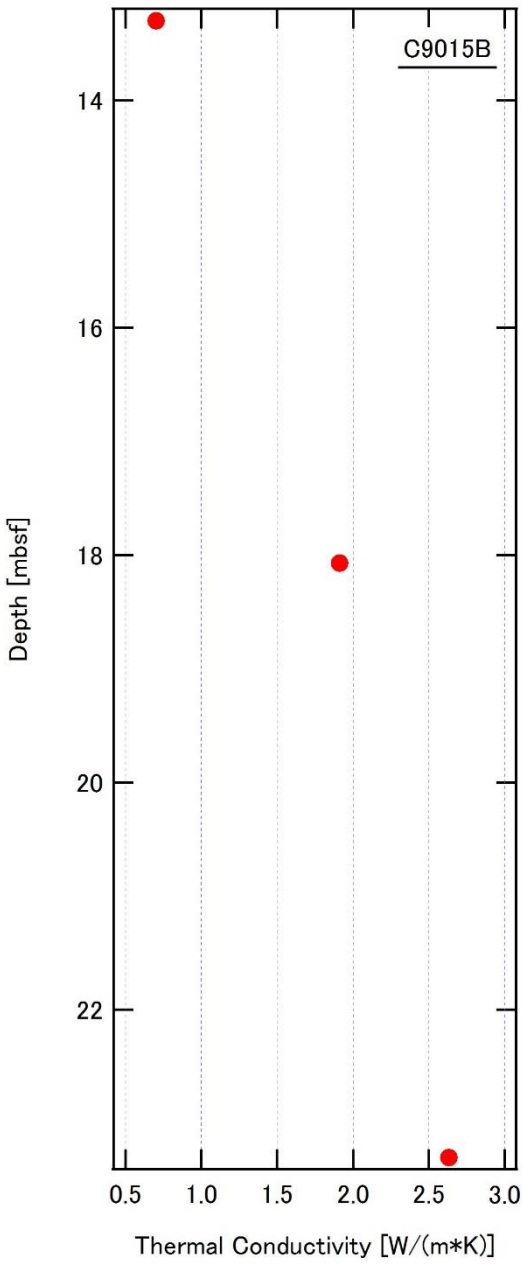

Fig. 3-19 : Depth profile of thermal conductivity at Hole C9015B

Chapter 4. Environmental surveys by remotely operated vehicle

Hiroyuki YAMAMOTO

An environmental assessment is a process used to estimate the consequence of any kind of disturbance on an environment or ecosystem. The drilling expedition on hydrothermal system involves a probability to alter the fluid pathway of subseafloor and affect the biogeographic pattern of organisms. This alternation is thought to be common phenomenon in hydrothermal system, caused by volcanic activity or deformation of geological structure. On the other hand, the hydrothermal system attracts mining company seeking valuable mineral resource. To provide estimation of the disturbance of future exploitation, baseline data on the ecosystem from surface to seabed should be collected to prepare a better management system of marine ecosystem.

IODP Expedition 331 on Iheya North Knoll had been carried out on September 2010, and three-years post-drilling survey discovered a dramatic succession of seafloor biota on the expedition areas, where an artificial thermal vent has been created. It is difficult to meet such succession process under natural condition, except sterilization by volcanic eruption or alternation by scientific drilling expedition.

CK14-04 drilling cruise planned an expedition to find the extent of subseafloor fluid pathway. We anticipated that a similar alteration after Ex331 might occur on some area of drilling point. In this cruise the following works have been done to collect the information on habitat condition, biota and microbial community.

4.1 Preparation of payload

Hiroyuki YAMAMOTO, Ryota NAKAJIMA, Yuka MASAKI
Masayuki WATANABE

D/V “Chikyu” has a remotely operated vehicle (ROV), which is operated by OCEANEERING International Inc., as supporting device in drilling activity. The ROV is a commercial product from HYDRA MAGNUM employing the side-entry cage system with tether cable connection. In this cruise, we planned to use this ROV equipped in DV “Chikyu” and for pre-drilling site-survey and sediment core sampling. To achieve this purpose, a payload basket was made by the ROV engineers. The basket could transport three MBARI push core samplers and a vacuum fluid sampler, and could be carried by hanging it on the beam of ROV cage (Fig 4.1-1). The CTD-pH sensor (XR 420 CTD with AMP pH combined sensor, RBR Limited) was installed a

left side of the vehicle, the stand-alone heat flow meter (SAHF) put on the beam of the ROV cage. Operations on the seabottom were shown in Fig 4.1-2.

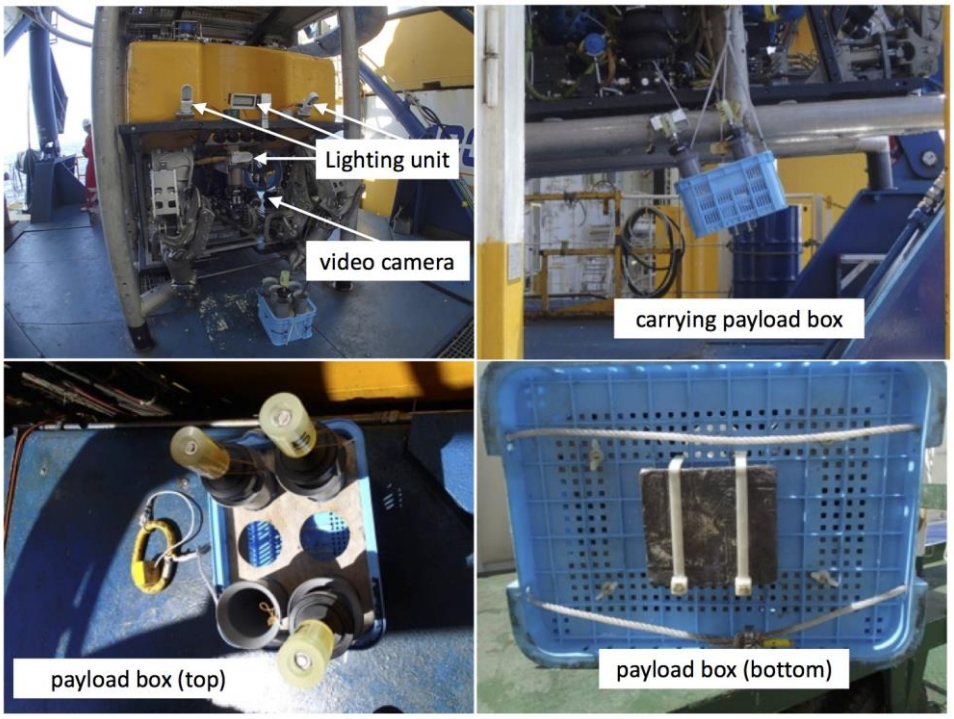

Fig 4.1-1 Appearance of ROV and payload basket

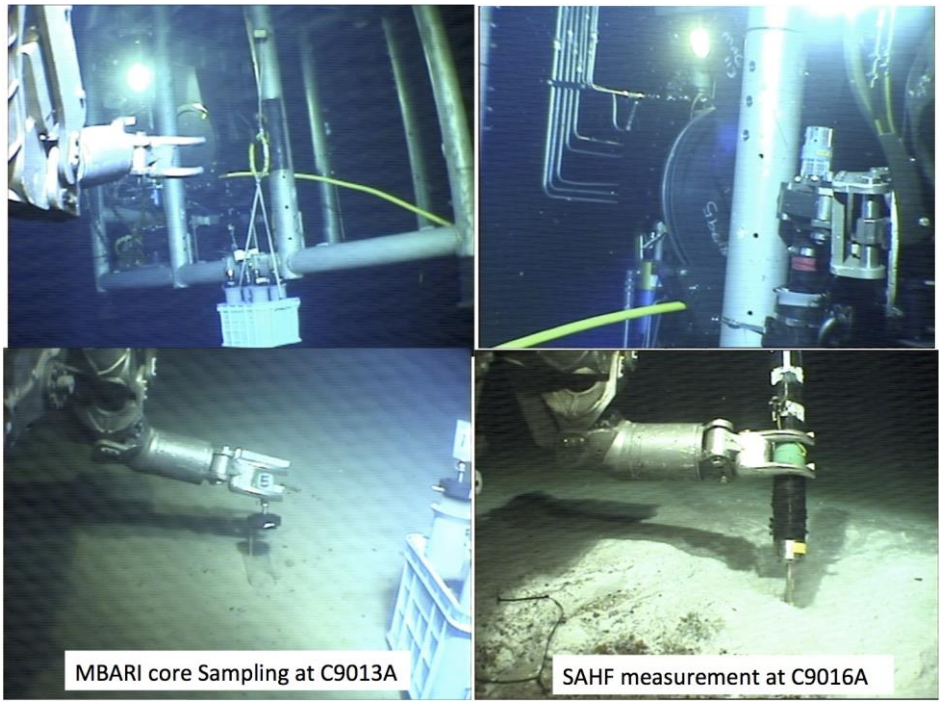

Fig 4.1-2 Operation by ROV

4.2 Site survey by video camera of ROV

Ryota NAKAJIMA Hiroyuki YAMAMOTO, Yuka MASAKI, Tomohiko FUKUSHIMA, Masayuki WATANABE

The video survey to determine habitat condition, colonization of mega-benthos, seabed characterization, and hydrothermal activity from borehole was performed by the video camera equipped on the vehicle. The resolution of video was NTSC SD quality, and the lighting consisted of three halogen lamps without metal reflector and a LED light. The video signal was converted to digital movie mode using a capture system, Intensity Extreme with Thunderbolt connection, produced by Blackmagic Design Pty. Ltd. The video signal without overlay information was provided from control panel of ROV operation system with BNC connector.

An altitude of 2meters from seafloor was the limit distance to keep a distinguishable quality of video image of the seafloor condition. The video survey was carried out within 50m-diameter from the drilling point, and on the line transects of north to south and west to east (Fig 4.2-1). The position of ROV was determined by SBL with 4 sec interval communication, but tracking data of ROV was not record in any storage, only appeared on the display.

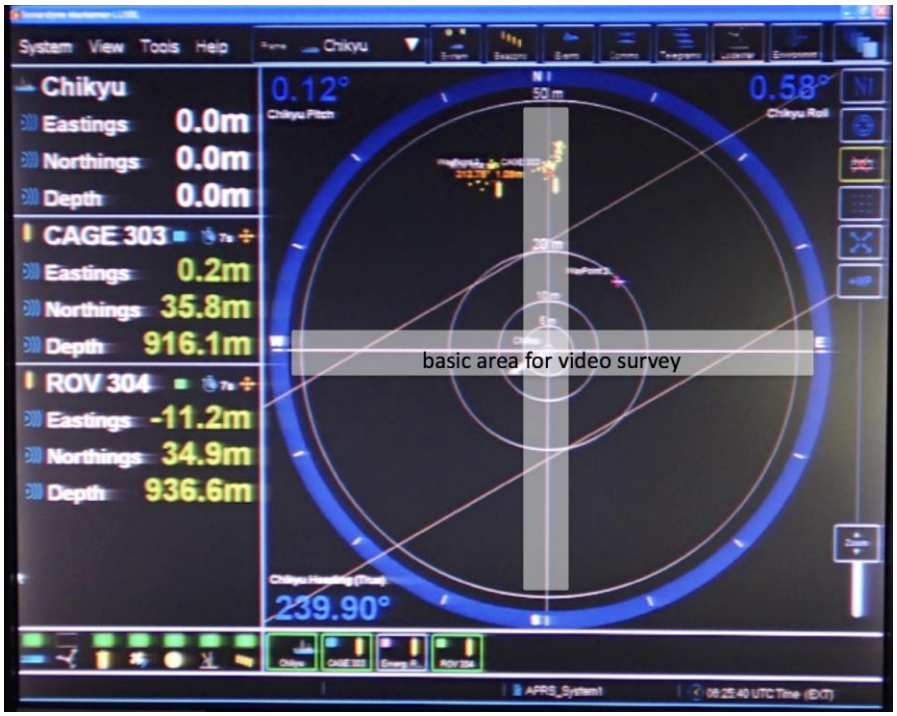

Fig 4.2-1 Console display the dynamic positioning system
The white zone pasted on the display image is the area surveyed by video.

Table 4.2-1 Summary of ROV Dive logs

Date	Time	Site	Hole	Dive#	Seabed vieo survy	Push-core	SHAF	CTD	Remarks
15-Jul	15:16	1	C9011A/B	1	Pre-drilling	-	-	○	
16-Jul	16:28			2	Post-drilling	-	-	○	plume
	20:25	11	C9012A	3	Pre-drilling	1	-	○	lost two MBARI core
17-Jul	18:40			4	Post-drilling	-	-	○	plume
18-Jul	13:44	7	C9013A	5	Post-drilling	3	-	○	
19-Jul	08:15	5	C9014A	6	Pre-drilling	-	-	○	
	17:39			7	Post-drilling	-	-	○	plume
	23:26	12	C9015A	8	Pre-drilling	-	-	○	
20-Jul	20:17			9	Post-drilling	-	-	○	
21-Jul	18:1	13	C9016A	10	Post-drilling	failed	○	○	no plume in video observation
23-Jul	20:30		C9016B	11	Pre-drilling	-	-	○	
24-Jul	23:40	12	C9015BC	12	Post-drilling	-	-	-	

4.3 Push core sampling of sediments

Hiroyuki YAMAMOTO, Frederic SINNGERS,
Hideto TAKAMI, Wataru ARAI

In order to estimate the biodiversity of organisms in the sediments we collected sediment cores in the drilling sites. The core samples were successfully collected at St 11 (27-47.50 N, 126-54.72 E, depth 1133m, Hole C9012A, Dive3) and St 07 (27-47.50 N, 126-54.72 E, depth 1133m, Hole C9013, Dive 5). St 11 corresponds to C0017 drilling site in Exp 331. The appearance of sediment core at St 11 was fine silt or mud. The sediment sample at St 07 was examined mineral component by X-ray diffraction analysis in onboard laboratory. The result showed that major mineral component was calcite and quartz, and distributed from surface to 20cmbsf.

4.4 Sensor measurements

Yuka MASAKI, Ryota NAKAJIMA, Hiroyuki YAMAMOTO

The temperature is a strong constraint for habitat condition and an indicator of hydrothermal plume and fluid flux in sediment layer. In this cruise, we measured water temperature and salinity using a CTD installed in the vehicle, and subseafloor heat flow by SAHF. SAHF is designed to measure a subseafloor heat flow with five thermistors set in 10cm intervals.

The heat flow measurement was performed only at St 12 (27-47.48'N/126-53.67'E, depth: 974mMSL, Hole C9015A), and detected significant heat-flow at 5m away from the Hole C9015A. The CTD continuously worked from 14 to 24 July, and all data was recovered successfully.

4.5 Microbial community of surface seawater

Masanobu KAWACHI

Surface seawater samples were collected for laboratory survey of the microbial community at the drilling expedition sites. Samples were collected by using bucket from the ship deck, and from the tap sea water pumping line of the ship bottom. Seawater was pre-filtered with polycarbonate filter (PCF, 10μm in pore-size) and then treated with the different methods listed in table 4.4-1. For the seawater samples collected with bucket, microorganisms in seawater sample were concentrated to 100 fold time by using tangential flow filtration (TFF) system (Vivaflow 200, Sartorius Ltd.) and then used for sub-culturing, cryopreservation, and light microscopic observations. As for the cryopreservation, 20 tubes per each sample containing 1ml of TFF concentrated specimens added with a cryoprotectant (5% DMSO in final concentration) were cooled with a rate of -1°C /min to -35°C by using a programmable freezer and then frozen rapidly to –196 °C into liquid nitrogen and were stored in a liquid nitrogen preservation tank. Since cryopreserved specimens are stable for long term storage and alive cells can be obtained after thawing so that these cryopreserved subsamples are going to be very useful material for subsequent culturing and genomic analysis.

Table 4.5-1 Sample list

Collection date	Collection tool	Latitude & longitude	Seawater temperature (°C)	Detail of samples
2014/7/17, 14:00	bucket	27-47.4759N; 126-54.6885E	30.1	DNA (1L, 0.2μm PCF, frozen), RNA (1L, 0.2μm PCF, soaked in RNA-Lock Reagent, 4°C) Chlorophyll a (1L, GF/F, soaked in DMF, 4°C) Nutrients (10ml, 0.4μm syringe filter, frozen) Salinity (frozen) Flowcytometry (frozen) Scanning electron microscopy (1L, 1μm PCF, desiccator) Pre-culturing (1ml, 100μl seawater sample, enriched with 3 medium, ESM, MNK and f/2)
2014/7/19, 14:00	bucket	27-47.6817N; 126-53.4708E	30.2	
2014/7/21, 12:00	tap	27-46.0841N; 126-54.0625E	30.3	
2014/7/21, 14:00	bucket	27-46.0841N; 126-54.0623E	30.3	
2014/7/22, 11:00	tap	27-46.0857N; 126-54.0582E	29.9	
2014/7/22, 17:00	tap	27-46.0826N; 126-54.0604E	30.2	
2014/7/22, 22:00	tap	27-46.0746N; 126-54.0738E	30.1	
2014/7/23, 6:00	tap	27-46.0756N; 126-54.0707E	30.0	

Direct observations on microbial community were also achieved by using an inverted light microscope. Nano- or micro-size phytoplanktons were recorded as digital images (Figs 4.4-1A-J). From these observation, limited by the low magnification and not as quantitative analysis, the preliminary results of the dominant phytoplankton groups could be simply recorded. Nitrogen-fixing filamentous cyanobacteria, *Trichodesmium* (Figs 4.4-1A-J) is one of the dominant and conspicuous species in the concentrated samples prepared with 10μm PCF. The other dominant plankton groups were dinoflagellates (Figs 4.4-1C, E, G), foraminifera (Fig. 4.4-1D), radiolarians (Fig. 4.4-1H), and diatoms (Figs 4.4-1I, J). Among such larger planktons, species with symbiotic relationship were frequently observed (Figs 4.4-1D, E, H, J). In addition to these dominant groups, diverse pico-size plankton were also detected in the TFF concentrated specimens (Fig. 4.4-1F). This area is strongly influenced by the Kuroshio Current intrusion. Its distinctive environment with warm seawater temperatures at 30°C and oligotrophic conditions are reflected in the microbial community consisting of nitrogen fixing cyanobacteria, diversified eukaryotic picoplankton and variety of symbiotic related species.

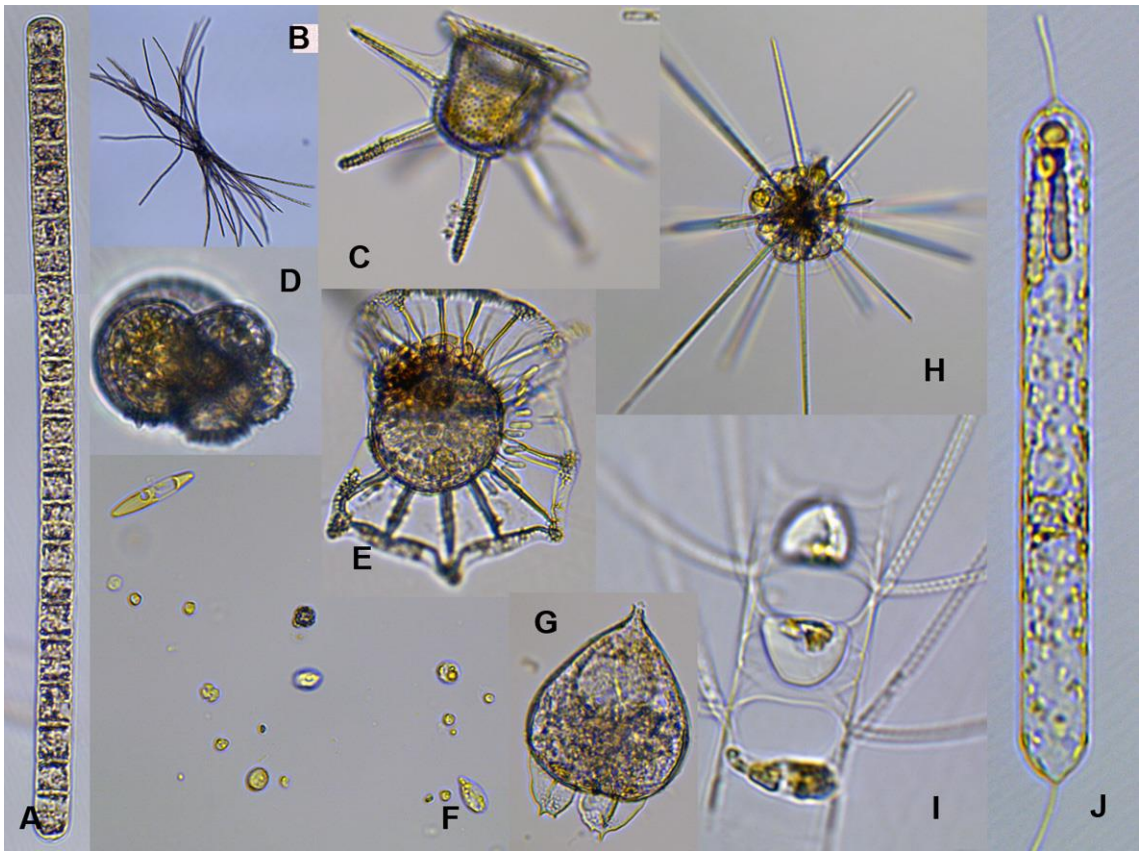

Fig. 4.5-1. Major planktonic species observed at the drilling expedition sites of CH14-04. A. *Trichodesmium*, B. lower magnification of *Trichodesmium*, C. *Ceratocorys*, D. planktonic foraminifera, E. *Ornithocercus*, G. *Podolampas*, H. radiolaria, I. *Chaetoceros*, J. *Rhizosolenia*.

Chapter 5. Operation

EPM-LSS

Chikyu left Shimizu Port at 16:00 on July 8, after all the loading work and crew change have been completed. Six scientists got onboard, including Chief Scientist Ken Takai. Chikyu headed SWS to avoid the approaching typhoon #8, and turned WSW at around 1700 h on July 10. Onboard scientists started preparation with ROV crew for sampling and data acquisition using ROV. There was also a pre-spud meeting with ship crew and a visit to LWD unit/tools on July 10.

While Chikyu continued sailing to Okinawa, rig preparation including making up ESCS, SD-RCB and RCB coring BHA. Simulation training of non-stop driller was carried out on July 12 and 13. LWD BHA was also made up before arriving at Nago Bay at 1130 on July 13.

Crew change was carried out on July 14 and the remaining 16 scientists got onboard. Chikyu moved to the core line winch test site at 27°45.14'N / 126°52.50'E. After installation of cursor rail at low current area, Chikyu arrived at the test site at 0130 on July 15. During the core line winch test, ROV dove with sample basket at 0230 but was recovered on deck at 0330 due to water ingress into termination box. After the core line winch turned out to be no problem, Chikyu started drifting at 0.5 kn to the site at 1030.

Here the altitude of rig-floor from the sea level was 28.5m. All operations were primarily recorded as the downward distances from the rig-floor, mBRT unit (Fig.5-1). Information of sites and cores are shown as Table 5-1 and 5-2-1 to 5-2-4, respectively.

C9011

Running LWD BHA started 1245 on Jul 15 at St.01, and reached 946 mBRT at 1800. ROV dove with MBARI push corer, water sampler, SAHF probe, and CTD sensor. Test operation with dummy SAHF probe was carried out on the seafloor after seabed survey. ROV was then recovered due to an electric trouble on starboard side hydraulic motor. ROV returned to the seafloor at 2130. Running LWD BHA resume to 975mBRT. After a slight adjustment of the site, we tagged the seabed at 978.5mBRT and spud-in at 2215.

C9011A was washed down to 983 mBRT and drilled to 995.4 mBRT.

However drilling was stopped due to drill string inclination. We pulled out of the hole and started a new hole C9011B at 2330 with rotation at 60 RPM, after tagging the seafloor at 979 mBRT.

Drilling reached 1199.8 mBRT at 0915 on Jul 16. ROP was controlled to 40 – 45 m/hr. Inclination and azimuth survey was carried out before connection without rotation. Pump rate was 500 gpm and ROP was 45 m/hr until 1074.4 mBRT, and 600 gpm and 40.5 m/hr respectively for 1074.4 – 1199.8 mBRT. ROV camera image was lost due to telemetry problem at 0030. ROV was recovered. Repeat log was taken at 1145 – 1155 mBRT.

Drill string was pulled out to 10 mBSF at 1245. After ROV arrived at the seafloor, drill bit was pulled out from the hole. After seabed observation, we pulled out to 680 mBRT at 1600.

C9012

Chikyu started drifting at 0.5 kn and arrived at St. 11 at 1837 on Jul 16. After a short seafloor observation and tagging the seafloor, hole C9012A was started at 2025. We drilled down to 60 mbsf with 60 rpm rotation and 400 gpm pumping, and reached to 1265 mBRT by the end of the day.

Drilling with LWD continued at C9012A until we reached 1502 mBRT(341.5 mbsf) at 1145. Flow rate was increased up to 700 gpm during drilling. Temperature increase up to 84degC (ARC) / 24degC (Telescope) was observed at 240mbsf

While pulling out from the hole bottom, repeat log was taken between 1435 and 1395mBRT(bit depth) with 45rpm and 33m/h POOH speed, but no temperature increase was observed. After pulling out above surface, the bit condition was observed no problem by ROV. Temperature measurement with SAHF was attempted on the seafloor at 1745. Drill string was pulled out to 650 mBRT and Chikyu started drifting to next site St. 07 at 19:44.

C9013

Chikyu arrived at St. 07 at 2144, but ROV was unavailable for troubleshooting of cable. Hole C9013A was started without ROV at 0300 on Jul 18 by drilling down with 60 rpm rotation and 500 gpm pumping. Drilling was terminated at 175.5 mbsf at 1115. During pulling out, ROV dove and collected push core samples on

the seafloor. After drill bit was pulled out from the hole, the condition of the hole was observed ROV image. ROV was then recovered on deck due to unstable communication. The drill string was fully recovered on surface and LWD memory data was downloaded at 1630. The drill bit was replaced with a new one.

C9014

Chikyu started moving to next site at 1440 and arrived at St. 05 at 1710. After arranging three NSD stands, running LWD BHA was started at 2000 on Jul 18. Spud-in hole C9014A was 0045 on Jul 19. We started the hole by drill down with 60rpm rotation and 500gpm pumping.Pack off occurred at 0600 at 1017.7mBRT, but the pipe was free after decreasing flow rate to 300gpm and working pipe. Drilling was resumed and continued to 1145.6mBRT.Torque and pressure increase was observed several times showing sign of pack off. Drilling was stopped at 1145.6 mBRT (230.6mbsf) at 1430. Drill bit condition was observed by ROV image after the bit was pulled out of the hole. Observation of outflow from the hole and temperature measurement was attempted near the hole. Pulling out continued to 650 mBRT at 1715.

C9015A

After rearranging NST triple stands, running in started at 1900 on Jul 19. ROV dove at 2140 after maintenance and checking junction box. Seabed survey was at new site St. 12 started at 2230 and C9015 was started at 0030 on Jul 20 by drilling down with 60 rpm rotation and 500 gpm pumping.Penetration rate was < 1 m/hr until 1050.9 mBRT, but ROP increased to ave. 25.5 m/hr for 1050.9 – 1206 mBRT. Rotation was increased to 70 rpm. Drilling was stopped at 1500 at 1206 mBRT (189 mbsf). Re-logging was carried out for 1075 – 1035 mBRT while pulling out of the hole. Observation of the seafloor and drill bit condition was carried out after pulling out the bit above seafloor, but the survey was carried out by ROV in the cage. Pulling out to 750 mBRT was completed at 1830.

C9016A

Chikyu moved to the new site St. 13 by 2230 on Jul 20, and started C9016A by drilling down with 60rpmrotation and 500gpm pumping at 0015 on Jul 21. ROV was unavailable for repair of transformer of the cage.Drilling LWD hole was finished at

1300 mBRT (176mbsf) at 0845.It was determined that we move to coring operation at the same site. LWD BHA was pulled out to surface at 1330, and memory data was downloaded. While rig up of core line BOP and change of saver sub was carried out, ROV attempted push core sampling and temperature measurement on the seafloor.

C9016B

Make up and running HPCS/ESCS core BHA started at 0000 on Jul 22. After adjusting the bit position near the previous C9016A hole by using ROV seafloor image, core 1H was cut with HPCS from the seafloor and recovered on deck at 0548 with 8.9 m recovery. Core 2X was cut with ESCS, and 2.8 m core was recovered from 15.5 m advance. Coring operation continued to core 7X, which was recovered on deck at 1700. Various advance was used depending on the priority of the interval. Temperature measurement was attempted by using Thermo-Resistant Downhole Temperature logger at 1189 mBRT, while pump was stopped with 10 rpm rotation. ESCS coring with short (5 – 6.5 m) advance continued to core 12X, which was recovered on deck at 0228 on July 23. Another four cores were cut from longer (10 – 25 m) advance. The last core 16X was recovered on deck at 1136. Coring operation at C9016B was terminated at the final depth of 150 mBRT. While pulling out from the hole, seabed survey was conducted with ROV. Then Chikyu started moving the next site St. 12A with ROV in 700 m water.

C9015B

After pulling out HPCS/ESCS BHA to surface, running SD-RCB assembly started at 1600 on Jul 23. After adjusting the spud-in location during seabed survey with ROV, drilling C9015B started at 2045 with SD-RCB core hole. Core 1R was cut from 1019 – 1027mBRT (0 – 8mbsf) and recovered on deck at 2152. Cores 2R and 3R were short advance (5 m). Coring operation with SD-RCB was stopped after core 5R, which was recovered on deck at 0453, Jul 24. Drill bit condition was confirmed OK by ROV observation.

C9015C

Before starting a new hole, ROV was recovered due to loose umbilical cable. C9015C was started without ROV. Coring operation with SD-RCB started at 1230 on

Jul 24 and a total of 5 cores were recovered until 2000. Retrieval of core 6R was unsuccessful, and ROV returned to seafloor for observation. It turned out that 7” drill collar was broken and the core barrel was lost in the hole. Pulling out started 0000 on Jul 25, and was completed at 0400.

Chikyu started sailing at 0900 after removing cursor rail at a low current area, and the expedition was completed when Chikyu arrived at Nakagusuku port in the morning of Jul 26.

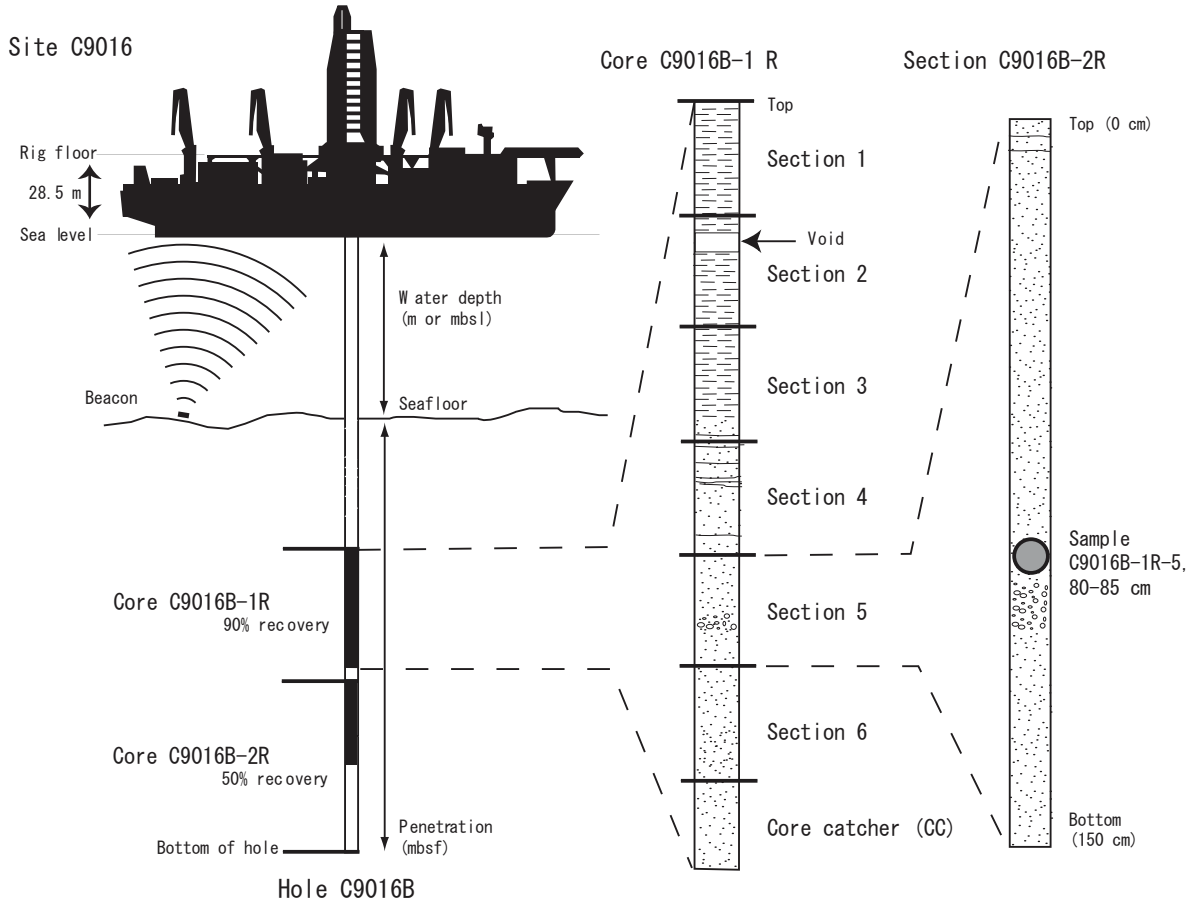

Figure 5-1: Schematic diagram of core, section and samples.

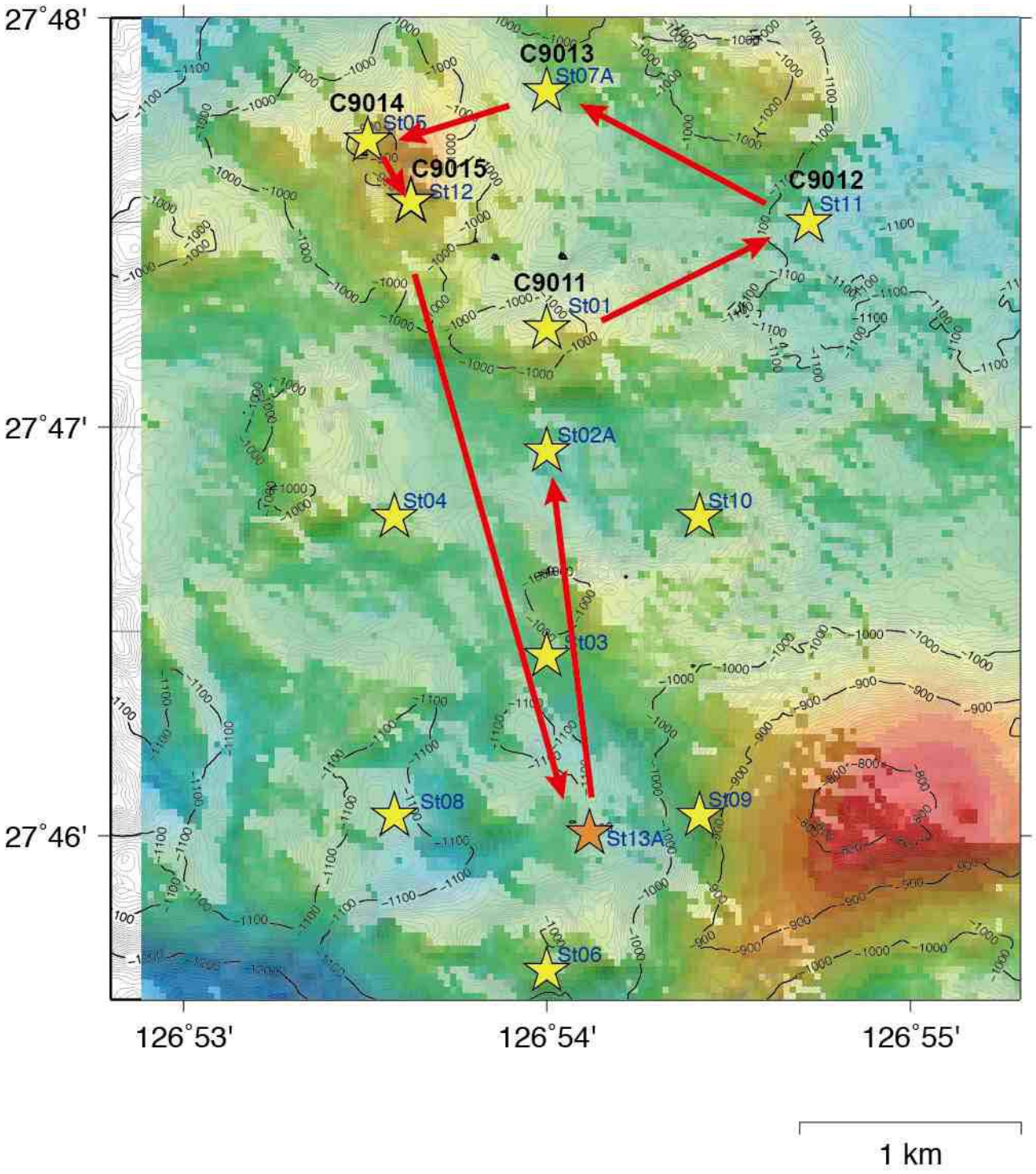

Figure 5-2: Stations proposed and revised in CK14-04 (Exp.907). The final station was St.13A, i.e. St.02A was not drilled.

Table 5-1. Site Summary

Site	Proposed Site Name	Hole	Location		Water Depth	Hole Depth	Remarks
			Lat. (N)	Long. (E)	mBRT	mBRT (mbsf)	
C9011	St. 01	A	27°47.2312'	126°53.9239'	978.5	996.0 (17.5)	LWD
		B	27°47.2430'	126°53.9080'	979.0	1200.0 (221.0)	
C9012	St. 11	A	27°47.5115'	126°54.7158'	1160.5	1502.0 (341.5)	LWD
C9013	St. 07A	A	27°47.6700'	126°54.0500'	1093.5	1269.0 (175.5)	LWD
C9014	St. 05	A	27°47.7000'	126°53.5070'	915.0	1145.5 (230.5)	LWD
C9015	St. 12A	A	27°47.4492'	126°53.7150'	1017.0	1206.0 (189.0)	LWD
		B	27°47.4462'	126°53.7266'	1019.0	1050.0 (31.0)	Core
	St. 12D	C	27°47.4667'	126°53.6667'	1006.0	1046.0 (40.0)	Core
C9016	St. 13A	A	27°46.1000'	126°54.1000'	1124.0	1300.0 (176.0)	LWD
		B	27°46.1097'	126°54.0942'	1125.0	1275.0 (150.0)	Core

Table 5-2-1. Core Summary

Hole	Core type	Num. core	Cored interval (m)	Recovered length (m)	Total recovery (%)
C9016B	H/X	16	150	32.6	21.7
C9015B	R (SD)	5	31	3.79	12.2
C9015C	R (SD)	5	30	6.48	21.6

Table 5-2-2. C9016B Core List

Core	Type	Core on Deck Time (JST)	Core Depth (mBRT)		Core Depth (mbsf)		Advance (m)	Initial Core Length (m)	Initial Recovery (%)
			Top	Bottom	Top	Bottom			
1	H	2014/07/22 05:48	1125.00	1134.50	0.0	9.50	9.50	8.90	93.7
2	X	2014/07/22 09:02	1134.50	1150.00	9.50	25.00	15.50	2.80	18.1
3	X	2014/07/22 10:26	1150.00	1154.50	25.00	29.50	4.50	0.51	11.3
4	X	2014/07/22 12:50	1154.50	1160.00	29.50	35.00	5.50	3.62	65.8
5	X	2014/07/22 14:03	1160.00	1165.00	35.00	40.00	5.00	3.59	71.8
6	X	2014/07/22 15:08	1165.00	1175.00	40.00	50.00	10.00	3.59	35.9
7	X	2014/07/22 17:00	1175.00	1192.00	50.00	67.00	17.00	1.68	9.9
8	X	2014/07/22 20:00	1192.00	1198.50	67.00	73.50	6.50	0.76	11.7
9	X	2014/07/22 21:24	1198.50	1205.00	73.50	80.00	6.50	0.46	7.1
10	X	2014/07/22 23:18	1205.00	1210.00	80.00	85.00	5.00	0.34	6.8
11	X	2014/07/23 01:00	1210.00	1215.00	85.00	90.00	5.00	1.42	28.4
12	X	2014/07/23 02:28	1215.00	1220.00	90.00	95.00	5.00	2.68	53.6
13	X	2014/07/23 04:17	1220.00	1230.00	95.00	105.00	10.00	0.70	7.0
14	X	2014/07/23 06:38	1230.00	1240.00	105.00	115.00	10.00	0.63	6.3
15	X	2014/07/23 09:30	1240.00	1265.00	115.00	140.00	25.00	0.55	2.2
16	X	2014/07/23 11:36	1265.00	1275.00	140.00	150.00	10.00	0.37	3.7

Total Initial Core Length (m): 32.60

Total Corrected Core Length (m): TBD

Table 5-2-3. C9015B Core List

Core	Type	Core on Deck Time (JST)	Core Depth (mBRT)		Core Depth (mbsf)		Advance (m)	Initial Core Length (m)	Initial Recovery (%)
			Top	Bottom	Top	Bottom			
1	R (SD)	2014/07/23 21:52	1019.00	1027.00	0.0	8.00	8.00	0.15	1.9
2	R (SD)	2014/07/23 22:46	1027.00	1032.00	8.00	13.00	5.00	0.89	17.8
3	R (SD)	2014/07/24 00:25	1032.00	1037.00	13.00	18.00	5.00	1.45	29.0
4	R (SD)	2014/07/24 02:48	1037.00	1042.00	18.00	23.00	5.00	0.40	8.0
5	R (SD)	2014/07/24 04:53	1042.00	1050.00	23.00	31.00	8.00	0.90	11.3
					Total Initial Core Length (m):		**3.79**		

Table 5-2-4. C9015C Core List

Core	Type	Core on Deck Time (JST)	Core Depth (mBRT)		Core Depth (mbsf)		Advance (m)	Initial Core Length (m)	Initial Recovery (%)
			Top	Bottom	Top	Bottom			
1	R (SD)	2014/07/24 14:02	1006.00	1016.00	0.0	10.00	10.00	5.89	58.9
2	R (SD)	2014/07/24 14:51	1016.00	1021.00	10.00	15.00	5.00	0.20	4.0
3	R (SD)	2014/07/24 16:16	1021.00	1026.00	15.00	20.00	5.00	0.06	1.2
4	R (SD)	2014/07/24 18:02	1026.00	1031.00	20.00	25.00	5.00	0.06	1.2
5	R (SD)	2014/07/24 20:03	1031.00	1036.00	25.00	30.00	5.00	0.25	5.0
					Total Initial Core Length (m):		**6.46**		

907-C9015B Core MISC Material Sample List

	J-CORES sample ID	Leg/Exp.	Sample source	Request number	Sample volume (cm3)	Top depth [m CSF-A, DSF, MSF, WSF]	Bottom Depth [m CSF-A, DSF, MSF, WSF]	Top Depth [m CSF-B, DSF, MSF, WSF]	Bottom Depth [m CSF-B, DSF, MSF, WSF]	Comment
1	CKY000000000000186150	907	C9015B-2R-1 W, 29.0--31.0 cm	907TAK	7	8.29	8.31	8.29	8.31	
2	CKY000000000000183950	907	C9015B-2R-CC W, 35.0--38.0 cm	907TY	51	8.88	8.91	8.88	8.91	
3	CKY000000000000186250	907	C9015B-3R-1 W, 19.0--21.0 cm	907TAK	7	13.19	13.21	13.19	13.21	
4	CKY000000000000186350	907	C9015B-3R-1 W, 58.0--60.0 cm	907TAK	7	13.58	13.6	13.58	13.6	
5	CKY000000000000184150	907	C9015B-3R-1 W, 71.0--76.0 cm	907TY	51	13.71	13.76	13.71	13.76	
6	CKY000000000000185250	907	C9015B-3R-1 W, 88.0--90.0 cm	907SYU	5	13.88	13.9	13.88	13.9	
7	CKY000000000000177250	907	C9015B-3R-1 WR, 96.5--100.5 cm	907KTG	5	13.965	14.005	13.965	14.005	2 vials
8	CKY000000000000177350	907	C9015B-3R-1 WR, 96.5--100.5 cm	907KTHS	5	13.965	14.005	13.965	14.005	2 vials
9	CKY000000000000184250	907	C9015B-3R-CC W, 0.0--6.0 cm	907TY	51	14.005	14.065	14.005	14.065	
10	CKY000000000000186450	907	C9015B-3R-CC W, 18.5--20.5 cm	907TAK	7	14.19	14.21	14.19	14.21	
11	CKY000000000000184650	907	C9015B-4R-CC W, 0.0--8.5 cm	907TN	34	18	18.085	18	18.085	
12	CKY000000000000184050	907	C9015B-4R-CC W, 8.5--14.0 cm	907TY	51	18.085	18.14	18.085	18.14	
13	CKY000000000000185450	907	C9015B-4R-CC W, 22.0--30.0 cm	907SYU	5	18.22	18.3	18.22	18.3	
14	CKY000000000000186550	907	C9015B-5R-1 W, 7.0--9.0 cm	907TN	42	23.07	23.09	23.07	23.09	
15	CKY000000000000185350	907	C9015B-5R-1 W, 9.0--12.5 cm	907SYU	5	23.09	23.125	23.09	23.125	
16	CKY000000000000184750	907	C9015B-5R-1 W, 12.5--16.0 cm	907TN	34	23.125	23.16	23.125	23.16	
17	CKY000000000000184350	907	C9015B-5R-1 W, 18.0--24.0 cm	907HK	5	23.18	23.24	23.18	23.24	
18	CKY000000000000184850	907	C9015B-5R-CC W, 0.0--7.5 cm	907TN	34	23.26	23.335	23.26	23.335	
19	CKY000000000000185650	907	C9015B-5R-CC W, 7.5--13.0 cm	907SYU	5	23.335	23.39	23.335	23.39	
20	CKY000000000000184550	907	C9015B-5R-CC W, 13.0--16.0 cm	907SAKI	5	23.39	23.42	23.39	23.42	
21	CKY000000000000185550	907	C9015B-5R-CC W, 18.0--23.0 cm	907SYU	5	23.44	23.49	23.44	23.49	
22	CKY000000000000184950	907	C9015B-5R-CC W, 24.0--26.0 cm	907TN	34	23.5	23.52	23.5	23.52	
23	CKY000000000000185050	907	C9015B-5R-CC W, 39.0--43.0 cm	907TN	34	23.65	23.69	23.65	23.69	
24	CKY000000000000185150	907	C9015B-5R-CC W, 46.0--50.0 cm	907TN	34	23.72	23.76	23.72	23.76	

[Note]
m CSF = depth of Core below Sea Floor in meters / m CSF-A: Distance from sea floor to sample within recovered core. This scale allows overlap at core and section boundaries. /
m CSF-B: Distance from sea floor to sample within recovered core is compressed, if core recovery > 100%.
JNK = Junk basket, Junk sub / SDB = Solid from Drill Bit, depth scale is "m DSF: Drilling depth below Sea Floor in meters".
SMW = Solids (cuttings) taken from Mud Water / LMW = Liquid (fluid) taken from Mud Water / LMT = Liquid (fluid) taken from Mud water Tank / GMW = Gas taken from Mud Water, depth scale is "m MSF: depth of Mud below Sea Floor in meters".

SWL = Solid taken by Wireline Logging tools / LWL = Liquid taken by Wireline Logging tools / GWL = Gas taken by Wireline Logging tools, depth scale is "m WSF: depth of Wireline log below Sea Floor in meters".
For further details, consult the "IODP Depth Scales Terminology" in the IODP web site (http://www.iodp.org/program-policies/).

907-C9015C Core MISC Material Sample List

	J-CORES sample ID	Leg/Exp.	Sample source	Request number	Sample volume (cm3)	Top depth [m CSF-A, DSF, MSF, WSF]	Bottom Depth [m CSF-A, DSF, MSF, WSF]	Top Depth [m CSF-B, DSF, MSF, WSF]	Bottom Depth [m CSF-B, DSF, MSF, WSF]	Comment
1	CKY000000000000186850	907	C9015C-1 WR	907KAWW	9999.9	0	0	0	0	Volume 10L
2	CKY000000000000182650	907	C9015C-1R-2 WR, 0.0--4.0 cm	907KTG	5	0.42	0.46	0.42	0.46	
3	CKY000000000000182750	907	C9015C-1R-2 WR, 0.0--4.0 cm	907KTHS	5	0.42	0.46	0.42	0.46	
4	CKY000000000000183250	907	C9015C-1R-2 WR, 15.0--35.0 cm	907KTIW	840	0.57	0.77	0.57	0.77	
5	CKY000000000000187350	907	C9015C-1R-2 WR, 15.0--35.0 cm	907KTIWS	192	0.57	0.77	0.57	0.77	
6	CKY000000000000187450	907	C9015C-1R-2 WR, 15.0--35.0 cm	907KTIWIC	30	0.57	0.77	0.57	0.77	
7	CKY000000000000182850	907	C9015C-1R-4 WR, 0.0--4.0 cm	907KTG	5	2.44	2.48	2.44	2.48	
8	CKY000000000000182950	907	C9015C-1R-4 WR, 0.0--4.0 cm	907KTHS	5	2.44	2.48	2.44	2.48	
9	CKY000000000000183350	907	C9015C-1R-4 WR, 20.0--40.0 cm	907KTIW	840	2.64	2.84	2.64	2.84	
10	CKY000000000000187550	907	C9015C-1R-4 WR, 20.0--40.0 cm	907KTIWS	192	2.64	2.84	2.64	2.84	
11	CKY000000000000187650	907	C9015C-1R-4 WR, 20.0--40.0 cm	907KTIWIC	30	2.64	2.84	2.64	2.84	
12	CKY000000000000183050	907	C9015C-1R-CC WR, 47.0--51.0 cm	907KTG	5	5.93	5.97	5.93	5.97	
13	CKY000000000000183150	907	C9015C-1R-CC WR, 47.0--51.0 cm	907KTHS	5	5.93	5.97	5.93	5.97	
14	CKY000000000000187150	907	C9015C-2R-CC W, 0.0--7.0 cm	907SYU	50	10	10.07	10	10.07	
15	CKY000000000000187050	907	C9015C-2R-CC W, 14.0--21.0 cm	907HK	50	10.14	10.21	10.14	10.21	
16	CKY000000000000186950	907	C9015C-4R-CC W, 0.0--5.0 cm	907HK	50	20	20.05	20	20.05	
17	CKY000000000000186650	907	C9015C-5R-CC WR, 11.0--15.0 cm	907KTG	5	25.11	25.15	25.11	25.15	
18	CKY000000000000186750	907	C9015C-5R-CC WR, 11.0--15.0 cm	907KTHS	5	25.11	25.15	25.11	25.15	
19	CKY000000000000187250	907	C9015C-5R-CC W, 18.0--23.0 cm	907SYU	50	25.18	25.23	25.18	25.23	

[Note]
m CSF = depth of Core below Sea Floor in meters / m CSF-A: Distance from sea floor to sample within recovered core. This scale allows overlap at core and section boundaries. /
m CSF-B: Distance from sea floor to sample within recovered core is compressed, if core recovery > 100%.
JNK = Junk basket, Junk sub / SDB = Solid from Drill Bit, depth scale is "m DSF: Drilling depth below Sea Floor in meters".
SMW = Solids (cuttings) taken from Mud Water / LMW = Liquid (fluid) taken from Mud Water / LMT = Liquid (fluid) taken from Mud water Tank / GMW = Gas taken from Mud Water, depth scale is "m MSF: depth of Mud below Sea Floor in meters".

SWL = Solid taken by Wireline Logging tools / LWL = Liquid taken by Wireline Logging tools / GWL = Gas taken by Wireline Logging tools, depth scale is "m WSF: depth of Wireline log below Sea Floor in meters".
For further details, consult the "IODP Depth Scales Terminology" in the IODP web site (http://www.iodp.org/program-policies/).

907-C9016A Core MISC Material Sample List

	J-CORES sample ID	Leg/Exp.	Sample source	Request number	Sample volume (cm3)	Top depth [m CSF-A, DSF, MSF, WSF]	Bottom Depth [m CSF-A, DSF, MSF, WSF]	Top Depth [m CSF-B, DSF, MSF, WSF]	Bottom Depth [m CSF-B, DSF, MSF, WSF]	Comment
1	CKY000000000000151150	907	C9016A-1 WR	907KAWW	9999	0	0	0	0	Volume:20L
2	CKY000000000000151250	907	C9016A-1 WR	907RNW	9999	0	0	0	0	Volume:20L

[Note]
m CSF = depth of Core below Sea Floor in meters / m CSF-A: Distance from sea floor to sample within recovered core. This scale allows overlap at core and section boundaries. /
m CSF-B: Distance from sea floor to sample within recovered core is compressed, if core recovery > 100%.
JNK = Junk basket, Junk sub / SDB = Solid from Drill Bit, depth scale is "m DSF: Drilling depth below Sea Floor in meters".
SMW = Solids (cuttings) taken from Mud Water / LMW = Liquid (fluid) taken from Mud Water / LMT = Liquid (fluid) taken from Mud water Tank / GMW = Gas taken from Mud Water, depth scale is "m MSF: depth of Mud below Sea Floor in meters".

SWL = Solid taken by Wireline Logging tools / LWL = Liquid taken by Wireline Logging tools / GWL = Gas taken by Wireline Logging tools, depth scale is "m WSF: depth of Wireline log below Sea Floor in meters".
For further details, consult the "IODP Depth Scales Terminology" in the IODP web site (http://www.iodp.org/program-policies/).

	J-CORES sample ID	Leg/Exp.	Sample source	Request number	Sample volume (cm3)	Top depth [m CSF-A]	Bottom depth [m CSF-A]	Top depth [m CSF-B]	Bottom depth [m CSF-B]	Comment
1	CKY000000000000167350	907	C9016B-1H-1 W, 1.0--3.0 cm	907TAK	7	0.01	0.03	0.01	0.03	
2	CKY000000000000159650	907	C9016B-1H-1 W, 17.5--23.0 cm	907TY	93.5	0.175	0.23	0.175	0.23	
3	CKY000000000000166750	907	C9016B-1H-1 W, 30.0--33.0 cm	907KAW	51	0.3	0.33	0.3	0.33	
4	CKY000000000000153750	907	C9016B-1H-1 WR, 50.0--80.0 cm	907KTIW	1020	0.5	0.8	0.5	0.8	
5	CKY000000000000175750	907	C9016B-1H-1 WR, 50.0--80.0 cm	907KTIWS	160	0.5	0.8	0.5	0.8	
6	CKY000000000000177450	907	C9016B-1H-1 WR, 50.0--80.0 cm	907KTIWIC	60	0.5	0.8	0.5	0.8	
7	CKY000000000000153850	907	C9016B-1H-1 WR, 80.0--101.0 cm	907KTWR	714	0.8	1.01	0.8	1.01	
8	CKY000000000000151350	907	C9016B-1H-1 WR, 97.0--101.0 cm	907KTG	5	0.97	1.01	0.97	1.01	
9	CKY000000000000151450	907	C9016B-1H-1 WR, 97.0--101.0 cm	907KTG	5	0.97	1.01	0.97	1.01	
10	CKY000000000000151550	907	C9016B-1H-1 WR, 97.0--101.0 cm	907KTHS	5	0.97	1.01	0.97	1.01	
11	CKY000000000000151650	907	C9016B-1H-1 WR, 97.0--101.0 cm	907KTHS	5	0.97	1.01	0.97	1.01	
12	CKY000000000000167450	907	C9016B-1H-2 W, 13.0--15.0 cm	907TAK	7	1.14	1.16	1.14	1.16	
13	CKY000000000000159750	907	C9016B-1H-2 W, 30.0--34.0 cm	907TY	68	1.31	1.35	1.31	1.35	
14	CKY000000000000159850	907	C9016B-1H-2 W, 44.5--49.5 cm	907TY	85	1.455	1.505	1.455	1.505	
15	CKY000000000000159950	907	C9016B-1H-2 W, 71.0--77.5 cm	907TY	110.5	1.72	1.785	1.72	1.785	
16	CKY000000000000167550	907	C9016B-1H-2 W, 87.0--89.0 cm	907TAK	7	1.88	1.9	1.88	1.9	
17	CKY000000000000151750	907	C9016B-1H-2 WR, 97.0--101.0 cm	907KTG	5	1.98	2.02	1.98	2.02	
18	CKY000000000000151850	907	C9016B-1H-2 WR, 97.0--101.0 cm	907KTG	5	1.98	2.02	1.98	2.02	
19	CKY000000000000151950	907	C9016B-1H-2 WR, 97.0--101.0 cm	907KTHS	5	1.98	2.02	1.98	2.02	
20	CKY000000000000152050	907	C9016B-1H-2 WR, 97.0--101.0 cm	907KTHS	5	1.98	2.02	1.98	2.02	
21	CKY000000000000167650	907	C9016B-1H-3 W, 13.0--15.0 cm	907TAK	7	2.15	2.17	2.15	2.17	
22	CKY000000000000160050	907	C9016B-1H-3 W, 40.0--44.5 cm	907TY	76.5	2.42	2.465	2.42	2.465	
23	CKY000000000000153950	907	C9016B-1H-3 WR, 50.0--65.0 cm	907KTIW	510	2.52	2.67	2.52	2.67	
24	CKY000000000000175850	907	C9016B-1H-3 WR, 50.0--65.0 cm	907KTIWS	128	2.52	2.67	2.52	2.67	
25	CKY000000000000177550	907	C9016B-1H-3 WR, 50.0--65.0 cm	907KTIWIC	30	2.52	2.67	2.52	2.67	
26	CKY000000000000154050	907	C9016B-1H-3 WR, 65.0--85.0 cm	907KTWR	680	2.67	2.87	2.67	2.87	
27	CKY000000000000154150	907	C9016B-1H-3 WR, 85.0--101.0 cm	907KTIW	544	2.87	3.03	2.87	3.03	
28	CKY000000000000175950	907	C9016B-1H-3 WR, 85.0--101.0 cm	907KTIWS	192	2.87	3.03	2.87	3.03	
29	CKY000000000000177650	907	C9016B-1H-3 WR, 85.0--101.0 cm	907KTIWIC	30	2.87	3.03	2.87	3.03	
30	CKY000000000000152150	907	C9016B-1H-3 WR, 97.0--101.0 cm	907KTG	5	2.99	3.03	2.99	3.03	
31	CKY000000000000152250	907	C9016B-1H-3 WR, 97.0--101.0 cm	907KTG	5	2.99	3.03	2.99	3.03	
32	CKY000000000000152350	907	C9016B-1H-3 WR, 97.0--101.0 cm	907KTHS	5	2.99	3.03	2.99	3.03	
33	CKY000000000000152450	907	C9016B-1H-3 WR, 97.0--101.0 cm	907KTHS	5	2.99	3.03	2.99	3.03	
34	CKY000000000000167750	907	C9016B-1H-4 W, 7.5--9.5 cm	907TAK	7	3.105	3.125	3.105	3.125	
35	CKY000000000000166850	907	C9016B-1H-4 W, 20.0--23.0 cm	907KAW	51	3.23	3.26	3.23	3.26	
36	CKY000000000000160150	907	C9016B-1H-4 W, 29.0--31.0 cm	907SAKI	34	3.32	3.34	3.32	3.34	
37	CKY000000000000160250	907	C9016B-1H-4 W, 31.0--33.0 cm	907TN	34	3.34	3.36	3.34	3.36	
38	CKY000000000000169650	907	C9016B-1H-4 W, 74.0--76.0 cm	907TAK	7	3.77	3.79	3.77	3.79	
39	CKY000000000000160350	907	C9016B-1H-4 W, 80.0--82.0 cm	907SAKI	34	3.83	3.85	3.83	3.85	
40	CKY000000000000160450	907	C9016B-1H-4 W, 82.0--84.0 cm	907TN	34	3.85	3.87	3.85	3.87	
41	CKY000000000000154250	907	C9016B-1H-5 WR, 0.0--30.0 cm	907KTIW	1020	4.035	4.335	4.035	4.335	
42	CKY000000000000176050	907	C9016B-1H-5 WR, 0.0--30.0 cm	907KTIWS	192	4.035	4.335	4.035	4.335	
43	CKY000000000000177750	907	C9016B-1H-5 WR, 0.0--30.0 cm	907KTIWIC	30	4.035	4.335	4.035	4.335	
44	CKY000000000000154350	907	C9016B-1H-5 WR, 30.0--50.0 cm	907KTWR	680	4.335	4.535	4.335	4.535	
45	CKY000000000000167850	907	C9016B-1H-5 W, 54.0--56.0 cm	907TAK	7	4.575	4.595	4.575	4.595	
46	CKY000000000000160550	907	C9016B-1H-5 W, 60.0--62.0 cm	907SAKI	34	4.635	4.655	4.635	4.655	
47	CKY000000000000160650	907	C9016B-1H-5 W, 62.0--64.0 cm	907TN	34	4.655	4.675	4.655	4.675	
48	CKY000000000000167950	907	C9016B-1H-6 W, 3.0--5.0 cm	907TAK	7	5.075	5.095	5.075	5.095	
49	CKY000000000000160750	907	C9016B-1H-6 W, 25.0--27.0 cm	907SAKI	34	5.295	5.315	5.295	5.315	
50	CKY000000000000160850	907	C9016B-1H-6 W, 27.0--29.0 cm	907TN	34	5.315	5.335	5.315	5.335	
51	CKY000000000000161950	907	C9016B-1H-6 W, 70.0--72.0 cm	907SAKI	34	5.745	5.765	5.745	5.765	

	J-CORES sample ID	Leg/Exp.	Sample source	Request number	Sample volume (cm3)	Top depth [m CSF-A]	Bottom depth [m CSF-A]	Top depth [m CSF-B]	Bottom depth [m CSF-B]	Comment
52	CKY000000000000160950	907	C9016B-1H-6 W, 72.0--74.0 cm	907TN	34	5.765	5.785	5.765	5.785	
53	CKY000000000000168050	907	C9016B-1H-6 W, 74.0--76.0 cm	907TAK	7	5.785	5.805	5.785	5.805	
54	CKY000000000000152550	907	C9016B-1H-6 WR, 97.5--101.5 cm	907KTG	5	6.02	6.06	6.02	6.06	
55	CKY000000000000152650	907	C9016B-1H-6 WR, 97.5--101.5 cm	907KTG	5	6.02	6.06	6.02	6.06	
56	CKY000000000000152750	907	C9016B-1H-6 WR, 97.5--101.5 cm	907KTHS	5	6.02	6.06	6.02	6.06	
57	CKY000000000000152850	907	C9016B-1H-6 WR, 97.5--101.5 cm	907KTHS	5	6.02	6.06	6.02	6.06	
58	CKY000000000000161050	907	C9016B-1H-6 W, 99.0--101.0 cm	907SYU	10	6.035	6.055	6.035	6.055	
59	CKY000000000000161150	907	C9016B-1H-7 W, 0.0--2.0 cm	907SAKI	34	6.06	6.08	6.06	6.08	
60	CKY000000000000161250	907	C9016B-1H-7 W, 2.0--4.0 cm	907TN	34	6.08	6.1	6.08	6.1	
61	CKY000000000000168150	907	C9016B-1H-7 W, 8.0--10.0 cm	907TAK	7	6.14	6.16	6.14	6.16	
62	CKY000000000000161350	907	C9016B-1H-7 W, 14.0--16.0 cm	907SAKI	34	6.2	6.22	6.2	6.22	
63	CKY000000000000161450	907	C9016B-1H-7 W, 16.0--18.0 cm	907TN	34	6.22	6.24	6.22	6.24	
64	CKY000000000000161550	907	C9016B-1H-7 W, 27.0--29.0 cm	907SAKI	34	6.33	6.35	6.33	6.35	
65	CKY000000000000161650	907	C9016B-1H-7 W, 29.0--31.0 cm	907TN	34	6.35	6.37	6.35	6.37	
66	CKY000000000000161750	907	C9016B-1H-7 W, 38.0--40.0 cm	907SAKI	34	6.44	6.46	6.44	6.46	
67	CKY000000000000161850	907	C9016B-1H-7 W, 40.0--42.0 cm	907TN	34	6.46	6.48	6.46	6.48	
68	CKY000000000000168250	907	C9016B-1H-7 W, 44.0--46.0 cm	907TAK	7	6.5	6.52	6.5	6.52	
69	CKY000000000000154450	907	C9016B-1H-7 WR, 50.0--70.0 cm	907KTIW	680	6.56	6.76	6.56	6.76	
70	CKY000000000000176150	907	C9016B-1H-7 WR, 50.0--70.0 cm	907KTIWS	192	6.56	6.76	6.56	6.76	
71	CKY000000000000177850	907	C9016B-1H-7 WR, 50.0--70.0 cm	907KTIWIC	30	6.56	6.76	6.56	6.76	
72	CKY000000000000154550	907	C9016B-1H-7 WR, 70.0--100.5 cm	907KTWR	1037	6.76	7.065	6.76	7.065	
73	CKY000000000000152950	907	C9016B-1H-7 WR, 96.5--100.5 cm	907KTG	5	7.025	7.065	7.025	7.065	
74	CKY000000000000153050	907	C9016B-1H-7 WR, 96.5--100.5 cm	907KTG	5	7.025	7.065	7.025	7.065	
75	CKY000000000000153150	907	C9016B-1H-7 WR, 96.5--100.5 cm	907KTHS	5	7.025	7.065	7.025	7.065	
76	CKY000000000000153250	907	C9016B-1H-7 WR, 96.5--100.5 cm	907KTHS	5	7.025	7.065	7.025	7.065	
77	CKY000000000000168350	907	C9016B-1H-8 W, 4.0--6.0 cm	907TAK	7	7.105	7.125	7.105	7.125	
78	CKY000000000000162050	907	C9016B-1H-8 W, 20.0--22.0 cm	907SAKI	34	7.265	7.285	7.265	7.285	
79	CKY000000000000162150	907	C9016B-1H-8 W, 22.0--24.0 cm	907TN	34	7.285	7.305	7.285	7.305	
80	CKY000000000000162250	907	C9016B-1H-8 W, 40.0--42.0 cm	907SAKI	34	7.465	7.485	7.465	7.485	
81	CKY000000000000162350	907	C9016B-1H-8 W, 42.0--44.0 cm	907TN	34	7.485	7.505	7.485	7.505	
82	CKY000000000000166950	907	C9016B-1H-8 W, 50.0--53.0 cm	907KAW	51	7.565	7.595	7.565	7.595	
83	CKY000000000000168450	907	C9016B-1H-8 W, 54.0--56.0 cm	907TAK	7	7.605	7.625	7.605	7.625	
84	CKY000000000000162450	907	C9016B-1H-8 W, 70.0--72.0 cm	907SAKI	34	7.765	7.785	7.765	7.785	
85	CKY000000000000162550	907	C9016B-1H-8 W, 72.0--74.0 cm	907TN	34	7.785	7.805	7.785	7.805	
86	CKY000000000000162650	907	C9016B-1H-8 W, 79.0--81.0 cm	907SAKI	34	7.855	7.875	7.855	7.875	
87	CKY000000000000162750	907	C9016B-1H-8 W, 81.0--83.0 cm	907TN	34	7.875	7.895	7.875	7.895	
88	CKY000000000000162850	907	C9016B-1H-8 W, 93.0--95.0 cm	907SAKI	34	7.995	8.015	7.995	8.015	
89	CKY000000000000162950	907	C9016B-1H-8 W, 95.0--97.0 cm	907TN	34	8.015	8.035	8.015	8.035	
90	CKY000000000000168550	907	C9016B-1H-9 W, 4.0--6.0 cm	907TAK	7	8.11	8.13	8.11	8.13	
91	CKY000000000000163050	907	C9016B-1H-9 W, 9.0--11.0 cm	907SAKI	34	8.16	8.18	8.16	8.18	
92	CKY000000000000163150	907	C9016B-1H-9 W, 11.0--13.0 cm	907TN	34	8.18	8.2	8.18	8.2	
93	CKY000000000000163250	907	C9016B-1H-9 W, 29.0--31.0 cm	907SAKI	34	8.36	8.38	8.36	8.38	
94	CKY000000000000163350	907	C9016B-1H-9 W, 31.0--33.0 cm	907TN	34	8.38	8.4	8.38	8.4	
95	CKY000000000000168650	907	C9016B-1H-9 W, 49.0--51.0 cm	907TAK	7	8.56	8.58	8.56	8.58	
96	CKY000000000000163450	907	C9016B-1H-9 W, 66.0--68.0 cm	907SAKI	34	8.73	8.75	8.73	8.75	
97	CKY000000000000163550	907	C9016B-1H-9 W, 68.0--70.0 cm	907TN	34	8.75	8.77	8.75	8.77	
98	CKY000000000000163650	907	C9016B-1H-9 W, 79.0--81.0 cm	907SAKI	34	8.86	8.88	8.86	8.88	
99	CKY000000000000163750	907	C9016B-1H-9 W, 81.0--83.0 cm	907TN	34	8.88	8.9	8.88	8.9	
100	CKY000000000000168750	907	C9016B-1H-10 W, 4.0--6.0 cm	907TAK	7	9.115	9.135	9.115	9.135	
101	CKY000000000000167050	907	C9016B-1H-10 W, 9.0--11.0 cm	907SAKI	34	9.165	9.185	9.165	9.185	
102	CKY000000000000163950	907	C9016B-1H-10 W, 11.0--13.0 cm	907TN	34	9.185	9.205	9.185	9.205	

	J-CORES sample ID	Leg/Exp.	Sample source	Request number	Sample volume (cm3)	Top depth [m CSF-A]	Bottom depth [m CSF-A]	Top depth [m CSF-B]	Bottom depth [m CSF-B]	Comment
103	CKY000000000000153350	907	C9016B-1H-CC WR, 0.0--4.0 cm	907KTG	5	9.275	9.315	9.275	9.315	
104	CKY000000000000153450	907	C9016B-1H-CC WR, 0.0--4.0 cm	907KTG	5	9.275	9.315	9.275	9.315	
105	CKY000000000000153550	907	C9016B-1H-CC WR, 0.0--4.0 cm	907KTHS	5	9.275	9.315	9.275	9.315	
106	CKY000000000000153650	907	C9016B-1H-CC WR, 0.0--4.0 cm	907KTHS	5	9.275	9.315	9.275	9.315	
107	CKY000000000000168850	907	C9016B-1H-CC W, 4.0--6.0 cm	907TAK	7	9.315	9.335	9.315	9.335	
108	CKY000000000000164050	907	C9016B-1H-CC W, 16.0--18.0 cm	907SYU	10	9.435	9.455	9.435	9.455	
109	CKY000000000000168950	907	C9016B-2X-1 W, 5.0--7.0 cm	907TAK	7	9.55	9.57	9.55	9.57	
110	CKY000000000000164150	907	C9016B-2X-1 W, 14.0--16.0 cm	907SAKI	34	9.64	9.66	9.64	9.66	
111	CKY000000000000164250	907	C9016B-2X-1 W, 16.0--18.0 cm	907TN	34	9.66	9.68	9.66	9.68	
112	CKY000000000000164350	907	C9016B-2X-1 W, 21.0--23.0 cm	907SYU	10	9.71	9.73	9.71	9.73	
113	CKY000000000000164450	907	C9016B-2X-1 W, 37.0--39.0 cm	907SAKI	34	9.87	9.89	9.87	9.89	
114	CKY000000000000164550	907	C9016B-2X-1 W, 39.0--41.0 cm	907TN	34	9.89	9.91	9.89	9.91	
115	CKY000000000000154650	907	C9016B-2X-2 WR, 0.0--4.0 cm	907KTG	5	9.93	9.97	9.93	9.97	2 vials
116	CKY000000000000154750	907	C9016B-2X-2 WR, 0.0--4.0 cm	907KTHS	5	9.93	9.97	9.93	9.97	2 vials
117	CKY000000000000164650	907	C9016B-2X-2 W, 1.0--3.0 cm	907SYU	10	9.94	9.96	9.94	9.96	
118	CKY000000000000169050	907	C9016B-2X-2 W, 4.0--6.0 cm	907TAK	7	9.97	9.99	9.97	9.99	
119	CKY000000000000164750	907	C9016B-2X-2 W, 14.0--16.0 cm	907SAKI	34	10.07	10.09	10.07	10.09	
120	CKY000000000000164850	907	C9016B-2X-2 W, 16.0--18.0 cm	907TN	34	10.09	10.11	10.09	10.11	
121	CKY000000000000164950	907	C9016B-2X-2 W, 34.0--36.0 cm	907SAKI	34	10.27	10.29	10.27	10.29	
122	CKY000000000000165050	907	C9016B-2X-2 W, 36.0--38.0 cm	907TN	34	10.29	10.31	10.29	10.31	
123	CKY000000000000155450	907	C9016B-2X-2 WR, 45.0--60.0 cm	907KTWR	510	10.38	10.53	10.38	10.53	
124	CKY000000000000155550	907	C9016B-2X-2 WR, 60.0--75.0 cm	907KTIW	510	10.53	10.68	10.53	10.68	
125	CKY000000000000176350	907	C9016B-2X-2 WR, 60.0--75.0 cm	907KTIWS	128	10.53	10.68	10.53	10.68	
126	CKY000000000000177950	907	C9016B-2X-2 WR, 60.0--75.0 cm	907KTIWIC	30	10.53	10.68	10.53	10.68	
127	CKY000000000000169150	907	C9016B-2X-2 W, 78.0--80.0 cm	907TAK	7	10.71	10.73	10.71	10.73	
128	CKY000000000000165150	907	C9016B-2X-2 W, 89.0--91.0 cm	907SAKI	34	10.82	10.84	10.82	10.84	
129	CKY000000000000165250	907	C9016B-2X-2 W, 91.0--93.0 cm	907TN	34	10.84	10.86	10.84	10.86	
130	CKY000000000000155650	907	C9016B-2X-3 WR, 0.0--15.0 cm	907KTIW	510	10.94	11.09	10.94	11.09	
131	CKY000000000000176450	907	C9016B-2X-3 WR, 0.0--15.0 cm	907KTIWS	160	10.94	11.09	10.94	11.09	
132	CKY000000000000178050	907	C9016B-2X-3 WR, 0.0--15.0 cm	907KTIWIC	30	10.94	11.09	10.94	11.09	
133	CKY000000000000154850	907	C9016B-2X-3 WR, 0.0--4.0 cm	907KTG	5	10.94	10.98	10.94	10.98	2 vials
134	CKY000000000000154950	907	C9016B-2X-3 WR, 0.0--4.0 cm	907KTHS	5	10.94	10.98	10.94	10.98	2 vials
135	CKY000000000000169250	907	C9016B-2X-3 W, 19.0--21.0 cm	907TAK	7	11.13	11.15	11.13	11.15	
136	CKY000000000000165350	907	C9016B-2X-3 W, 48.0--50.0 cm	907SAKI	34	11.42	11.44	11.42	11.44	
137	CKY000000000000167150	907	C9016B-2X-3 W, 50.0--52.0 cm	907TN	34	11.44	11.46	11.44	11.46	
138	CKY000000000000165450	907	C9016B-2X-3 W, 55.0--57.0 cm	907SYU	10	11.49	11.51	11.49	11.51	
139	CKY000000000000167250	907	C9016B-2X-3 W, 70.0--73.0 cm	907KAW	51	11.64	11.67	11.64	11.67	
140	CKY000000000000169350	907	C9016B-2X-3 W, 74.0--76.0 cm	907TAK	7	11.68	11.7	11.68	11.7	
141	CKY000000000000165550	907	C9016B-2X-3 W, 81.0--83.0 cm	907SYU	10	11.75	11.77	11.75	11.77	
142	CKY000000000000165750	907	C9016B-2X-3 W, 86.0--88.0 cm	907SAKI	34	11.8	11.82	11.8	11.82	
143	CKY000000000000165650	907	C9016B-2X-3 W, 88.0--90.0 cm	907TN	34	11.82	11.84	11.82	11.84	
144	CKY000000000000165850	907	C9016B-2X-3 W, 91.0--93.0 cm	907SYU	10	11.85	11.87	11.85	11.87	
145	CKY000000000000165950	907	C9016B-2X-CC W, 5.0--7.0 cm	907SYU	10	12	12.02	12	12.02	
146	CKY000000000000169450	907	C9016B-2X-CC W, 9.0--11.0 cm	907TAK	7	12.04	12.06	12.04	12.06	
147	CKY000000000000166050	907	C9016B-2X-CC W, 14.0--16.0 cm	907SAKI	34	12.09	12.11	12.09	12.11	
148	CKY000000000000166150	907	C9016B-2X-CC W, 16.0--18.0 cm	907TN	34	12.11	12.13	12.11	12.13	
149	CKY000000000000166250	907	C9016B-2X-CC W, 18.0--20.0 cm	907SYU	10	12.13	12.15	12.13	12.15	
150	CKY000000000000166350	907	C9016B-2X-CC W, 21.0--23.0 cm	907SYU	10	12.16	12.18	12.16	12.18	
151	CKY000000000000166450	907	C9016B-2X-CC W, 25.5--30.0 cm	907SYU	10	12.205	12.25	12.205	12.25	
152	CKY000000000000169750	907	C9016B-2X-CC W, 27.0--30.0 cm	907HK	20	12.22	12.25	12.22	12.25	
153	CKY000000000000155050	907	C9016B-2X-CC WR, 28.5--32.5 cm	907KTG	5	12.235	12.275	12.235	12.275	

	J-CORES sample ID	Leg/Exp.	Sample source	Request number	Sample volume (cm3)	Top depth [m CSF-A]	Bottom depth [m CSF-A]	Top depth [m CSF-B]	Bottom depth [m CSF-B]	Comment
154	CKY000000000000155150	907	C9016B-2X-CC WR, 28.5--32.5 cm	907KTHS	5	12.235	12.275	12.235	12.275	
155	CKY000000000000169550	907	C9016B-2X-CC W, 37.0--39.0 cm	907TAK	7	12.32	12.34	12.32	12.34	
156	CKY000000000000170550	907	C9016B-3X-1 W, 0.0--5.0 cm	907TN	1	25	25.05	25	25.05	
157	CKY000000000000170650	907	C9016B-3X-1 W, 3.0--5.0 cm	907SYU	10	25.03	25.05	25.03	25.05	
158	CKY000000000000173550	907	C9016B-3X-1 W, 4.0--6.0 cm	907TAK	7	25.04	25.06	25.04	25.06	
159	CKY000000000000170750	907	C9016B-3X-1 W, 10.0--12.0 cm	907SYU	10	25.1	25.12	25.1	25.12	
160	CKY000000000000155250	907	C9016B-3X-CC WR, 0.0--4.0 cm	907KTG	5	25.19	25.23	25.19	25.23	2 vials
161	CKY000000000000155350	907	C9016B-3X-CC WR, 0.0--4.0 cm	907KTHS	5	25.19	25.23	25.19	25.23	2 vials
162	CKY000000000000170850	907	C9016B-3X-CC W, 11.0--13.0 cm	907SYU	10	25.3	25.32	25.3	25.32	
163	CKY000000000000173650	907	C9016B-3X-CC W, 15.0--17.0 cm	907TAK	7	25.34	25.36	25.34	25.36	
164	CKY000000000000170950	907	C9016B-3X-CC W, 26.0--28.0 cm	907SYU	10	25.45	25.47	25.45	25.47	
165	CKY000000000000171950	907	C9016B-4X-1 W, 4.0--7.0 cm	907TN	51	29.54	29.57	29.54	29.57	
166	CKY000000000000173750	907	C9016B-4X-1 W, 6.0--8.0 cm	907TAK	7	29.56	29.58	29.56	29.58	
167	CKY000000000000169950	907	C9016B-4X-1 W, 11.0--13.0 cm	907SAKI	34	29.61	29.63	29.61	29.63	
168	CKY000000000000157150	907	C9016B-4X-2 WR, 0.0--15.0 cm	907KTIW	510	29.645	29.795	29.645	29.795	
169	CKY000000000000176250	907	C9016B-4X-2 WR, 0.0--15.0 cm	907KTIWS	128	29.645	29.795	29.645	29.795	
170	CKY000000000000178150	907	C9016B-4X-2 WR, 0.0--15.0 cm	907KTIWIC	17	29.645	29.795	29.645	29.795	
171	CKY000000000000157250	907	C9016B-4X-2 WR, 15.0--30.0 cm	907KTWR	510	29.795	29.945	29.795	29.945	
172	CKY000000000000171050	907	C9016B-4X-2 W, 35.0--39.0 cm	907SYU	30	29.995	30.035	29.995	30.035	
173	CKY000000000000170050	907	C9016B-4X-2 W, 59.0--61.0 cm	907SAKI	34	30.235	30.255	30.235	30.255	
174	CKY000000000000173850	907	C9016B-4X-2 W, 66.0--68.0 cm	907TAK	7	30.305	30.325	30.305	30.325	
175	CKY000000000000175550	907	C9016B-4X-2 W, 72.0--74.0 cm	907TN	34	30.365	30.385	30.365	30.385	
176	CKY000000000000175650	907	C9016B-4X-2 W, 92.0--95.0 cm	907TN	51	30.565	30.595	30.565	30.595	
177	CKY000000000000155750	907	C9016B-4X-2 WR, 96.0--100.0 cm	907KTG	5	30.605	30.645	30.605	30.645	2 vials
178	CKY000000000000155850	907	C9016B-4X-2 WR, 96.0--100.0 cm	907KTHS	5	30.605	30.645	30.605	30.645	2 vials
179	CKY000000000000171150	907	C9016B-4X-3 W, 3.0--5.0 cm	907SYU	10	30.675	30.695	30.675	30.695	
180	CKY000000000000173950	907	C9016B-4X-3 W, 21.0--23.0 cm	907TAK	7	30.855	30.875	30.855	30.875	
181	CKY000000000000172050	907	C9016B-4X-3 W, 24.0--30.0 cm	907TN	102	30.885	30.945	30.885	30.945	
182	CKY000000000000172150	907	C9016B-4X-3 W, 60.0--70.0 cm	907TN	170	31.245	31.345	31.245	31.345	
183	CKY000000000000174050	907	C9016B-4X-3 W, 73.0--75.0 cm	907TAK	7	31.375	31.395	31.375	31.395	
184	CKY000000000000155950	907	C9016B-4X-3 WR, 96.0--100.0 cm	907KTG	5	31.605	31.645	31.605	31.645	2 vials
185	CKY000000000000156050	907	C9016B-4X-3 WR, 96.0--100.0 cm	907KTHS	5	31.605	31.645	31.605	31.645	2 vials
186	CKY000000000000174150	907	C9016B-4X-4 W, 8.0--10.0 cm	907TAK	7	31.725	31.745	31.725	31.745	
187	CKY000000000000157350	907	C9016B-4X-4 WR, 45.0--65.0 cm	907KTIW	680	32.095	32.295	32.095	32.295	
188	CKY000000000000176550	907	C9016B-4X-4 WR, 45.0--65.0 cm	907KTIWS	192	32.095	32.295	32.095	32.295	
189	CKY000000000000178250	907	C9016B-4X-4 WR, 45.0--65.0 cm	907KTIWIC	30	32.095	32.295	32.095	32.295	
190	CKY000000000000174250	907	C9016B-4X-4 W, 72.0--74.0 cm	907TAK	7	32.365	32.385	32.365	32.385	
191	CKY000000000000172250	907	C9016B-4X-4 W, 75.0--79.0 cm	907TN	68	32.395	32.435	32.395	32.435	
192	CKY000000000000172350	907	C9016B-4X-4 W, 87.0--93.0 cm	907TN	102	32.515	32.575	32.515	32.575	
193	CKY000000000000172450	907	C9016B-4X-CC W, 4.0--13.0 cm	907TN	153	32.685	32.775	32.685	32.775	
194	CKY000000000000173450	907	C9016B-4X-CC W, 16.0--20.0 cm	907KAW	68	32.805	32.845	32.805	32.845	
195	CKY000000000000156450	907	C9016B-4X-CC WR, 22.5--26.5 cm	907KTHS	5	32.87	32.91	32.87	32.91	2 vials
196	CKY000000000000170150	907	C9016B-4X-CC W, 25.0--27.0 cm	907SAKI	34	32.895	32.915	32.895	32.915	
197	CKY000000000000174350	907	C9016B-4X-CC W, 35.0--37.0 cm	907TAK	7	32.995	33.015	32.995	33.015	
198	CKY000000000000171550	907	C9016B-4X-CC W, 44.0--46.0 cm	907SYU	10	33.085	33.105	33.085	33.105	
199	CKY000000000000156350	907	C9016B-4X-CC WR, 44.5--48.5 cm	907KTG	5	33.09	33.13	33.09	33.13	2 vials
200	CKY000000000000174450	907	C9016B-5X-1 W, 16.0--18.0 cm	907TAK	7	35.16	35.18	35.16	35.18	
201	CKY000000000000158250	907	C9016B-5X-2 WR, 0.0--20.0 cm	907KTIW	680	35.205	35.405	35.205	35.405	
202	CKY000000000000176650	907	C9016B-5X-2 WR, 0.0--20.0 cm	907KTIWS	256	35.205	35.405	35.205	35.405	
203	CKY000000000000178350	907	C9016B-5X-2 WR, 0.0--20.0 cm	907KTIWIC	30	35.205	35.405	35.205	35.405	
204	CKY000000000000158350	907	C9016B-5X-2 WR, 20.0--35.0 cm	907KTWR	680	35.405	35.555	35.405	35.555	

	J-CORES sample ID	Leg/Exp.	Sample source	Request number	Sample volume (cm3)	Top depth [m CSF-A]	Bottom depth [m CSF-A]	Top depth [m CSF-B]	Bottom depth [m CSF-B]	Comment
205	CKY000000000000172550	907	C9016B-5X-2 W, 46.0--47.0 cm	907TN	34	35.665	35.675	35.665	35.675	
206	CKY000000000000174550	907	C9016B-5X-2 W, 54.0--56.0 cm	907TAK	7	35.745	35.765	35.745	35.765	
207	CKY000000000000171250	907	C9016B-5X-2 W, 71.0--73.0 cm	907SYU	10	35.915	35.935	35.915	35.935	
208	CKY000000000000156750	907	C9016B-5X-2 WR, 96.0--100.0 cm	907KTG	5	36.165	36.205	36.165	36.205	
209	CKY000000000000156850	907	C9016B-5X-2 WR, 96.0--100.0 cm	907KTHS	5	36.165	36.205	36.165	36.205	
210	CKY000000000000172650	907	C9016B-5X-2 W, 98.0--99.0 cm	907TN	34	36.185	36.195	36.185	36.195	
211	CKY000000000000174650	907	C9016B-5X-3 W, 29.0--31.0 cm	907TAK	7	36.495	36.515	36.495	36.515	
212	CKY000000000000158450	907	C9016B-5X-3 WR, 80.0--100.5 cm	907KTIW	697	37.005	37.21	37.005	37.21	
213	CKY000000000000176750	907	C9016B-5X-3 WR, 80.0--100.5 cm	907KTIWS	192	37.005	37.21	37.005	37.21	
214	CKY000000000000178450	907	C9016B-5X-3 WR, 80.0--100.5 cm	907KTIWIC	30	37.005	37.21	37.005	37.21	
215	CKY000000000000156550	907	C9016B-5X-3 WR, 96.0--100.0 cm	907KTG	5	37.165	37.205	37.165	37.205	
216	CKY000000000000156650	907	C9016B-5X-3 WR, 96.0--100.0 cm	907KTHS	5	37.165	37.205	37.165	37.205	
217	CKY000000000000171350	907	C9016B-5X-4 W, 0.0--2.0 cm	907SYU	10	37.21	37.23	37.21	37.23	
218	CKY000000000000172750	907	C9016B-5X-4 W, 4.0--9.0 cm	907TN	85	37.25	37.3	37.25	37.3	
219	CKY000000000000174750	907	C9016B-5X-4 W, 29.0--31.0 cm	907TAK	7	37.5	37.52	37.5	37.52	
220	CKY000000000000170250	907	C9016B-5X-4 W, 64.0--67.0 cm	907SAKI	51	37.85	37.88	37.85	37.88	
221	CKY000000000000172850	907	C9016B-5X-4 W, 83.0--89.0 cm	907TN	102	38.04	38.1	38.04	38.1	
222	CKY000000000000172950	907	C9016B-5X-CC W, 8.0--11.0 cm	907TN	51	38.285	38.315	38.285	38.315	
223	CKY000000000000174850	907	C9016B-5X-CC W, 11.0--13.0 cm	907TAK	7	38.315	38.335	38.315	38.335	
224	CKY000000000000171450	907	C9016B-5X-CC W, 17.0--19.0 cm	907SYU	10	38.375	38.395	38.375	38.395	
225	CKY000000000000169850	907	C9016B-5X-CC W, 20.0--39.0 cm	907HK	323	38.405	38.595	38.405	38.595	
226	CKY000000000000156950	907	C9016B-5X-CC WR, 35.5--39.5 cm	907KTG	5	38.56	38.6	38.56	38.6	
227	CKY000000000000157050	907	C9016B-5X-CC WR, 35.5--39.5 cm	907KTHS	5	38.56	38.6	38.56	38.6	
228	CKY000000000000171850	907	C9016B-6X-1 W, 2.0--4.0 cm	907SYU	10	40.02	40.04	40.02	40.04	
229	CKY000000000000174950	907	C9016B-6X-1 W, 13.0--15.0 cm	907TAK	7	40.13	40.15	40.13	40.15	
230	CKY000000000000173050	907	C9016B-6X-1 W, 15.0--18.0 cm	907TN	51	40.15	40.18	40.15	40.18	
231	CKY000000000000157450	907	C9016B-6X-2 WR, 0.0--4.0 cm	907KTG	5	40.26	40.3	40.26	40.3	
232	CKY000000000000157550	907	C9016B-6X-2 WR, 0.0--4.0 cm	907KTHS	5	40.26	40.3	40.26	40.3	
233	CKY000000000000170350	907	C9016B-6X-2 W, 8.0--12.0 cm	907SAKI	68	40.34	40.38	40.34	40.38	
234	CKY000000000000173150	907	C9016B-6X-2 W, 23.0--26.0 cm	907TN	51	40.49	40.52	40.49	40.52	
235	CKY000000000000171650	907	C9016B-6X-2 W, 28.0--30.0 cm	907SYU	10	40.54	40.56	40.54	40.56	
236	CKY000000000000175050	907	C9016B-6X-2 W, 39.0--41.0 cm	907TAK	7	40.65	40.67	40.65	40.67	
237	CKY000000000000158650	907	C9016B-6X-2 WR, 80.0--100.0 cm	907KTIW	680	41.06	41.26	41.06	41.26	
238	CKY000000000000176850	907	C9016B-6X-2 WR, 80.0--100.0 cm	907KTIWS	192	41.06	41.26	41.06	41.26	
239	CKY000000000000178550	907	C9016B-6X-2 WR, 80.0--100.0 cm	907KTIWIC	30	41.06	41.26	41.06	41.26	
240	CKY000000000000175150	907	C9016B-6X-3 W, 19.0--21.0 cm	907TAK	7	41.45	41.47	41.45	41.47	
241	CKY000000000000171750	907	C9016B-6X-3 W, 35.0--37.0 cm	907SYU	10	41.61	41.63	41.61	41.63	
242	CKY000000000000170450	907	C9016B-6X-3 W, 48.0--51.0 cm	907SAKI	51	41.74	41.77	41.74	41.77	
243	CKY000000000000173250	907	C9016B-6X-3 W, 61.0--64.0 cm	907TN	51	41.87	41.9	41.87	41.9	
244	CKY000000000000175250	907	C9016B-6X-3 W, 69.0--71.0 cm	907TAK	7	41.95	41.97	41.95	41.97	
245	CKY000000000000173350	907	C9016B-6X-3 W, 81.0--83.0 cm	907TN	34	42.07	42.09	42.07	42.09	
246	CKY000000000000157650	907	C9016B-6X-3 WR, 95.5--99.5 cm	907KTG	5	42.215	42.255	42.215	42.255	
247	CKY000000000000157750	907	C9016B-6X-3 WR, 95.5--99.5 cm	907KTHS	5	42.215	42.255	42.215	42.255	
248	CKY000000000000175350	907	C9016B-6X-4 W, 29.0--31.0 cm	907TAK	7	42.545	42.565	42.545	42.565	
249	CKY000000000000158750	907	C9016B-6X-4 WR, 65.0--85.0 cm	907KTIW	680	42.905	43.105	42.905	43.105	
250	CKY000000000000176950	907	C9016B-6X-4 WR, 65.0--85.0 cm	907KTIWS	160	42.905	43.105	42.905	43.105	
251	CKY000000000000178650	907	C9016B-6X-4 WR, 65.0--85.0 cm	907KTIWIC	30	42.905	43.105	42.905	43.105	
252	CKY000000000000158850	907	C9016B-6X-4 WR, 85.0--100.5 cm	907KTWR	527	43.105	43.26	43.105	43.26	
253	CKY000000000000157850	907	C9016B-6X-CC WR, 0.0--4.0 cm	907KTG	5	43.26	43.3	43.26	43.3	
254	CKY000000000000157950	907	C9016B-6X-CC WR, 0.0--4.0 cm	907KTHS	5	43.26	43.3	43.26	43.3	
255	CKY000000000000175450	907	C9016B-6X-CC W, 10.0--12.0 cm	907TAK	7	43.36	43.38	43.36	43.38	

	J-CORES sample ID	Leg/Exp.	Sample source	Request number	Sample volume (cm3)	Top depth [m CSF-A]	Bottom depth [m CSF-A]	Top depth [m CSF-B]	Bottom depth [m CSF-B]	Comment
256	CKY000000000000156150	907	C9016B-7X-1 W, 14.0--16.0 cm	907TAK	7	50.14	50.16	50.14	50.16	
257	CKY000000000000158950	907	C9016B-7X-2 WR, 0.0--20.0 cm	907KTIW	680	50.25	50.45	50.25	50.45	
258	CKY000000000000177050	907	C9016B-7X-2 WR, 0.0--20.0 cm	907KTIWS	160	50.25	50.45	50.25	50.45	
259	CKY000000000000178750	907	C9016B-7X-2 WR, 0.0--20.0 cm	907KTIWIC	30	50.25	50.45	50.25	50.45	
260	CKY000000000000156250	907	C9016B-7X-2 W, 29.0--31.0 cm	907TAK	7	50.54	50.56	50.54	50.56	
261	CKY000000000000163850	907	C9016B-7X-2 W, 69.0--71.0 cm	907TAK	7	50.94	50.96	50.94	50.96	
262	CKY000000000000180250	907	C9016B-7X-2 W, 76.0--78.0 cm	907TY	34	51.01	51.03	51.01	51.03	
263	CKY000000000000166650	907	C9016B-7X-CC W, 23.5--25.5 cm	907TAK	7	51.49	51.51	51.49	51.51	
264	CKY000000000000158050	907	C9016B-7X-CC WR, 38.0--42.0 cm	907KTG	5	51.635	51.675	51.635	51.675	
265	CKY000000000000158150	907	C9016B-7X-CC WR, 38.0--42.0 cm	907KTHS	5	51.635	51.675	51.635	51.675	
266	CKY000000000000179950	907	C9016B-8X-1 W, 18.0--20.0 cm	907SYU	17	67.18	67.2	67.18	67.2	
267	CKY000000000000181350	907	C9016B-8X-1 W, 26.5--28.5 cm	907TAK	7	67.265	67.285	67.265	67.285	
268	CKY000000000000181250	907	C9016B-8X-CC W, 8.0--19.0 cm	907HK	374	67.44	67.55	67.44	67.55	
269	CKY000000000000180350	907	C9016B-8X-CC W, 20.0--23.0 cm	907TY	51	67.56	67.59	67.56	67.59	
270	CKY000000000000178950	907	C9016B-8X-CC W, 26.0--30.0 cm	907SYU	34	67.62	67.66	67.62	67.66	
271	CKY000000000000181450	907	C9016B-8X-CC W, 31.0--33.0 cm	907TAK	7	67.67	67.69	67.67	67.69	
272	CKY000000000000158550	907	C9016B-8X-CC WR, 36.5--40.5 cm	907KTHS	5	67.725	67.765	67.725	67.765	
273	CKY000000000000180750	907	C9016B-9X-CC W, 4.0--5.0 cm	907TN	34	73.64	73.65	73.64	73.65	
274	CKY000000000000180850	907	C9016B-9X-CC W, 8.0--9.0 cm	907TN	34	73.68	73.69	73.68	73.69	
275	CKY000000000000179050	907	C9016B-9X-CC W, 13.0--15.0 cm	907SYU	17	73.73	73.75	73.73	73.75	
276	CKY000000000000181550	907	C9016B-9X-CC W, 18.0--20.0 cm	907TAK	7	73.78	73.8	73.78	73.8	
277	CKY000000000000179150	907	C9016B-9X-CC W, 26.0--30.0 cm	907SYU	34	73.86	73.9	73.86	73.9	
278	CKY000000000000159050	907	C9016B-9X-CC WR, 31.0--35.0 cm	907KTHS	5	73.91	73.95	73.91	73.95	
279	CKY000000000000181150	907	C9016B-10X-CC W, 19.0--26.0 cm	907HK	10	80.19	80.26	80.19	80.26	
280	CKY000000000000180450	907	C9016B-10X-CC W, 29.0--33.0 cm	907TY	68	80.29	80.33	80.29	80.33	
281	CKY000000000000181650	907	C9016B-11X-1 W, 19.0--21.0 cm	907TAK	7	85.19	85.21	85.19	85.21	
282	CKY000000000000180950	907	C9016B-11X-1 W, 36.0--37.0 cm	907TN	34	85.36	85.37	85.36	85.37	
283	CKY000000000000181050	907	C9016B-11X-1 W, 47.0--48.0 cm	907TN	34	85.47	85.48	85.47	85.48	
284	CKY000000000000179250	907	C9016B-11X-1 W, 57.0--62.0 cm	907SYU	42.5	85.57	85.62	85.57	85.62	
285	CKY000000000000181750	907	C9016B-11X-1 W, 69.0--71.0 cm	907TAK	7	85.69	85.71	85.69	85.71	
286	CKY000000000000180550	907	C9016B-11X-1 W, 82.5--85.0 cm	907TY	42.5	85.825	85.85	85.825	85.85	
287	CKY000000000000159250	907	C9016B-11X-CC WR, 0.0--4.0 cm	907KTHS	5	86.005	86.045	86.005	86.045	2 vials
288	CKY000000000000179350	907	C9016B-11X-CC W, 19.0--22.0 cm	907SYU	25.5	86.195	86.225	86.195	86.225	
289	CKY000000000000181850	907	C9016B-11X-CC W, 29.0--31.0 cm	907TAK	7	86.295	86.315	86.295	86.315	
290	CKY000000000000179450	907	C9016B-12X-1 W, 11.0--17.0 cm	907SYU	51	90.11	90.17	90.11	90.17	
291	CKY000000000000181950	907	C9016B-12X-1 W, 18.0--20.0 cm	907TAK	7	90.18	90.2	90.18	90.2	
292	CKY000000000000180050	907	C9016B-12X-2 W, 9.0--12.0 cm	907SAKI	34	90.37	90.4	90.37	90.4	
293	CKY000000000000179550	907	C9016B-12X-2 W, 35.0--39.0 cm	907SYU	34	90.63	90.67	90.63	90.67	
294	CKY000000000000182050	907	C9016B-12X-2 W, 49.0--51.0 cm	907TAK	7	90.77	90.79	90.77	90.79	
295	CKY000000000000179650	907	C9016B-12X-2 W, 75.0--79.0 cm	907SYU	34	91.03	91.07	91.03	91.07	
296	CKY000000000000159350	907	C9016B-12X-2 WR, 96.0--100.0 cm	907KTHS	5	91.24	91.28	91.24	91.28	2 vials
297	CKY000000000000182150	907	C9016B-12X-3 W, 9.0--11.0 cm	907TAK	7	91.37	91.39	91.37	91.39	
298	CKY000000000000159550	907	C9016B-12X-3 WR, 19.0--49.0 cm	907KTIW	1020	91.47	91.77	91.47	91.77	
299	CKY000000000000177150	907	C9016B-12X-3 WR, 19.0--49.0 cm	907KTIWS	160	91.47	91.77	91.47	91.77	
300	CKY000000000000178850	907	C9016B-12X-3 WR, 19.0--49.0 cm	907KTIWIC	30	91.47	91.77	91.47	91.77	
301	CKY000000000000179750	907	C9016B-12X-3 W, 66.0--69.0 cm	907SYU	25.5	91.94	91.97	91.94	91.97	
302	CKY000000000000182250	907	C9016B-12X-3 W, 79.0--81.0 cm	907TAK	7	92.07	92.09	92.07	92.09	
303	CKY000000000000159150	907	C9016B-12X-CC WR, 0.0--4.0 cm	907KTHS	5	92.29	92.33	92.29	92.33	2 vials
304	CKY000000000000182350	907	C9016B-12X-CC W, 29.0--31.0 cm	907TAK	7	92.58	92.6	92.58	92.6	
305	CKY000000000000179850	907	C9016B-12X-CC W, 36.0--40.0 cm	907SYU	34	92.65	92.69	92.65	92.69	
306	CKY000000000000182450	907	C9016B-13X-1 W, 17.0--19.0 cm	907TAK	7	95.17	95.19	95.17	95.19	

	J-CORES sample ID	Leg/Exp.	Sample source	Request number	Sample volume (cm3)	Top depth [m CSF-A]	Bottom depth [m CSF-A]	Top depth [m CSF-B]	Bottom depth [m CSF-B]	Comment
307	CKY000000000000180150	907	C9016B-13X-CC W, 9.0--11.0 cm	907SAKI	34	95.35	95.37	95.35	95.37	
308	CKY000000000000159450	907	C9016B-13X-CC WR, 10.0--14.0 cm	907KTHS	5	95.36	95.4	95.36	95.4	2 vials
309	CKY000000000000180650	907	C9016B-13X-CC W, 13.0--15.5 cm	907TY	42.5	95.39	95.415	95.39	95.415	
310	CKY000000000000182550	907	C9016B-13X-CC W, 19.0--21.0 cm	907TAK	7	95.45	95.47	95.45	95.47	
311	CKY000000000000185750	907	C9016B-14X-1 W, 14.0--16.0 cm	907TAK	7	105.14	105.16	105.14	105.16	
312	CKY000000000000183850	907	C9016B-14X-CC W, 0.0--3.0 cm	907TN	1	105.25	105.28	105.25	105.28	
313	CKY000000000000185850	907	C9016B-14X-CC W, 14.0--16.0 cm	907TAK	7	105.39	105.41	105.39	105.41	
314	CKY000000000000166550	907	C9016B-14X-CC WR, 25.0--29.0 cm	907KTHS	5	105.5	105.54	105.5	105.54	2 vials
315	CKY000000000000184450	907	C9016B-14X-CC W, 28.0--32.0 cm	907SAKI	34	105.53	105.57	105.53	105.57	
316	CKY000000000000183550	907	C9016B-14X-CC W, 29.0--32.0 cm	907SYU	10	105.54	105.57	105.54	105.57	
317	CKY000000000000183650	907	C9016B-15X-1 W, 0.0--5.0 cm	907SAKI	5	115	115.05	115	115.05	
318	CKY000000000000183750	907	C9016B-15X-1 W, 7.0--10.0 cm	907SYU	10	115.07	115.1	115.07	115.1	
319	CKY000000000000183450	907	C9016B-15X-CC W, 7.0--10.0 cm	907TY	42.5	115.25	115.28	115.25	115.28	
320	CKY000000000000185950	907	C9016B-15X-CC W, 19.0--21.0 cm	907TAK	7	115.37	115.39	115.37	115.39	
321	CKY000000000000186050	907	C9016B-16X-CC W, 26.0--28.0 cm	907TAK	7	140.26	140.28	140.26	140.28	

[Note]
m CSF = depth of Core below Sea Floor in meters.
m CSF-A: Distance from sea floor to sample within recovered core. This scale allows overlap at core and section boundaries.
m CSF-B: Distance from sea floor to sample within recovered core is compressed, if core recovery > 100%.
For further details, consult the "IODP Depth Scales Terminology" in the IODP web site (http://www.iodp.org/program-policies/).